Sensitivity Analysis for Measurements of Multipath Parameters Pertinent to TOA based Indoor Geolocation

by

Yunxing Ye

A Thesis Submitted to the Faculty of the

WORCESTER POLYTECHNIC INSTITUTE

In partial fulfillment of the requirements for the

Degree of Master of Science

in

Electrical and Computer Engineering

by

November 2009

Professor Kaveh Pahlavan
Thesis Advisor
ECE Department

Professor Allen Levesque
Thesis Committee member
ECE Department

Professor Xinming Huang
Thesis Committee member
ECE Department

Abstract

Recently, indoor geolocation technologies has been attracting tremendous attention. For indoor environments, the fine time resolution of ultra-wideband (UWB) signals enables the potential of accurate distance measurement of the direct path (DP) between a number of reference sources and the people or assets of interest. However, Once the DP is not available or is shadowed, substantial errors will be introduced into the ranging measurements, leading to large localization errors when measurements are combined from multiple sources. The measurement accuracy in undetected direct path (UDP) conditions can be improved in some cases by exploiting the geolocation information contained in the indirect path measurements. Therefore, the dynamic spatial behavior of paths is an important issue for positioning techniques based on TOA of indirect paths.

The objectives of this thesis are twofold. The first is to analyze the sensitivity of TOA estimation techniques based on TOA of the direct path. we studied the effect of distance, bandwidth and multipath environment on the accuracy of various TOA estimation techniques.The second is to study the sensitivity of multipath parameters pertinent to TOA estimation techniques based on the TOA of the indirect paths. We mainly looked into the effect of distance, bandwidth, threshold for picking paths, and multipath environment on the number of multipath components(MPCs) and path persistency.

Our results are based on data from a new measurement campaign conducted on the 3rd floor of AK laboratory. For the TOA estimation techniques based on DP, the line of sight (LOS) scenario provides greatest accuracy and these TOA estimation techniques are most sensitive to bandwidth availability in obstructed line of sight (OLOS) scenario. All the TOA estimation algorithms perform poorly in the UDP scenario although the use of higher bandwidth can reduce the ranging error to some extent. Based on our processed

results, The proposal for selecting the appropriate TOA estimation technique with certain constrains is given.

The sensitivity study of multipath parameters pertinent to indirect-path-based TOA estimation techniques shows that the number of MPCs is very sensitive to the threshold for picking paths and to the noise threshold. It generally decreases as the distance increase while larger bandwidth always resolves more MPCs. The multipath components behave more persistently in line of sight (LOS) and obstructed line of sight (OLOS) scenarios than in UDP scenarios, and the use of larger bandwidth and higher threshold for picking paths also result in more persistent paths.

Acknowledgements

Foremost, I am greatly thankful to my thesis advisor, Dr. Kaveh Pahlavan, not only for his guidance, support in academics and research, but also enlightening me with the general philosophy of life. His insight, knowledge and experience helped me attain the objectives of this research.

I am extremely grateful to members of the thesis committee, Dr. Allen Levesque and Dr. Xinmin Huang. I appreciate their advice and feedback in spite of tight schedules.

Many thanks go in particular to Ferit Ozan Akgul for his valuable guidence, discussion, comments through this research. During our collaboration, I also benefited from Ferit's help with his skill in programming and handling equipments. I gratefully thank other fellow friends, Nayef Alsindi, Mohammad Heidari, Biao Li, Yi Wang, Umair Ishaq, for their help, support, friendship, and nice working atmosphere they provided.

I would also like to thank Dr. Fred Looft as the department head of Electrical and Computer Engineering department in WPI who gave me the opportunity of continue my studies here in WPI as a TA.

Simply, I could not have reached where I am today without my father, Mr. Yuezhong Ye, my mother, Ms. Xingyue Wang. Without their unconditional love and support, this work wouldn't have been possible.

Table of Contents

List of Figures

List of Tables

Glossary

AK Atwater Kent, 21

AOA Angle of Arrival, 7

APD Average Path Displacement, 87

APL Average Path Life Time, 87

CWINS Center for Wireless Network Studies, 4

CZT Chirp Z transform, 37

DDP Detected Direct Path, 16

DLOS Direct Line of Sight, 17

DME Distance Measurement Error, 36

DP Direct Path, 1

DSSS Direct Sequence Spread Spectrum, 38

FBCM Forward Backward Correlation Matrix, 43

FDP First Detected Path, 37

GPS Global Positioning System, 2

IFT Inverse Fourier Transform, 37

LNA Low Noise Amplifier, 26

LOS Line of Sight, 1

MPCs Multipath Components, 5

MT Mobile Terminal, 3

NLOS None Line of Sight, 4

NUDP Natural Undetected Direct Path, 23

OLOS Obstructed Line of Sight, 1

RF Radio Frequency, 7

RMS Root Mean Square, 35

RSS Received Signal Strength, 7

SP Strongest Path, 87

SUDP Shadowed Undetected Direct Path, 23

TDOA Time Difference of Arrival, 70

TOA Time of Arrival, 1

UDP Undetected Direct Path, 1

UWB Ultra Wideband, 1

WLAN Wireless LAN, 7

Chapter 1

Introduction

This Chapter is divided into three sections. Section 1.1 provides the background and motivation for this research. Section Section 1.2 highlights the major contributions made through this research. Section 1.3 provides an outline of the remaining chapters in this thesis.

1.1 Background and Motivation

The use of radio signals for localization was originated in World War II when the requirement for locating military targets and soldiers appeared. During the Vietnam war, the Global positioning system (GPS) [3] was introduced by launching a series of satellites to support the military application. This technology became accessible to commercial and private use around 1990, and is still the most popular localization technology until now. Another existing location finding system, the wireless enhanced 911 (E911), was introduced by the FCC in 1996 and is used to provide relatively accurate positioning for the outdoor environment [4]. These technologies, although reliable and accurate in outdoor environments, can not achieve the satisfactory accuracy in indoor and urban areas with

serious multipath conditions and frequent occurrence of Undetected direct path (UDP) conditions.

Indoor geolocation is motivated by a variety of envisioned applications for indoor location sensing in commercial, public safety, and military settings [5, 1]. Examples of such applications include tracking people with special needs, locating instrumentation and other equipment in hospitals, locating equipment in warehouses, locating public safety and military personnel in their indoor missions, and various personal robotics applications [6].

As a result of the potential for such applications and services, many researchers have worked on various aspects of indoor geolocation. For the indoor environment, the fine time resolution of ultra-wideband (UWB) signals enables the potentiality of accurate distance measurement of the direct path (DP) between a number of reference sources and the people or assets of interest. However, the rich multipath environment often causes the received signal strength (RSS) of indirect paths to be greater than that of the direct path, sometimes resulting in undetected direct path (UDP) conditions [1]. Once the DP is not available or shadowed, substantial errors will be introduced into the ranging measurements hence leading to large localization errors when measurements are combined from multiple sources [7]. Discussions of these UDP conditions and how they affect the ranging/positioning accuracy can be found in [8, 9].

The measurement accuracy in UDP conditions can be improved in some cases by exploiting the geolocation information contained in the indirect path measurements [7], or exploiting multipath signals by using them as additional measurements within a nonlinear filter [10]. Both of these approaches will need the help of other indirect paths in addition to the DP component. The intuition for using multipath is that even in the absence of DP, there will be multipath components that might show stable and persistent behavior and thus can be related to the DP to aid in more precise localization. Therefore, the dynamic

behavior of paths, which is time varying due to the motion of the mobile terminal (MT) and changes in the surrounding objects, is an important issue in mitigating the UDP error.

In this thesis, a comprehensive dynamic UWB channel measurement database has been created to study the sensitivity of time of arrival (TOA) based indoor localization techniques. For direct path based TOA estimation, we mainly looked into the sensitivity of distance measurement error (DME). For multipath diversity based TOA estimation, the distance dependency of the available number of MPCs for geolocation has been modeled for both line of sight (LOS) and non-line of sight (NLOS) conditions. In addition, the effect of bandwidth, path detection threshold and NLOS occurrence on multipath parameters such as number of MPCs , and path persistency, is analyzed to provide a deeper insight into wireless channel modeling for indoor geolocation.

1.2 Contribution of the Thesis

The contribution of the thesis can be summarized as follows:

1. Dynamic UWB channel measurements were conducted for four different scenarios: Mixed loop scenario, LOS corridor scenario, NLOS scenario and UDP scenario. The main difference between this measurement campaign and the previous UWB channel measurement campaigns conducted in the Center for Wireless Information Network Study (CWINS) is this: the interval between consecutive measurement points is much smaller than in the previous measurements: 5 and 10cm distance for the dynamic measurements compared with several meters for previous measurements).

2. The sensitivity of TOA estimation accuracy for DP based techniques was analyzed. The effect of bandwidth, threshold for picking paths, and NLOS, UDP occurrence on

distance measurement error (DME) was evaluated. The performance of different TOA estimation techniques was also compared using various constraints to build a reference for the selection of TOA estimation techniques

3. The sensitivity of measured multipath parameters pertinent to TOA estimation techniques using multipath diversity was also analyzed. The distance dependency of the available number of MPCs was modeled for each measurement scenario. The effect of bandwidth, threshold for picking paths, and NLOS, UDP occurrence on the multipath parameters such as number of MPCs, and path persistency was evaluated using the comprehensive measurement data base tailored to indoor geolocation.

1.3 Outline of the Thesis

The thesis is divided into six chapters. Chapter 1provides an overview of the thesis.

Chapter 2 provides an overview of the indoor geolocation systems. The system architecture and geolocation specific matrices are explained. Furthermore, the classification of typical indoor channel environments is introduced.

Chapter 3 outlines the procedure for the measurement campaign that was conducted along with detailed procedure for post-processing the measured data. The measurement scenario is also depicted.

Chapter 4 first introduces the direct-path-based TOA estimation algorithms used in thesis and then provides the sensitivity study of these algorithms affected by adjusting bandwidth, threshold for picking paths, and multipath environments.

Chapter 5 provides the sensitivity analysis results of multipath parameters pertinent to indirect path based TOA estimation algorithms. This includes a proposed model for the distance dependency of number of MPCs in LOS scenario and NLOS scenario and also

the effect of bandwidth, threshold for picking paths, and UDP occurrence on number of MPCs and path persistency.

Finally, Chapter 6 concludes the thesis and discusses possible directions of future work.

Chapter 2

Indoor Geolocation and Channel behavior

Localization and tracking are of great interest in many application fields, such as robotics and emergency systems. In terms of functioning environment, we can distinguish between indoor and outdoor positioning systems. Outdoor positioning systems, such as GPS or GSM, are designed for application in wide areas. They usually provide satisfactory coverage and accuracy in open areas, but can't perform as well in indoor environments and urban canyon areas. Indoor systems are designed to determine a precise position inside buildings or at locations where GPS does not perform satisfactorily.

Apart from systems based on use of cameras and certain sensors (such as inertial sensors), most positioning systems use some kind of a signal metric to infer the distance between the fixed elements (beacons) and the mobile terminal that is to be located. The metrics that are usually used are time of arrival(TOA), received signal strength(RSS) and angle of arrival(AOA), which will be further explained later.

Radiofrequency (RF) is the signal that is most commonly used to perform indoor localization, because it is the backbone signal for wireless communications. Reusing

RF signals to perform localization can be accomplished without additional hardware, reducing the total cost of the localization system significantly. Many research groups are currently working on localization using a standard protocol such as 802.11 (WLAN) or 802.15.3 (UWB).

A wide variety of algorithms have been tested for position calculation , but they all suffer from none-line-of-sight(NLOS) errors: the problem of finding the intersection of several spheres centered on the beacons and radius equals their distances to the mobile terminal accurately. In the concluding section of this chapter, we introduce different channel profiles and their characteristics as the preparation for later discussion.

2.1 Indoor Geolocation Systems Architecture

Figure 2.1 illustrates a block diagram of the main components in a wireless geolocation system. The location sensing devices measure the location metrics between the mobile terminal (MT) with respect to some number of known reference points (RPs). The location metrics include angle of arrival (AOA), time of arrival (TOA), received signal strength (RSS), and carrier signal phase of arrival (POA). The positioning algorithm processes the reported metrics to estimate the location coordinates of the receiver. The display system exhibits the location of the mobile terminal relative to the user. The accuracy of location estimation is a function of the accuracy of the location metrics and the complexity of the positioning algorithm [2].

There are two common approaches to implementing a wireless indoor geolocation system. The first approach is to design a signaling system and a network infrastructure of location sensors focused primarily on geolocation applications [1]. The second approach is to use an existing wireless network infrastructure such as a cellular network or wireless LAN (WLAN) to locate a MT. The advantage of the first approach is that the physical

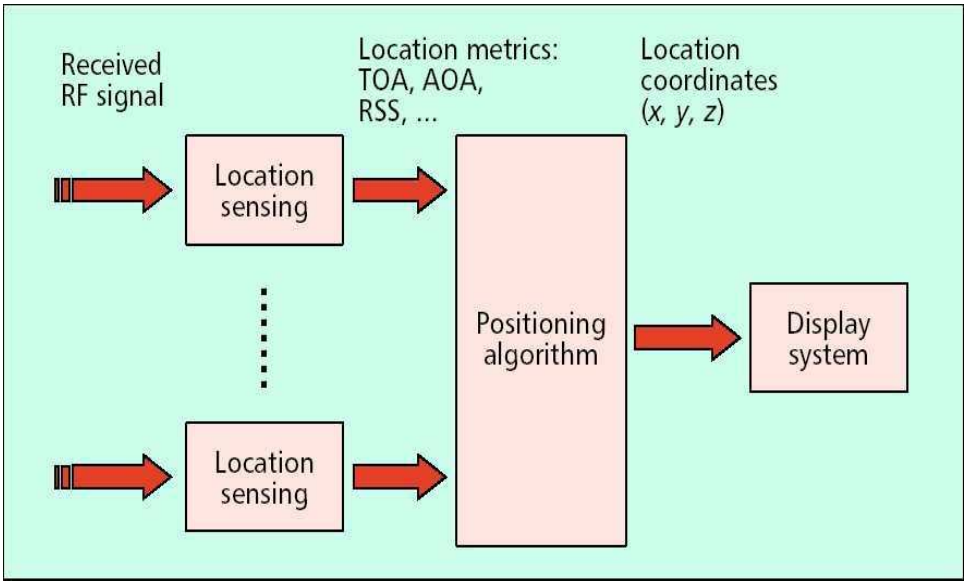

Figure 2.1: Functional block diagram of a wireless geolocation system [1]

specialization, and therefore the overall design, is under the control of the system designer. As a result, the MTs can be designed as small wearable tags or stickers and the complexity and density of the locating infrastructure can be customized to the accuracy required for different applications. The advantage of the second approach is that it avoids expensive and time-consuming infrastructure deployment. However, more intelligent algorithms are needed in such systems to compensate for the low accuracy of the reported metrics.

When considering system implementation, the advantage of the first approach is that it is easier to implement super-resolution algorithm for higher time-domain resolution. The system captures snapshots in the frequency domain and then through the spectral estimation, it is possible to obtain an accurate representation of the time domain. Another emerging approach that has better accuracy and potential is Ultra wideband (UWB) technology [1]. The large bandwidth provides high time domain resolution which in return provides better ranging accuracy.

For the second approach, the use of the network infrastructure in indoor geolocation

is also feasible but more complex algorithms are needed in order to compensate for overall performance. One current example is Ekahau positioning software which utilizes the existing WLAN infrastructure. Unlike the other positioning technologies, Ekahau does not apply propagation methods that suffer from multipath, scattering and attenuation effects. Instead, Ekahau collects radio network sample points from different site location. Each sample point contains received signal intensity (RSSI) and the related map coordinates, stored in an area-specific positioning model for accurate tracking. Ekahau provides average positioning accuracy approaching 1 meter. The software works with industry-standard Wi-Fi (IEEE 802.11b,g) networks [11]. When it comes to system deployment, a positioning model is created first. Then the positioning model is calibrated using RSSI samples collected from the different points on the map. Then the tracking or positioning can start as soon as the system is calibrated. In other words, this positioning algorithm works with the WLAN infrastructure and no information about the access point location is required. Such technology depends on complex positioning algorithms and does not concentrate on the physical layer. In fact, it uses RSS as a metric instead of trying to extract the TOA or AOA, which is more challenging task at the physical layer. Needless to say, when following the RSS method and bypassing the propagation issues the complexities lie in the software itself.

2.2 Positioning Metrices

Wireless localization sensors operating in different environment measure RSS, AOA, POA, TOA, and the signature of the delay power profile as location metrics [1].

2.2.1 Angle of Arrival

In AOA-based indoor geolocation, directional antenna or antenna arrays are used to triangulate the MT. Two or more reference points (RPs) are needed to determine the axis value of the MT as shown in Fig 2.2. Commonly, measurements of POA and AOA in large indoor and urban areas provide very unreliable results due to severe multipath propagation and heavy shadow-fading conditions. The accuracy of the AOA measurement

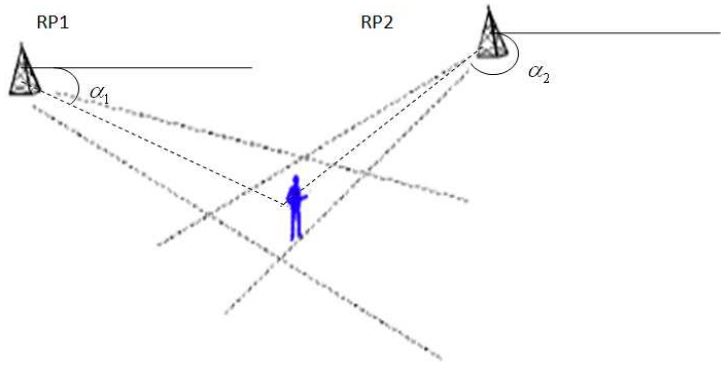

Figure 2.2: AOA technique for geolocation

system is determined by the resolution of the directional antenna or antenna array and the algorithms used to estimate the AOA simultaneously. Given the accuracy of AOA measurement system, the number of reference points is determined by the MT position with respect to the reference points. When the MT lies between the two reference points. AOA measurements will not be able to provide the exact location of the MT on the line between the two reference points. Hence, more than two reference points are normally needed to improve the location accuracy.

2.2.2 Received Signal Strength

The first RSS-based indoor geolocation system is the RADAR [12]. In RSS-based indoor geolocation, the distance between the RP and MT can be calculated using the measured power and a distance-power relationship. In wideband measurements, the effects of multipath fading are averaged over the spectrum of the signal. For narrowband systems, where we have only one arriving pulse with fluctuating amplitude according to the multipath fading characteristics, we need to average the signal over a longer period to make sure that the multipath fading is averaged out [2]. Many statistical models are available for relating RSS to the distance, developed mainly for telecommunication applications. The common principle behind all statistical models for calculating the RSS in a distance d is given by [2]:

$$RSS_d = 10log_{10}P_r = 10log_{10}P_t - 10\alpha log_{10}d + X \tag{2.1}$$

where P_t is the transmitted power, d is the distance between the transmitter and the receiver, and α is the distance-power gradient of the environment. The random variable X. The path loss model in indoor environment is highly site-specific. For example, the value of power-distance gradient, which is a parameter of path loss model, varies over a wide range between 15-20dB/decade and a value as high as 70dB/decade. Moreover, the shadow fading will further decrease the stability of RSS value. As a result, the distance calculated from RSS is not very reliable. An alternative solution is the ray-tracing algorithms, which can provide much more reliable RSS values by using the layout of the building [2]. However, the drawback of ray-tracing algorithms is the computational complexity and the labor cost incurred in getting the fine grained building floor plan as well as information on construction materials.

2.2.3 Time of Arrival

The TOA-based system measure distance based on an estimate of signal propagation delay between a transmitter and a receiver since in free space or air, radio signals travel at the constant speed of light. The TOA can be measured by either measuring the phase of received narrowband carrier signal or directly measuring the arrival time of a wideband narrow pulse [1]. The important parameters for TOA-based localization system is the TOA of the direct line of sight (DLOS) path since it is the direct representation of the physical distance between the transmitter and receiver. An example of the indoor multipath and the geolocation specific parameters is shown in Fig 2.3.

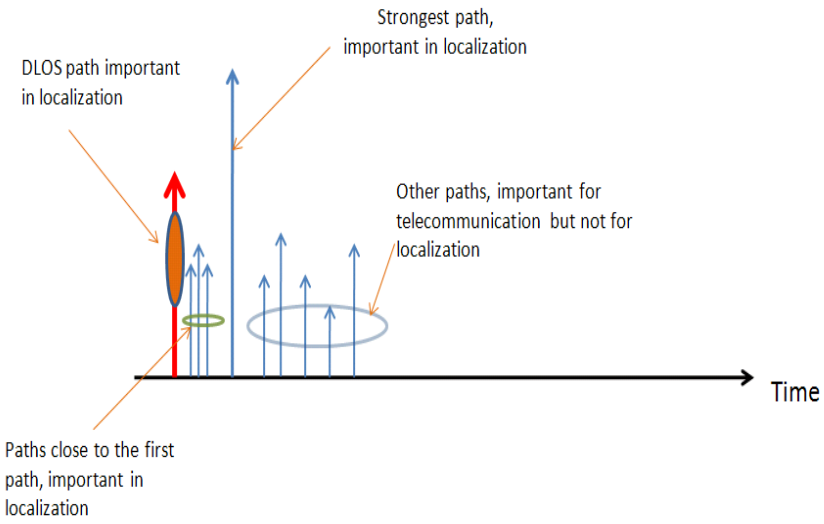

Figure 2.3: Multipath profile and important paths for geolocation [1]

Using the narrowband ranging technique, the phase of a received carrier signal, ϕ, and the TOA of the signal, τ, are related by $\tau = \phi/\omega_c$, where ω_c is the carrier frequency in radians. In outdoor scenario applications such as GPS, the DLOS path always exists, and accurate measurement of the carrier phase is possible. But in indoor environments,

the severe multipath environment causes huge measurement errors, sometimes larger than the actual distance between the transmitter and receiver. Therefore, the conclusion is that the phase-based distance measurement using narrowband carrier signal is not a suitable solution for indoor geolocation.

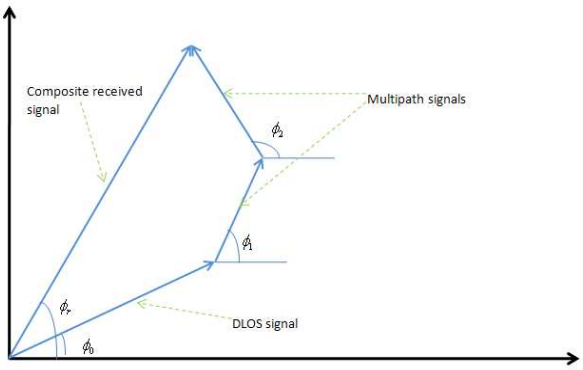

Figure 2.4: Phasor diagram for narrowband signaling on a multipath channel [2]

Another widely used technique is the wideband signal approach where the direct sequence spread spectrum (DSSS) method is the most commonly used form, as this technique performs better than competing systems at suppressing interference [13]. In such a system a known pseudo-noise (PN) signal, which is modulated using a modulation technique (such as BPSK, QPSK, etc), is multiplied by the carrier signal, which is thus replaced by a wide bandwidth signal with a spectrum equivalent to that of the noise signal.

Usually, in order to measure the time of arrival of the signal, a sliding correlator or a matched filter is used at the receiver which cross-correlates the received signal with a stored reference PN sequence. The arrival time of the first correlation peak is used as the time measurement.

Due to the scarcity of the available bandwidth in practice, DSSS ranging systems may not be able to provide adequate accuracy. On the other hand, it is always desirable to

achieve higher ranging accuracy using the same bandwidth. Inspired by high resolution spectrum estimation techniques, a number of researchers have studied super-resolution techniques for time-domain analysis [14].

Finally, the most recent accurate and promising technique is the UWB approach. As the bandwidth of UWB systems is usually several GHz, the ranging accuracy is of the order of centimeter. This fact can be determined from the relationship:

$$d = \frac{c}{BW} \tag{2.2}$$

where d denotes the absolute resolution, and BW is the bandwidth of the signal. The large bandwidth of UWB systems enables them to resolve multiple paths and combat multipath fading and interference. However, such systems have a limited range and building penetration, due to the high attenuation associated with the high-frequency content of the signal. From our measurement experience, the coverage range of UWB signal for an obstructed line of sight (0LOS) scenario is only about 16 meter. The actual deployment of the UWB systems in the US is subject to FCC approval. The main concern of the FCC is the interference of the UWB devices to, among other licensed services such as GPS systems operating in the 1.5GHz frequency band. A significant amount of research work is underway to assess the effect of the UWB interference on the GPS receivers.

2.3 TOA and Channel Profile in indoor areas

As the MT travels in an indoor environment, the multipath profile between the transmitter and MT keeps changing. For geolocation applications, we focus on the behavior of the DLOS path. The performance of TOA estimation varies substantially in different environments. Here, we classify the channel profile based on the behavior of DLOS path. The channel profiles were obtained by applying the inverse Chirp-Z transform to the frequency

domain measurement followed by a Hanning window.

The measurement is classified according to the availability and the strength of the DLOS path. The factors that affect categorizing the different profiles are receiver sensitivity and system dynamic range. The receiver sensitivity is the noise floor level of the system where any paths below that level are treated as noise because the receiver can not differentiate them from noise. The threshold for picking paths is defined as the ratio of the power of the strongest path to the power of the weakest detectable path in a measured profile. For this categorization, a threshold was used in order to distinguish between a detected direct path (DDP), non-dominant direct path (NDDP) and a undetected direct path (UDP). This threshold was selected based on the larger value of the measured system noise floor (receiver sensitivity) and the side-lobes of the filtering window used (threshold for picking paths). This ensured that the first peak of the channel profile is detected correctly. From these multipath conditions, DDP is the easiest to detect from the profile as can be seen from Fig 2.5.

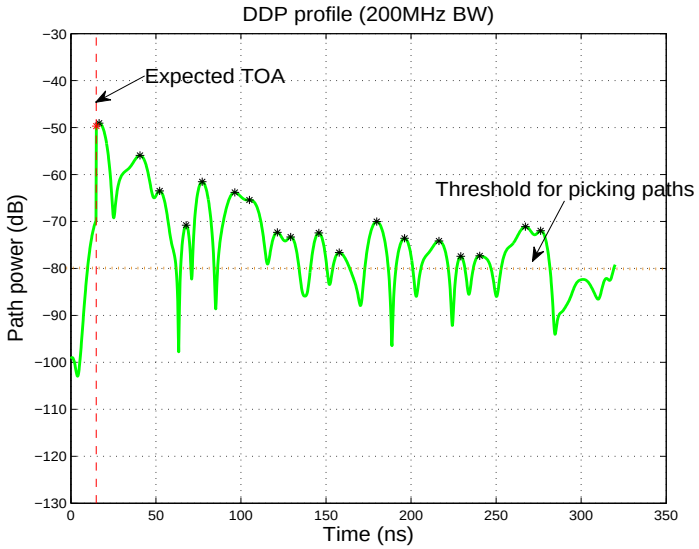

Figure 2.5: DDP measured channel profile at 200MHz bandwidth

Because it has a distinct strong first path, this category has an advantage in TOA

estimation accuracy.

When the first detected path becomes weaker but remains above the threshold, the profile is categorized as NDDP, which is shown in Fig 2.6. For this case, the inaccuracy of TOA estimation can be mitigated significantly by using a more complex RAKE receiver to resolve the multipath and intelligently detect the TOA of the DLOS path.

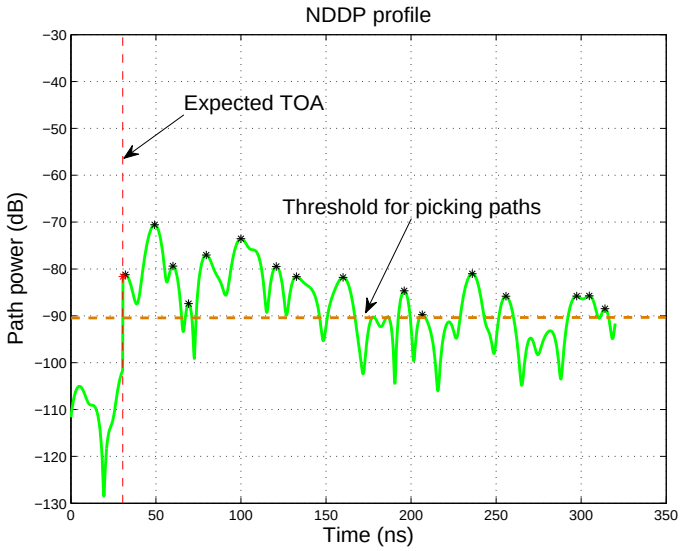

Figure 2.6: NDDP measured channel profile at 200MHz bandwidth

For the UDP profile, which is shown in Fig 2.7, substantial error in TOA estimation can occur due to the loss of DLOS path. The power of the first path is below the path detection threshold and another path which is not the representation of physical distance between the transmitter and receiver is mistakenly interpreted as the DLOS path. This causes significant error in indoor positioning applications. In this unfavorable situation, neither GPS nor a RAKE receiver can accurately detect the TOA. If practical considerations regarding the dynamic range of the system are neglected, then there are essentially two categories: DDP and NDDP. However, in reality, the implemented receiver will have limitations such as sensitivity and dynamic range and this will create situations where the DLOS path can't be detected. The existence of these UDP conditions and how they affect

the ranging accuracy are discussed in [8, 9]. Since the UDP condition brings most of the troubles to indoor geolocation applications when compared to other conditions, identification of UDP profile and mitigating the ranging errors in UDP condition are crucial to positioning applications. In [15], the author proposed the method of using a binary hypothesis test on multipath parameters such as received power of the first path and RMS delay spread to identify UDP conditions, and from our measurement results, we found that the ratio between the five strongest paths' power and the total received signal power is also a feasible metric to differentiate UDP condition from other conditions [16]. Normally, in DDP and NDDP condition, the DLOS path and a few strongest path contribute a significant portion of the received power. However, in UDP condition, they are not the dominant portion of received signal power. After UDP identification, the next step for

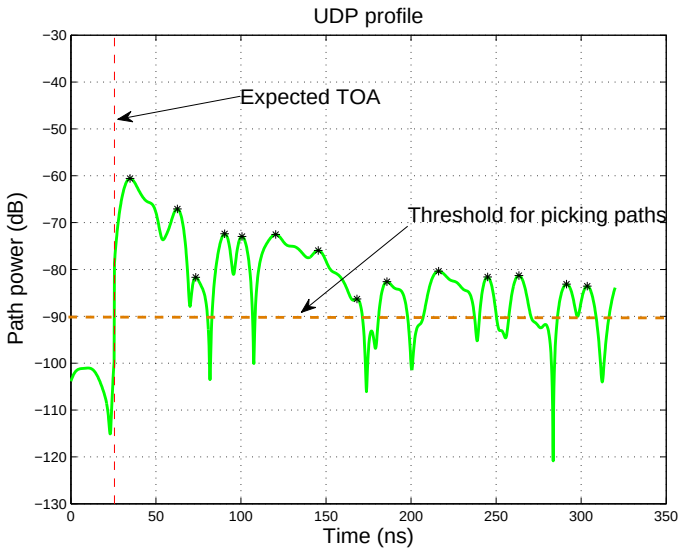

Figure 2.7: UDP measured channel profile at 200MHz bandwidth

accurate indoor positioning would be mitigating the errors caused by UDP influence. The measurement accuracy in UDP conditions can be improved in some cases by exploiting the geolocation information contained in the indirect path measurements, as described in [7], or exploiting multipath signals by using them as additional measurements within a

nonlinear filter [10]. An effective solution would be to exploit other multipath components to aid in the localization by using time difference of arrival (TDOA) of consecutive locations on the receiver's pathway, given that a specific path can be tracked using AOA information.

Chapter 3

UWB Measurement Campaign

In the previous chapters, we have introduced the concept of dynamic channel measurement, which is a challenging task due to the measurement system limitation. In the early days, all wide band measurements were aimed at telecommunication applications, where the interests are mainly around the coverage and rms delay spread analysis, which is directly related to the achievable throughput. The main objective of the indoor channel measurements is to establish a realistic foundation for the evaluation of indoor channel models. Measurements targeted for indoor geolocation application have been carried out in Center for Wireless information Networks (CWINS) since 1998 [17, 18, 19]. These measurement campaigns, however, did not focus on the dynamic behavior since the data sets are all collected at separated points at least 1 meter apart from each other. They were mainly conducted to study the distance measurement error behavior for different environments such as LOS environment, OLOS environment and UDP environment. For the purpose of our research, we developed a new measurement system which is suitable for dynamic channel measurement. Dynamic sounding is much more challenging than traditional static measurement, since it requires consecutive measurements during the movement of the MT (receiver), and the step between two consecutive measurements should

be kept the same for all the measurement locations, which requires accurate control of the MT's motion. Moreover, since the step size in dynamic measurement is much smaller than in static measurement, a manual dynamic measurement campaign can be extremely time consuming and the measured database huge. For example, our first measurement scenario is the loop around the CWINS lab. With the measurement step size of 5cm, we took measurements at 931 different locations to traverse the 46.55 meter distance around the loop.

The measurement campaign which we will discuss in detail in this chapter is an effort to study the dynamic behavior of a multipath channel and the influence of bandwidth, threshold for picking paths and UDP occurrence on multipath parameters pertinent to indoor geolocation. The measurement campaign is composed of two experimental steps. Step 1 is designed to study the effect of bandwidth, threshold for picking paths, and UDP occurrence on multipath parameters. The transmitter location was fixed and the receiver moved around a loop which contains different propagation conditions. Step 2 is to study the distance effect on multipath parameters and compare the influence of micro-metal and macro-metal obstructions on multipath parameters. In this chapter, we first describe the measurement system and then explain the procedure for post-processing the data. Finally, the measurement scenario is outlined.

Section 3.1 outlines the measurement scenario and explains the reason for selecting these scenarios. Section 3.2 provides a detailed description of the measurement system used to collect the data samples and the data post-processing technology. Section 3.3 presents the preliminary measurement results and proposes a UDP detection technology.

3.1 Measurement Scenario

The campaign of measurement was conducted on the third floor of Atwater Kent(AK) Labratories at Worcester Polytechnic Institute(WPI). The AK building was built in 1906 and underwent two major remodelings and additions in 1934 and 1981. Therefore, in some areas within the building, there is more than one exterior-type wall. The exterior walls of this building are heavy brick, the interior walls are made of aluminum studs and sheet rock, the floors are made with metallic beams, the doors and windows are metallic, and many other metallic objects are spread over various laboratory areas. The excessive number of metallic objects and heavy and multiple external walls makes this building a very harsh environment for radio propagation. As a result, this environment is suitable for the indoor geolocation experiment since the DLOS path will be attenuated seriously in most locations. The measurement campaign was conducted on the third floor of AK building. The first step of the campaign procedure is to select the location of measurement points.

The main purpose of the first set of measurements is to study the effect of bandwidth, threshold for picking paths and UDP occurrence on multipath parameters. We used the loop around AK 320 (CWINS lab) as the measurement site.

Fig 3.1 shows the measurement site plan and the measured points. The transmitter antenna was fixed at a position inside the CWINS laboratory as shown in fig 3.1, close to a metallic beam on the upper left side. The receiver antenna was secured on a bar carried by the robot.This loop was designed to include different receiver location classes. We controlled the robot to move 5 cm at a time, each time stopping to take two measurements. The total distance of the loop was 46.55m which corresponds to 931 different receiver locations and $931 \times 2 = 1862$ bandwidth swept measurements by the VNA. The solid green line part in the loop denotes the DDP conditions in which there is no

blockage between transmitter and receiver or only one wall with window between them. The dashed line part denotes the Shadowed UDP (SUDP) conditions in which the DP between the transmitter and receiver is undetectable due to metallic obstruction. The blue line part denotes the Natural UDP (NUDP) conditions in which several walls along with long distance between transmitter and receiver cause the DP to drop below the threshold for picking paths, making it undetectable.

In other words, prior to conducting the measurement, it was desirable to see what happens to the multipath parameters as the receiver moves between DDP, SUDP and NUDP conditions. Would the measured channel profile change from DDP to SUDP and NUDP as the power of the first path weakens? Would the number of MPCs increase at UDP locations? Would the path become less persistent in UDP locations? The answers to these questions can provide insight into how the channel behaves dynamically. In radio propagation, it is well known that metallic objects reflect most of the propagating wave and weaken the transmitted signal. Hence, it would be interesting to see whether or not the metallic chamber, metallic beam, and metallic objects would produce UDP conditions or not.

The main purpose of the second set of measurements is to relate the effect of distance on multipath parameters and provide comparison for the later scenarios with similar receiver route but different transmitter location producing different propagation condition between the receiver and transmitter. We used the corridor on the third floor of AK laboratory as the route of the receiver. The transmitter was fixed on a point in the corridor, and the receiver moved smoothly from the transmitter with a measurement step size 0.1m as shown in Fig 3.2. The distance range of this scenario is 1 to 30m, because there is no blockage between the transmitter and receiver, as well as possibly waveguide effect of the corridor, making the UWB signal covers this range.

The purpose of the third set of measurements is to study the effect of micro-metal

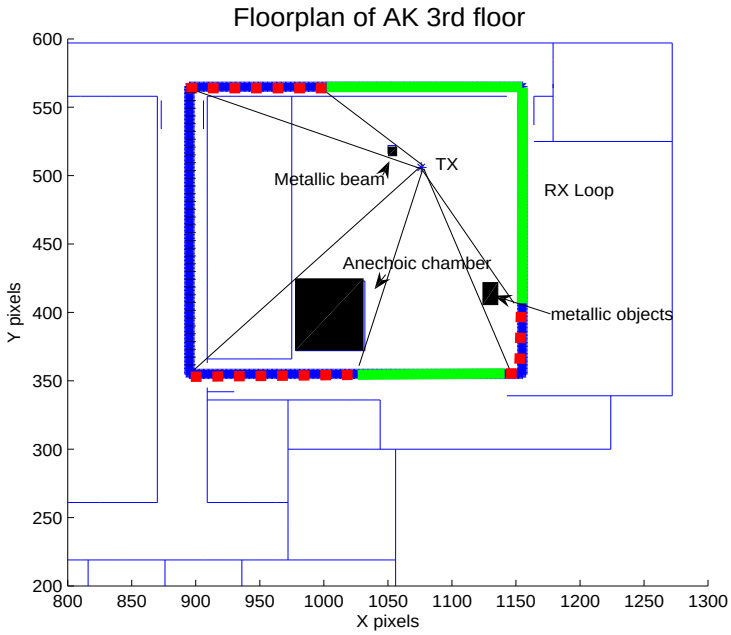

Figure 3.1: Measurement scenario 1 at 3rd floor of AK laboratory

objects blockage on multipath parameters and compare this result with that of the LOS measurements. We used the same receiver route but moved the transmitter inside the CWINS lab to a location that is the symmetric point of the transmitter location used for scenario 2 behind the wall. The distance range of this scenario is 1 to 16m, corresponding to 161 different measurement locations. Because of the attenuation caused by micro-metal objects and wall, the UWB signal lost its coverage beyond the distance of 16m.

The purpose of the fourth set of measurements is to analyze the effect on macro-metal objects blockage (here referring to the anechoic chamber) on multipath parameters and compare this result with the results of the LOS measurements and OLOS measurements, we define this scenario the UDP scenario. Since we intended to have the anechoic chamber blockage all the time for this scenario, the route of the receiver is slightly different from the LOS scenario and the OLOS scenario. However, we again moved the receiver from the proximity of the transmitter to locations further apart from the transmitter. The

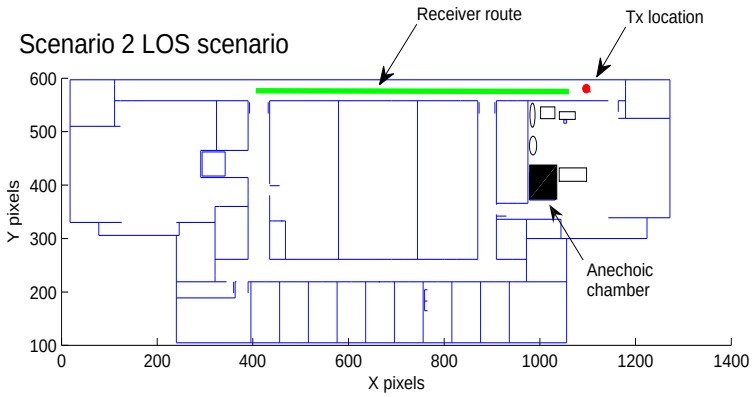

Figure 3.2: Measurement scenario 2 ,LOS senario

signal coverage in UDP condition is only around 10 meters.

3.2 Measurement Setup and Post Processing Technology

With frequency domain sounders, the RF signal is generated and received using a vector network analyzer (VNA), which makes the measurement setup quite simple. The sounding signal is a set of narrow-band sinusoids that are swept across the band of interest. The maximum sweep time is limited by the channel coherence time. If the sweep time is longer than than the channel coherence time, the channel may change during the sweep. Therefore, in order to prevent the channel from fast variation, we conducted measurements when there were fewer people or other scatterers in the area.

The performance of the frequency domain sounding is also limited by the maximum

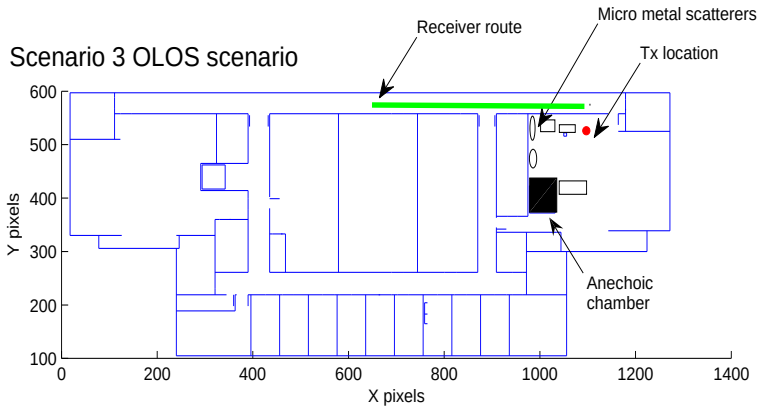

Figure 3.3: Measurement scenario 3 ,OLOS senario

channel delay. the upper bound for the detectable delay τ_{max} can be defined by the number of frequency points used per sweep and the bandwidth B (frequency span to be swept), as given by:

$$\tau_{max} = (N_{smp} - 1)/B \tag{3.1}$$

where N_{smp} is the number of sampled frequency points. The main component of our measurement system is a 40GHz HP-8363B network analyzer. Fig 3.5shows the measurement system and its components.

The measurement system is composed of the network analyzer, two UWB antennas, a power amplifier at the transmitter end, a low noise amplifier at the receiver end, and the 'ER1' robot system. The network analyzer is controlled by a laptop computer through wireless network, where a program is used to select the desired parameters of the measurement scenario. The laptop initializes the network analyzer preceding each measure-

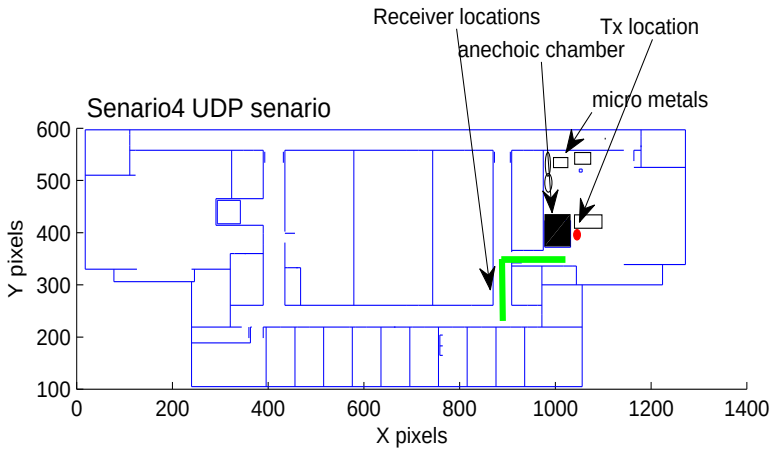

Figure 3.4: Measurement scenario 3 ,UDP senario

ment, where start and stop sweeping frequencies are selected along with the number of desired samples and the data collected at the completion of each measurement. The transmitted signal passes through a 30dB amplifier before going to the channel. The receiver attenuates and pre-amplifies the incoming signal with a low noise amplifier (LNA) before passing it to the network analyzer. For the analysis in the thesis, The VNA was used to sweep the frequency spectrum of 3-8GHz with 1.5625MHz sampling interval, yielding 3200 frequency domain measurement samples at each location. The transmitter and receiver are a pair of disc-cone UWB antennas connected to the VNA by low-loss, high quality doubly shielded cables.

Both the transmitter and receiver are fixed at a height of 1.3m during the measurement. The overall measurement system has a noise level of -90dB. A power amplifier at the transmitter side and a low noise amplifier (LNA) at the receiver side are used to supply

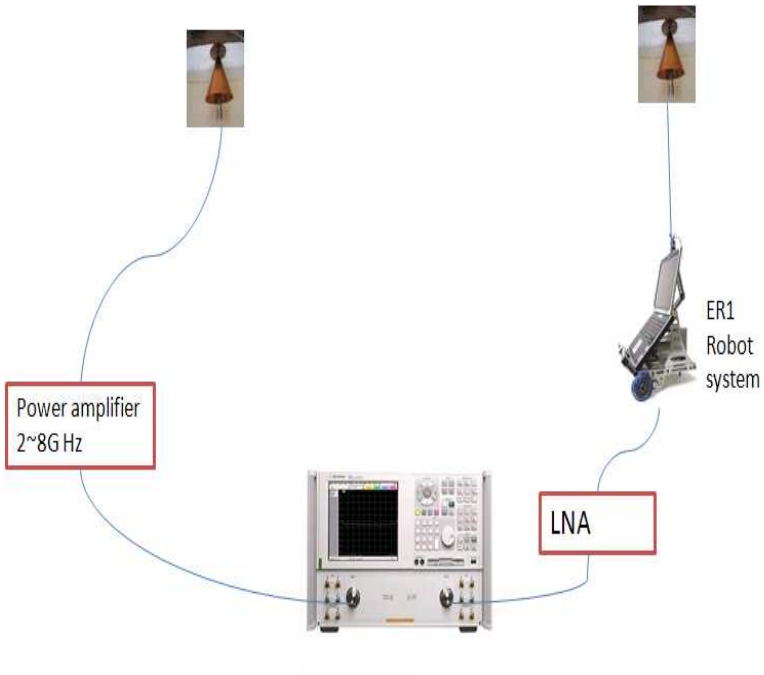

Figure 3.5: Frequency dynamic measurement system

Figure 3.6: Ultrawide band cone antennas

the experimental system with enough power to propagate as far as 30 meters in LOS scenario.

System calibration involves connecting the cables back-to-back without the antennas.

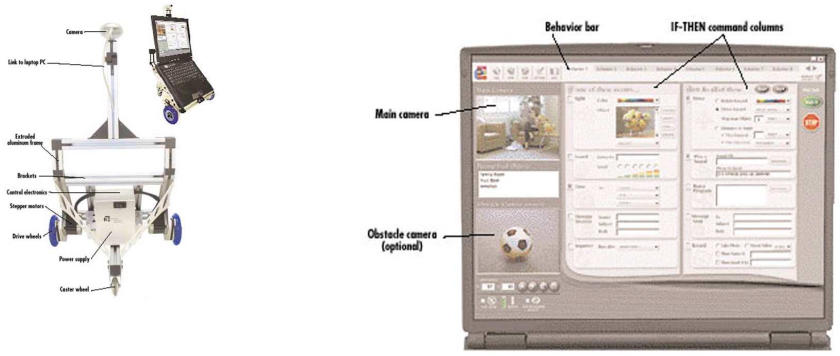

(a) architecture of Er1 robot system (b) User interface

Figure 3.7: ER1 robot system

This removes the delay and attenuation of the cables. The second step of system calibration is connecting the antennas and performing a 1-meter LOS free space calibration. This removes the delay and gain caused by the antennas. As a result, the CIR after calibration in this case would be a single path occurring at 0ns.

The dynamic measurements were conducted by enrolling the 'ER1' robot system to carry our receiver antenna during the measurement campaign [20]. We used software to control the robot moving with a step size of 5cm (for the first scenario), 10cm (for the other scenarios), then stopping to take two measurements. The 'ER1' robot system has three wheels, one of which is implemented with directional sensor, there's also a camera on top of the robot system, hence we can make sure that the robot was moving along a straight path during the measurement. The speed and step size of movement can also be precisely controlled from the user end.

The measured frequency response data was windowed with a Hanning window in order to reduce the noise sidelobes. Although some other window functions such as Kaiser window provides higher dynamic range, the Hanning window is selected for its much faster decaying sidelobes which significantly reduces the interfering effect of strong

multipath components in peak detection. For the analysis in this thesis, 5GHz down to 50MHz bandwidth chunks were parsed out of the measured frequency domain data with a center frequency of 5.5GHz. After obtaining frequency domain measurements, we used an inverse chirp Z transform to obtain channel impulse response (CIR) [19]. Specifically, 50MHz of bandwidth provides time-domain resolution in the order of $\triangle t_{50MHz} = 20ns \Longrightarrow 6m(accuracy)$, while 5GHz provides$\triangle t_{5GHz} = 0.2ns \Longrightarrow 0.06m(accuracy)$. The desired parameters such as amplitudes and delay of each path are detected from the time-domain channel profile using a peak detection algorithm.

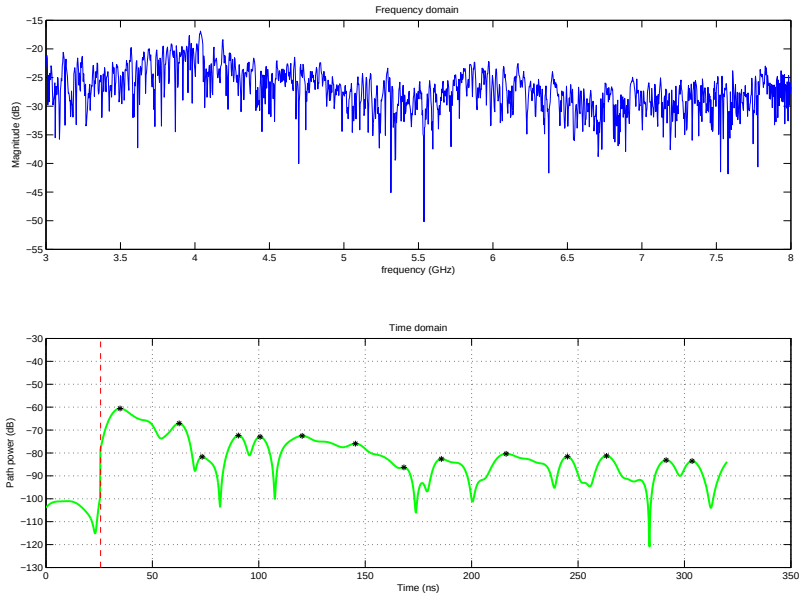

Figure 3.8: Sample frequency domain and time domain channel profile

Figure 3.8 shows a sample frequency domain measurement and its corresponding time-domain profile. Notice the frequency selective fading in the frequency domain and the time-domain profile illustrating multipath components arriving at different delays.

3.3 Preliminary Results and a UDP Identification Technology

In this section, we present some measurement results in order to illustrate the different channel behavior in different scenarios. Fig 3.9 shows there are more MPCs at UDP loca-

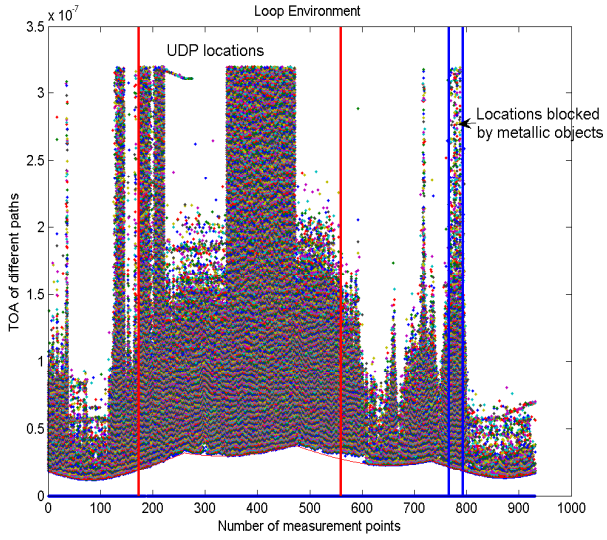

Figure 3.9: TOA of different paths for the Loop scenario

tions than the number of MPCs at DDP locations for the loop scenario. One explanation would be that the power of the strongest path in UDP conditions is weaker compared to that in DDP conditions, bringing more MPCs above the threshold for picking paths. Because the distance between transmitter and receiver does not keep increasing, we can't find any relationship between the distance and number of MPCs in this figure.

Figure 3.10 shows that for the LOS condition, the time of arrival (TOA) of the strongest LOS component increases as the robot moves away from the Tx. Also observable in the graph are the higher order reflections. These reflections are caused by the back and forth reflections at the two end of the corridor, which can be shown by comparing their path length to the actual geometric reflected path length. The delay, distance profile shown in

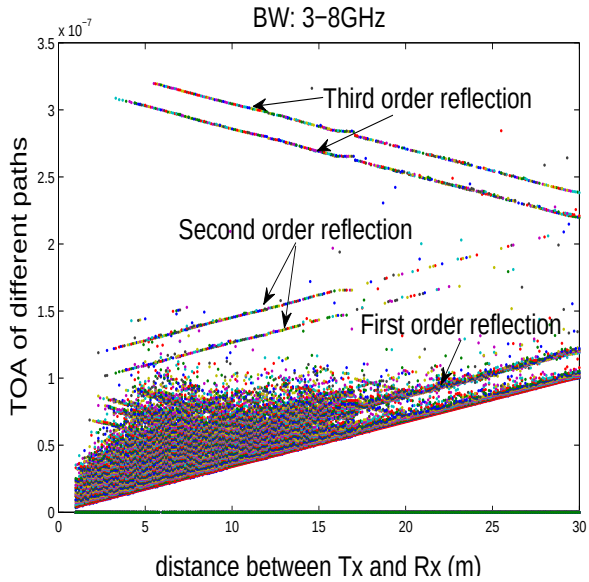

Figure 3.10: TOA of different paths for the LOS scenario

Figure 3.10 further substantiate the following observations: When the Tx is close to the Rx, the number of MPCs is small due to the strong LOS component and the threshold for picking paths (which means we only consider those paths within α dB of the strongest paths as eligible paths). Most MPCs are below the threshold at the beginning. As the Rx moves away from the Tx, more paths will be resolved due to the reduction of the gain of the strongest path. After a certain break point, the number of MPCs will start to decrease due to distance reducing the gain of more paths and decreasing them to below the noise floor threshold.

However, for OLOS condition, due to at least one wall separation, even when the Tx and Rx are at the closest distance, the strongest path between them is much weaker compared to that in LOS condition. Hence, all the resolvable paths above the noise floor will be counted as eligible paths. The cutoff effect of threshold for picking paths is weaker. As the receiver moves away, the number of MPCs will keep decreasing due to more paths becoming weaker and falling below the noise floor. In the end, resolvable paths disappear when the receiver moves beyond the coverage range of the Tx. In our case, this limitation

for OLOS is around 16m.

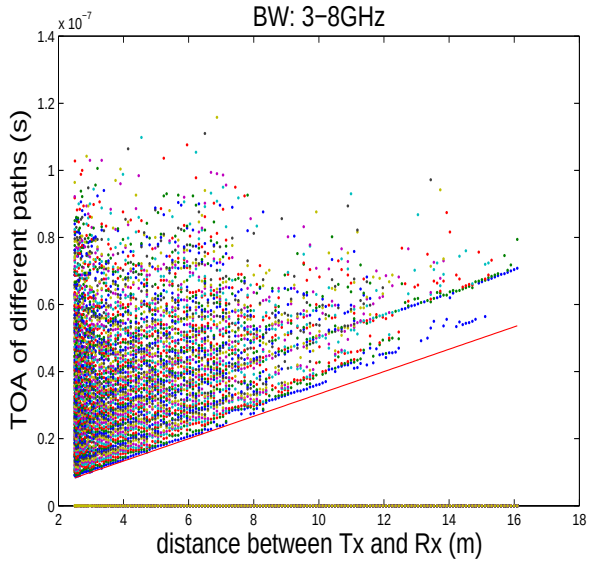

Figure 3.11: TOA of different paths for the OLOS scenario

When there is the metallic chamber between the Tx and Rx, the coverage of the UWB signal is further reduced to around 9m, which is expected because of the very short wavelength and low transmission power of the UWB signal.

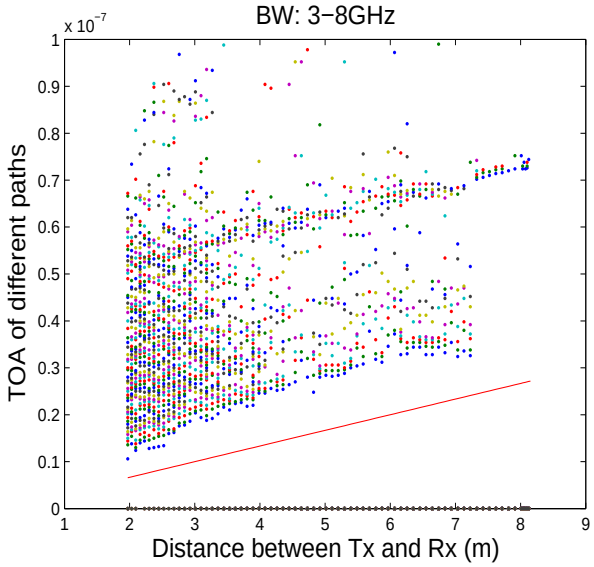

Figure 3.12: TOA of different paths for the UDP scenario

As the UDP occurrence has a strong effect on multipath parameters, and our measurement scenario 1, the loop scenario, contained mixed conditions including DDP, SUDP and NUDP. After pre-examining our measurement results from scenario 1, we found a methodology to distinguish between DDP and UDP conditions by investigating the ratio between the sum of the power of the 5 strongest paths to the total received signal power.This idea comes from [21] in which the authors state that: the strongest return does not carry significant power with respect to the other returns in None-Line-of-Sight (NLOS) locations. So we investigated the ratio of the sum of the 5 strongest paths' powers to the total received power: $\varepsilon = \frac{P_{5strongestpaths}}{P_{total}}$. Those locations with ε larger than a certain threshold ζ, are considered to be DDP locations; whereas the locations with ε smaller than ζ are considered to be UDP locations.

We can denote this as:

$$\begin{cases} H_0: \quad \varepsilon \geq \zeta, \quad DDP|d = c\tau_1 \\ \\ H_1: \quad \varepsilon < \zeta, \quad UDP|d < c\tau_1 \end{cases} \tag{3.2}$$

Where τ_1 is the TOA of the FDP. For our measurement scenario, we find $\zeta = 0.2$ is a suitable value to identify the UDP conditions. The identification result is shown in Fig 3.13(a).

Compared with Fig 2, results match well with the physical environment. We also examined another established UDP identification method [22] which basically uses the influence of UDP occurrence on τ_{rms} to identify it. The author in [22] observed that the distance influences the delay spread of UWB environments as :

$$\tau_{rms}(d) = 10d^{0}.3nsec \tag{3.3}$$

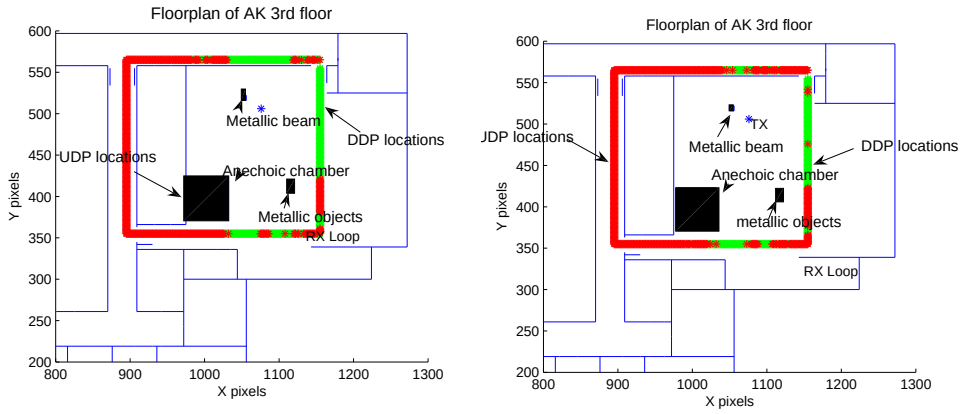

(a) Power ratio method (b) τ_{rms} method

Figure 3.13: Power ratio method and τ_{rms} method for UDP identification

In addition, the following dependency of the threshold for picking paths δ_{ds} can be derived:

$$\tau_{rms}(\delta_{ds}, d) = (-4.13\delta_{ds}^{-0.75} + 1.44)\tau_{RMS}^2 0dB(d) \tag{3.4}$$

Where $\tau_{RMS}^2 0dB(d)$ is the RMS delay spread with a threshold for picking paths of 20dB. Therefore, the combined threshold used in this method to distinguish DDP and UDP condition is:

$$\Theta_{ds,n} = \begin{cases} \tau_{RMS}(\delta_{ds}, \hat{d}) + \tau_{min} & \theta_{ds} > \tau min \\ \\ \Theta_{ds,n-1} & \theta_{ds} \leq \tau min \end{cases} \tag{3.5}$$

Using this method, the identification result is shown in Fig 3.13(b).

Comparing Fig 3.1 with Fig 3.13(a) and 3.13(b), our ratio method provides more consistent result, since the τ_{rms} method marks measurement locations at the upper right part and lower right part of the loop as UDP locations which are actually DDP locations.

Chapter 4

Sensitivity Analysis for Direct Path Estimation

For TOA based localization system, the biggest challenge is to estimate the TOA of the direct path (DP) accurately. NLOS and UDP are critical conditions that substantially degrade the accuracy of the estimation and in turn lower the performance of the whole positioning system. One of the ways to fight against these effects is to utilize the other indirect paths when the DP is blocked. However, there is another source of TOA estimation error, which can only be mitigated by increasing the system bandwidth or employing super-resolution algorithms [14], that is the multipath error. It is well known that increasing system bandwidth enhances the time-domain resolution and as a result improve the accuracy of TOA estimation. Another way to improve the time domain resolution is to implement advanced signal processing techniques called frequency-domain super-resolution TOA estimation technique designed by applying the super-resolution spectrum estimation techniques to the frequency-domain channel response, which can be modeled as a harmonic signal model. Different TOA estimation algorithms provide different time domain resolutions and create different levels of difficulties in implementation. For DP

based method We compare their performances in different environments and with different bandwidth availability by looking at the parameter DME:

$$DME = (TOA_{FDP} - TOA_{DLOS}) \cdot C \tag{4.1}$$

where TOA_{FDP} is the TOA estimation of the first detected path (FDP) and TOA_{DLOS} is the real TOA of the direct line of sight (DLOS) path, and C is the speed of light. Usually, we use the FDP of the channel profile, received above the detection threshold, to estimate the TOA of the DLOS path, and therefore, determine the distance between a transmitter and a receiver. As explained in [2], the wireless signal power in free space decreases with the square of distance and for FDP, the power distance gradient is even higher. Hence, the performance of different TOA estimation algorithms is very sensitive to distance variation. When the receiver is moved beyond a certain range to the transmitter, the FDP can not be correctly picked by TOA estimation algorithms.

4.1 TOA Estimation Algorithms

In the narrowband ranging technique, the phase difference between received and transmitted carrier signals is used to measure the distance between two points. The TOA of signal τ , and phase ϕ, are related by $\tau = \phi/\omega_c$, where ω_c is the carrier frequency in radians. However, unlike the situation for outdoor applications such as GPS, the severe multipath condition of the indoor geolocation environment causes substantial errors in phase measurements. Hence, phase-based distance measurement using a narrowband carrier signal can't provide an accurate estimate of distance in a heavy multipath environment.

Since the narrowband ranging technique is not suitable for indoor positioning applications, naturally, we would seek solutions using wideband signals. The simplest TOA estimation algorithm is directly using the Inverse Fourier Transform (IFT) after window-

ing the frequency domain measurement data. For this application,a Hanning window is used to avoid leakage and false peaks by reducing the side-lobes of the time domain response at the cost in reduced resolution. When the time domain response over part of the time period is desired, the chirp-z transform (CZT) is preferred, providing flexibility in the choice of time domain parameters at a cost in longer computational times as compared with the IFT. The peak detection algorithm then selects the peak that is closest to the real TOA.

Figure 4.1: Block diagram of an IFT TOA estimation algorithm

Another wideband signal that has been widely used in ranging system is the direct-sequence spread-spectrum (DSSS) signal. In such a system, a signal coded by a known pseudo-noise (PN) sequence is transmitted. Then a receiver cross-correlates the received signal with a locally generated PN sequence using a sliding correlator or a matched filter [23, 2]. In order to simulate DSSS signal-based cross-correlation technique, the frequency response of a raised-cosine pulse with roll-off factor 0.25 is first applied to the frequency domain response. Then, the resultant frequency response is converted to the time domain using the IFT for TOA estimation. Figure 4.2 shows the process implementing a DSSS estimation algorithm. As mentioned earlier, a peak detection algorithm is used to estimate the TOA of the DLOS path.

One of the hurdles for accurate TOA estimation is the limited bandwidth and its high

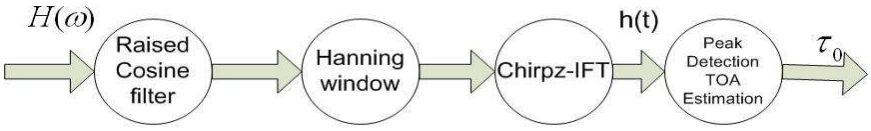

Figure 4.2: Block diagram of DSSS TOA estimation algorithm

price. Meanwhile, it is always desirable to achieve higher ranging accuracy using the same bandwidth. These requirements entail the use of super-resolution techniques for time-domain analysis such as described in [14].

The multipath indoor radio propagation channel is usually modeled as a low-pass equivalent impulse response given by:

$$h(t) = \sum_{k=0}^{L_p-1} \alpha_k \delta(t - \tau_k) \tag{4.2}$$

where L_p is the total number of multipath components, $\alpha_k = |\alpha_k| e^{j\theta_k}$ and τ_k are the complex attenuation and propagation delay of the kth path, respectively. The multipath components are indexed such that the propagation delays τ_k, $0 \leq k \leq L_p - 1$, are in ascending order. Therefore, τ_0 is the TOA of DLOS path and important for accurate ranging. The Fourier transform of (4.2) is the frequency domain channel response:

$$H(f) = \sum_{k=0}^{L_p-1} \alpha_k e^{-j2\pi f \tau_k} \tag{4.3}$$

This model is well known in the spectral estimation field [24]. Consequently, any spectral estimation techniques that are suitable for a harmonic signal model can be applied to the frequency response of multipath indoor radio channel to perform time-domain

analysis. In the reminder of the thesis, the MUSIC algorithm [25] is used to demonstrate the performance of super-resolution TOA estimation algorithm.

The discrete measurement data are obtained by sampling channel frequency response $H(f)$ at L equally spaced frequencies. Considering additive white noise in the measurement process, the sampled discrete frequency-domain channel response is given by

$$x(l) = H(f_l) + \omega(l) = \sum_{k=0}^{L_p-1} \alpha_k e^{-j2\pi(f_0+l\Delta f)\tau_k} + \omega(k) \tag{4.4}$$

where $l = 0, 1, ...L-1$ and $\omega(l)$ denotes additive white measurement noise with zero mean and variance σ_ω^2. We can then write this signal model in vector form as

$$\mathbf{x=H+w=Va+w} \tag{4.5}$$

where

$$\begin{aligned}
\mathbf{x} &= [x(0) \quad x(1) \quad ... \quad x(L-1)]^T \\
\mathbf{H} &= [H(f_0) \quad H(f_1) \quad ... \quad H(f_{L-1})]^T \\
\mathbf{w} &= [\mathrm{w(0)} \quad \mathrm{w(1)} \quad ... \quad \mathrm{w(L\text{-}1)}]^T \\
\mathbf{V} &= [\mathrm{v}(\tau_0) \quad \mathrm{v}(\tau_1) \quad ... \quad \mathrm{v}(\tau_{L_p-1})]^T \\
\mathbf{a} &= [\alpha'_0 \quad \alpha'_1 \quad ... \quad \alpha'_{L_p-1}]^T
\end{aligned}$$

and

$$\mathbf{v}(\tau_k) = [1 \; e^{-j2\pi\Delta f\tau_k} \; ... \; e^{-j2\pi(L-1)\Delta f\tau_k}]^T$$

$$\alpha'_k = \alpha_k e^{-j2\pi f_0\tau_k},$$

The MUSIC super-resolution algorithm is based on eigen-decomposition of the auto-correlation matrix of the preceding signal model in (4.5).

$$\mathbf{R_{XX}} = E\{\mathbf{x}\mathbf{x}^H\} = \mathbf{V}\mathbf{A}\mathbf{V}^H + \sigma_w^2\mathbf{I}, \tag{4.6}$$

where $A = E\{aa^H\}$ and superscript H denotes the Hermitian, conjugate transpose, of a matrix. Since the propagation delays τ_k in (4.2) can be reasonably assumed all different, the matrix V has full column rank, which means that the column vectors of V are linearly independent. If the magnitudes α_k is assumed a constant and phase a uniform random variable in $[0, 2\pi]$, the $L_p \times L_p$ covariance matrix A is non-singular. Therefore, from the theory of linear algebra, by assuming $L > L_p$, the rank of the matrix VAV^H is L_p, or from another point of view, the $L - L_p$ smallest eigenvalues of $R_{\mathbf{xx}}$ are all equal to σ_w^2. The eigenvectors corresponding to $L - L_p$ smallest eigenvalues of $R_{\mathbf{xx}}$ are called noise eigenvectors while the eigenvectors corresponding to the L_p largest eigenvalues are called signal eigenvectors. Hence, the L-dimensional subspace that contains the signal vector x is split into two orthogonal subspaces, known as signal subspace and noise subspace, by the signal eigenvectors and noise eigenvectors, respectively [14]. Then the projection matrix of the noise subspace is given by:

$$\mathbf{P}_w = \mathbf{Q}_w(\mathbf{Q}_w^H\mathbf{Q}_w)^{-1}\mathbf{Q}_w^H = \mathbf{Q}_w\mathbf{Q}_w^H \tag{4.7}$$

where $Q_w = [q_{Lp} \quad q_{Lp+1} \quad \dots \quad q_{L-1}]$ and q_k, $L_p \leq k \leq L-1$, are noise eigenvectors. Since the vector $\mathbf{v}(\tau_k)$, $0 \leq k \leq L_p - 1$, must lie in the signal subspace, we have:

$$\mathbf{P}_w\mathbf{v}(\tau_k) = 0, \tag{4.8}$$

From this, the multipath delays τ_k, $0 \leq k \leq L_p - 1$, can be determined by finding the delay values at which the time-domain MUSIC pseudospectrum reaches peak value.

$$\begin{aligned} S_{MUSIC}(\tau) &= \frac{1}{\| \mathbf{P}_w\mathbf{v}(\tau) \|^2} = \frac{1}{\mathbf{v}^H(\tau)P_w^H P_w\mathbf{v}(\tau)} \\ &= \frac{1}{\mathbf{v}^H(\tau)P_w\mathbf{v}(\tau)} = \frac{1}{\| Q_w^H\mathbf{v}(\tau) \|^2} \end{aligned}$$

$$= \frac{1}{\sum_{k=L_p}^{L-1} \mid q_k^H \mathbf{v}(\tau) \mid^2}$$

Up to this point, the theoretical correlation matrix $\mathbf{R_{XX}}$ was used. In practice, the correlation matrix must be estimated from the measured data samples. Figure 4.3 illustrates the function block diagram of super-resolution TOA estimation algorithm.

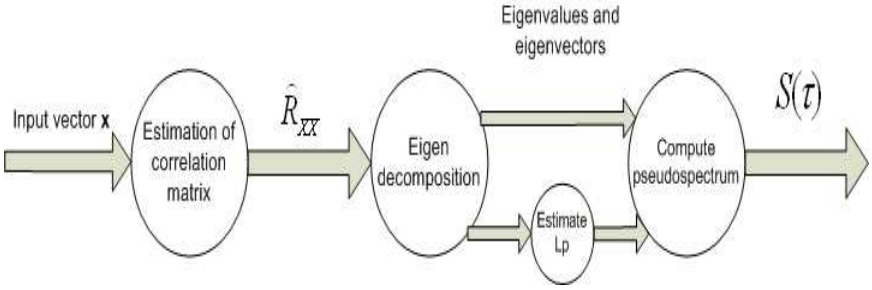

Figure 4.3: Block diagram of Super resolution TOA estimation algorithm

The input data vector, $i.e.$, the estimate of channel frequency response given in (4.5) is first used to estimate the correlation matrix $\mathbf{R_{XX}}$. Then the eigen-decomposition is performed to determine the L_p signal eigenvalues and their corresponding eigenvectors and $L - L_p$ noise eigenvalues and their corresponding eigenvectors. Once the pseudospectrum is obtained, a peak detection algorithm selects the first peak to estimate the TOA of the signal.

If we have P snapshots of the measurement data, the estimate of the correlation matrix is obtained from

$$\hat{\mathbf{R}}_{\mathbf{XX}} = \frac{1}{P} \sum_{k=1}^{P} \mathbf{x}(k)\mathbf{x}(k)^H \tag{4.9}$$

If only one snapshot of the measurement data of length N is available, the data sequence is divided into M consecutive segments of length L and then the correlation matrix is estimated as

$$\hat{\mathbf{R}}_{\mathbf{XX}} = \frac{1}{M}\sum_{k=1}^{M}\mathbf{x}(k)\mathbf{x}(k)^H \tag{4.10}$$

where $M = N - L + 1$ and $x(k) = [x(k) \quad ... \quad x(k+L-1)]^T$

For the super-resolution TOA estimation algorithm, the measurement data vector **x** is obtained by sampling the channel frequency response uniformly over a given frequency band. In order to avoid aliasing in the time domain, similar to the time-domain Nyquist sampling theorem, the frequency-domain sampling interval Δf is determined so as to satisfy the condition $1/\Delta f \geq 2\tau_{max}$, where $\tau_{max} = max(\tau_{L_p-1})$ is the maximum delay of the measured multipath radio propagation channel [14].

One issue that is not fulfilled in practice is the stationary data assumption. Without this assumption, the correlation matrix $\mathbf{R_{XX}}$ is not Hermitian,i.e., conjugate symmetric, and Toeplitz,i.e., having equal elements along all diagonals. The estimate of the correlation matrix can be improved using the following forward-backward correlation matrix (FBCM).

$$\hat{\mathbf{R}}_{\mathbf{XX}}^{(FB)} = \frac{1}{2}(\hat{\mathbf{R}}_{\mathbf{XX}} + J\hat{\mathbf{R}}_{\mathbf{XX}}^{*}J) \tag{4.11}$$

where the superscript $*$ denotes conjugate, superscript FB stands for forward-backward estimation, and J is the $L \times L$ exchange matrix whose components are zero except for ones on the anti-diagonal. This technique is widely used in spectral estimation with the name modified covariance method and in linear least-square signal estimation with the name forward-backward linear prediction (FBLP) [24].

One implicit assumption in the MUSIC method is that the noise eigenvalues are all equal,i.e., $\lambda_k = \sigma_w^2$ for $L_p \leq k \leq L-1$, which means the noise is white. However, when the correlation matrix is estimated from a limited number of data samples in practice, the noise eigenvalues are not equal. A slightly improved version on the MUSIC algo-

rithm, known as the Eigenvector (EV) method, can be used to account for the potentially different noise eigenvalues [14]. The pseudospectrum of the EV algorithm is defined as:

$$\hat{\mathbf{R}}_{EV}(\tau) = \frac{1}{\sum_{k=L_p}^{L-1} \frac{1}{\lambda_k} \mid \mathbf{q}_k^H v(\tau) \mid^2} \tag{4.12}$$

where $\lambda_k, L_p \leq k \leq L-1$, are the noise eigenvalues. The pseudospectrum of each eigenvector is normalized by its corresponding eigenvalue. The EV method equals MUSIC method if the noise eigenvalues are equal. The performance of EV method is less sensitive to inaccurate estimate of the parameter L_p, which is highly desirable in practical implementation [24]. In the following of this thesis, the EV method with FBCM is used to estimate the TOA of the DLOS path.

4.2 Sensitivity of the TOA Estimation Techniques

Usually, we use the FDP of the channel profile, received above the detection threshold, to estimate the TOA of the DLOS path, and therefore, determine the distance between a transmitter and a receiver. As explained in [2], the wireless signal power in free space decreases as the square of distance and for FDP, the power distance gradient is even higher. Hence, the performance of different TOA estimation algorithms is very sensitive to distance variation. When the receiver is moved beyond a certain range to the transmitter, the FDP can not be correctly picked by TOA estimation algorithms.

Another source of TOA estimation error is the limited bandwidth. In a single path environment, the expected result is perfect. However, multipath environment, which always exists, seriously degrades the system performance by shifting the real peak to one that comes from the combination of peaks around DLOS path, resulting in significant TOA estimation error. As the transmission bandwidth of the system increases, the pulses

arriving from different paths become narrower and easier to distinguish. As a result, the estimate of TOA by FDP becomes closer to the expected TOA of the DLOS path, resulting in a smaller distance measurement error.

The influence of threshold selection on the performance of algorithms should not be underestimated either. The threshold can be set based solely on the noise level, which requires noise variance estimation prior to leading edge selection. From our experiment experience, setting the threshold only based on noise level is not satisfactory, since if the FDP is much weaker than the strongest path, some side-lobe peaks which are above the noise floor level and earlier than than the DLOS path would be mistakenly interpreted as the DLOS path. Moreover, different algorithms and windowing function will produce different sidelobe intensity. There are two important quantities related to the detection of MPCs at the receiver. The first is the sensitivity (ϕ) of the receiver, which determines the ability of the receiver to detect signals above noise threshold. Signals below the sensitivity of the receiver would not be detected. The second parameter is the dynamic range (α) of the receiver which determines the ability of the receiver to detect weak signals in the presence of stronger signals [26]. Hence, the eligible MPCs which can be detected should fulfill the following requirements:

$$\frac{|\beta_{SP}|^2}{|\beta_i|^2} \leq \alpha \tag{4.13}$$

$$|\beta_i|^2 > \phi \tag{4.14}$$

where β_{SP} is the path gain of the strongest path and β_i is the path gain of each MPC.

As we mentioned before, in OLOS conditions, when the DLOS path falls below the detection threshold, we have a UDP condition. Under these conditions the FDP in the profile has no relationship to the arrival time of the DLOS path. The system exhibits sub-

stantially high distance measurement errors that can not be eliminated with the increase in the bandwidth of the system. Two classes of unavoidable UDP conditions occur in typical indoor positioning scenario. The first kind of UDP is caused by large metallic object such as a metallic beam, elevator or a chamber blocks the DLOS path between the transmitter and receiver, which is referred as shadowed UDP (SUDP) in literature [27]. The second type of UDP condition occurs in areas of low received power in OLOS environments when, due to the large distance between the transmitter and receiver, the power of the DLOS path falls below the detection threshold level. This category of UDP is called natural UDP (NUDP) in literature [27].

It is interesting to adjust one of these elements and hold others stationary to see to what extent the different TOA estimation algorithms are influenced by that element and what is the optimal condition for the performance of different TOA estimation algorithms. In the following part of this section, the TOA estimation algorithms along with our new dynamic measurement database are used for statistical analysis. The parameter we used to compare the performance of TOA estimation algorithms in different environment is the distance measurement error (DME):

$$\hat{d} = (TOA_{FDP} - TOA_{DLOS}) \cdot C \tag{4.15}$$

where TOA_{FDP} is the TOA estimation of the FDP and TOA_{DLOS} is the real TOA of the DLOS path, C is the speed of light.

4.2.1 Effect of Distance on TOA Estimation

Earlier works in modeling of distance measurement error are based on simulation results and static empirical data with the constraint of limited distance range as well as sparse bandwidth availability. Besides, the DME was calculated only by the simplest IFT algo-

rithm [28]. The author in [28] proposed a DME-distance model for LOS scenario as:

$$\hat{d} = d(1 + G(0, \sigma_L)) \tag{4.16}$$

where $\hat{d}$ is the DME in meters, d is the distance between Tx and Rx and G is a random variable with zero mean and standard deviation σ_L. The effect of distance on DME in OLOS scenario is modeled as:

$$\hat{d} = d + W_G \cdot G(0, \sigma_G) + W_{EXP} Exp(\lambda) \tag{4.17}$$

The DME distribution is considered as a mixture of two functions. The first one, is the normal distribution G with 0 mean and standard deviation σ_G, while the second one is an exponential distribution with mean $\frac{1}{\lambda}$. Furthermore, the DME-distance model for UDP scenario was not stressed in [28].

In this thesis, due to the improvement of the measurement system (we used a UWB disc cone antenna ($3 \sim 10$GHz) instead of traditional patched antenna ($0.8 \sim 1.2$GHz) and robot spatial measurement setup), wider coverage, smaller measurement sample interval, and finer time domain resolution of MPCs are available. We also examined the effect of distance on DME using two other advanced algorithms for performance comparison purpose.

The effect of distance on DME for LOS scenario when bandwidth is 120MHz is shown in Figures 4.4,4.5 and 4.6.

Notice that for the LOS scenario, the DME behaves differently when the Tx-Rx distance is within 25m and beyond 25m. Three different algorithms performs similarly when the Tx is close to Rx, but the CZT method shows some advantage at longer distance. The DLOS path can be correctly detected most of the time when the distance between Tx and Rx is small. For those measurement points, The DME is mainly caused by the limitation

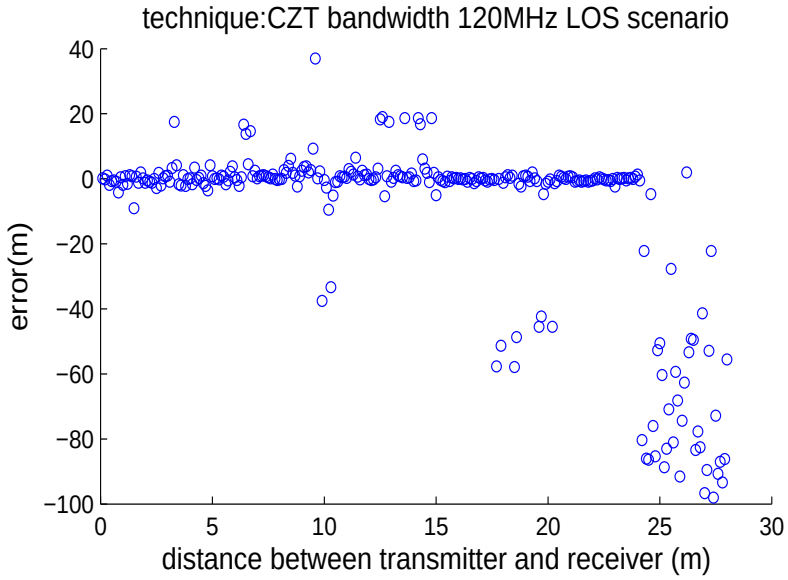

Figure 4.4:

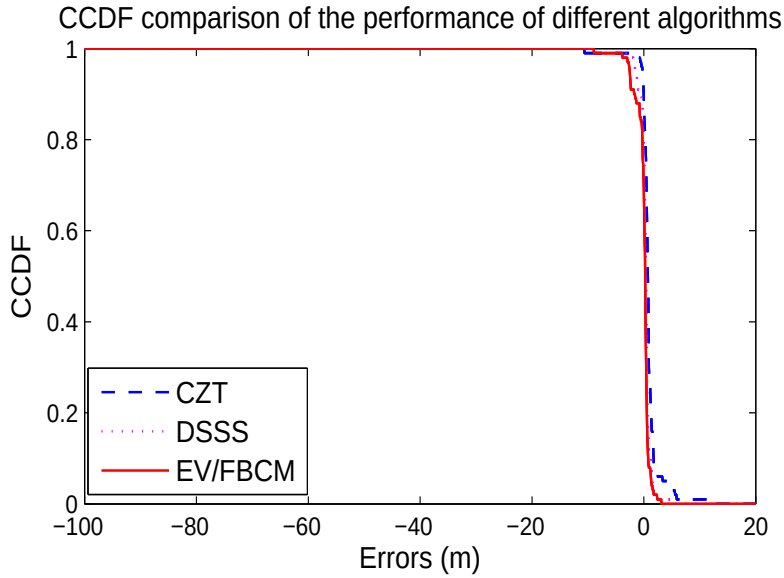

Figure 4.5: LOS scenario $0 \sim 10$m performance comparison of 3 algorithms

of bandwidth and the DME value is quite small as shown in figure 4.7.

However, there are a few measurement points within 25 meter distance showing significant ranging error, which may cased by bandwidth limitation shifting the real DLOS peak to the combined peak with other MPCs. One example channel profile and estimation

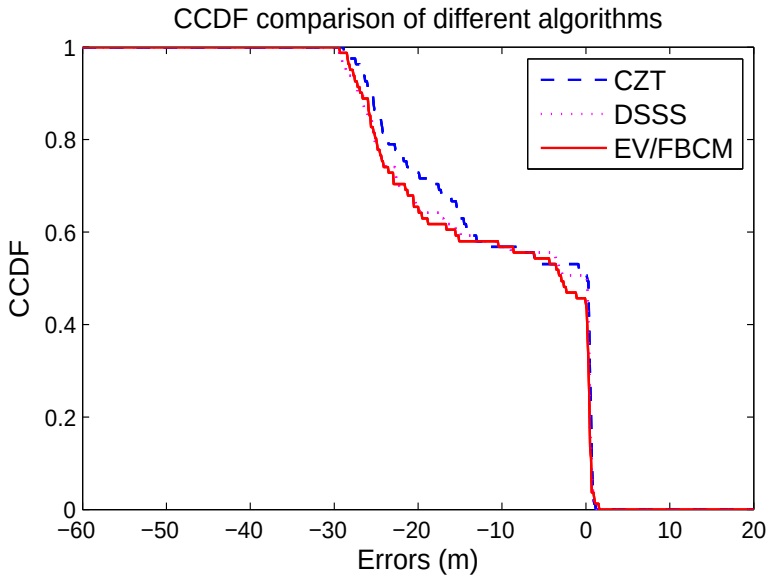

Figure 4.6: LOS scenario $>$ 20m performance comparison of 3 algorithms

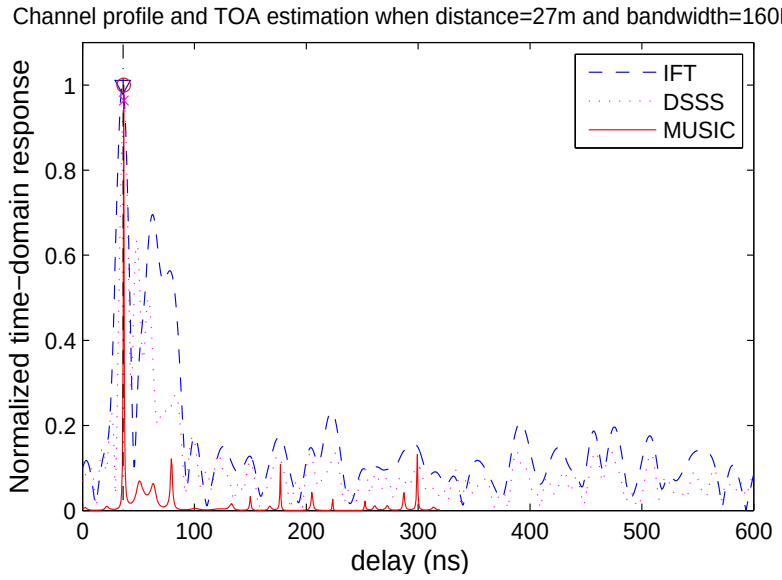

Figure 4.7: Channel profile and TOA estimation results(10m distance)

result is shown in Fig 4.8.

As the distance between Tx and Rx increases, the degradation of TOA estimation is caused by the dynamic range of the receiver which means when the power of the strongest MPC in the channel profile drops to a certain level, the system mistakenly interprets some

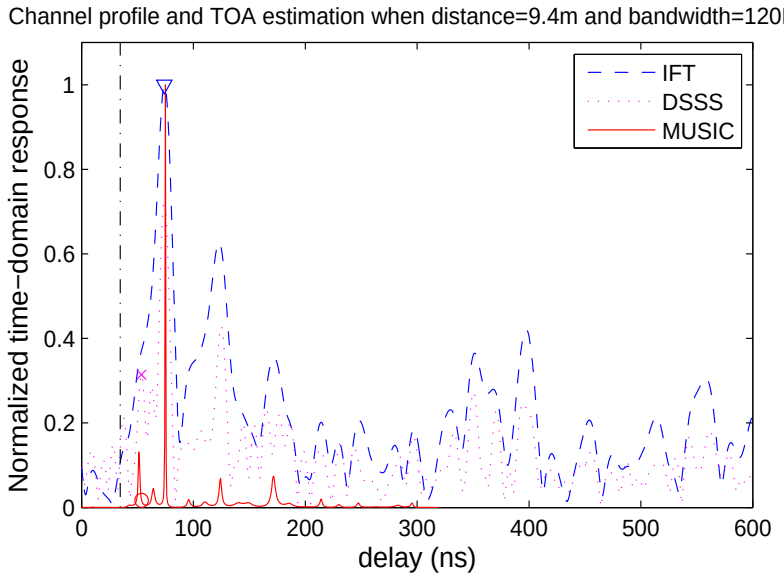

Figure 4.8: Channel profile and TOA estimation results for LOS scenario(9.4m distance)

sidelobe peaks as the DLOS path, which are actually impossible to be real MPCs. It is also interesting to notice that the CZT algorithm, which requires minimum calculation load, outperforms the other two more complex algorithms at longer distance measurement points in the LOS scenario. One example of such a channel profile is illustrated in Fig 4.9. From this figure, it is clear that super-resolution algorithm is more sensitive to sidelobe influence at higher distance value.

The effect of distance on DME for OLOS scenario when bandwidth is 120MHz is shown in Fig 4.10 and 4.11.

Notice that there are both positive and negative DME value at different measurement points. At the beginning, the DME increases with distance, however, the DME moves gradually toward large negative value. From this behavior of DME with distance, we suspect there are two factors influencing the DME and their combined function determines the DME value finally.

Our speculation is confirmed by the following channel profiles.

Figure 4.12 confirms that when the Tx is close to the Rx, the DME is mostly intro-

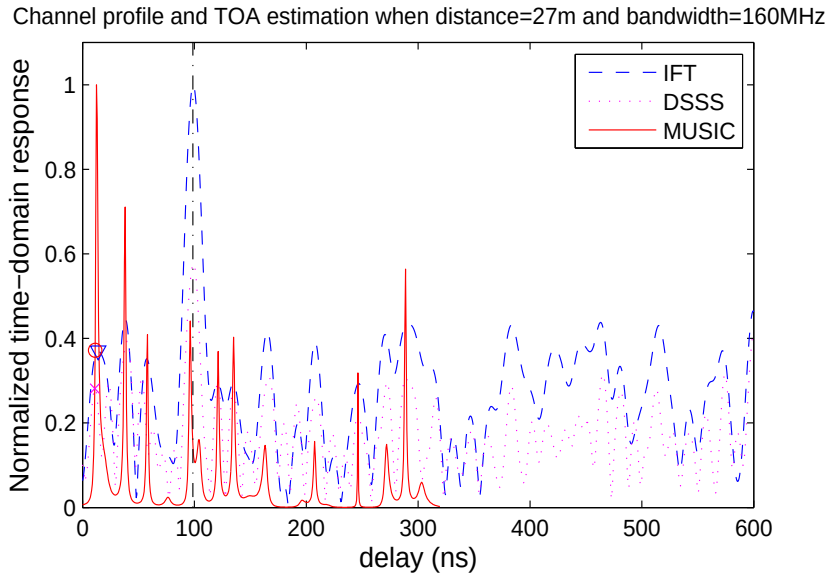

Figure 4.9: Channel profile and TOA estimation results for LOS scenario(27m distance)

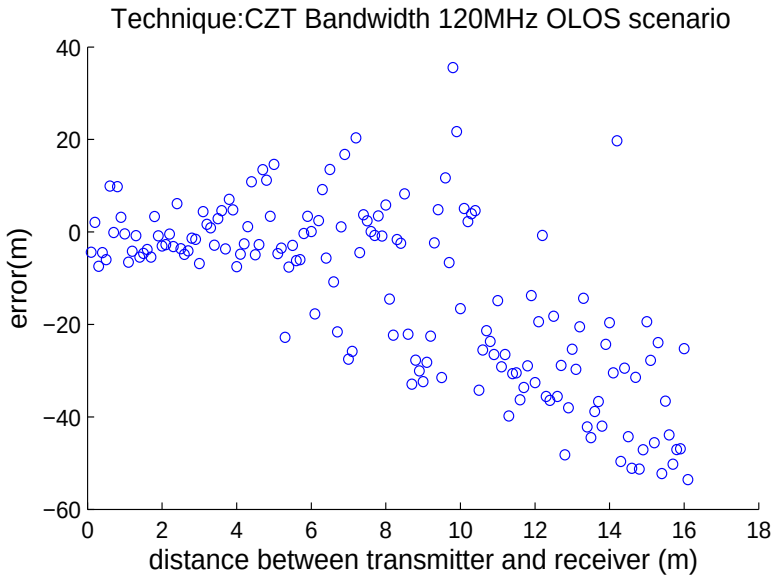

Figure 4.10:

duced by the MPCs' clutter and lack of bandwidth. The MPCs' clutter is caused by the reflections and transmissions in OLOS scenario, making the MPCs arriving at the receiver in clutters. Hence, if the available bandwidth is not wide enough to resolve MPCs inside each clutter, the FDP would be shifted from the DLOS path to a later arrived combined

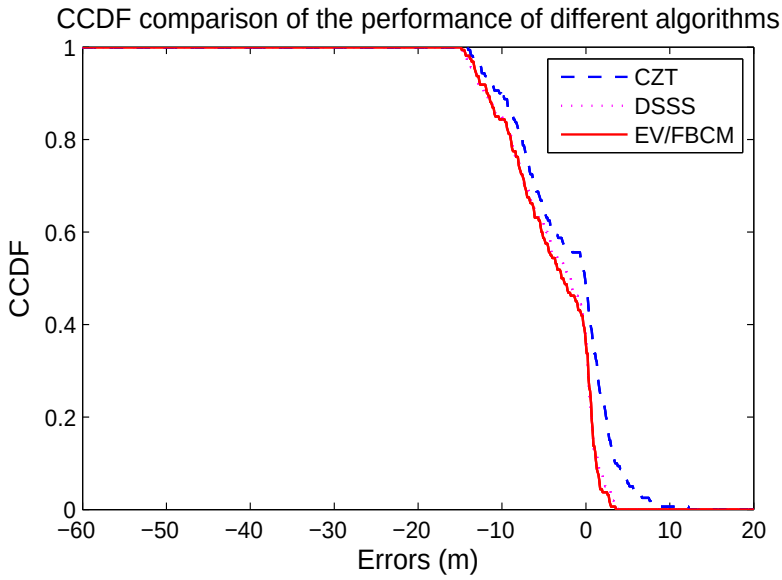

Figure 4.11: OLOS scenario performance comparison of 3 algorithms

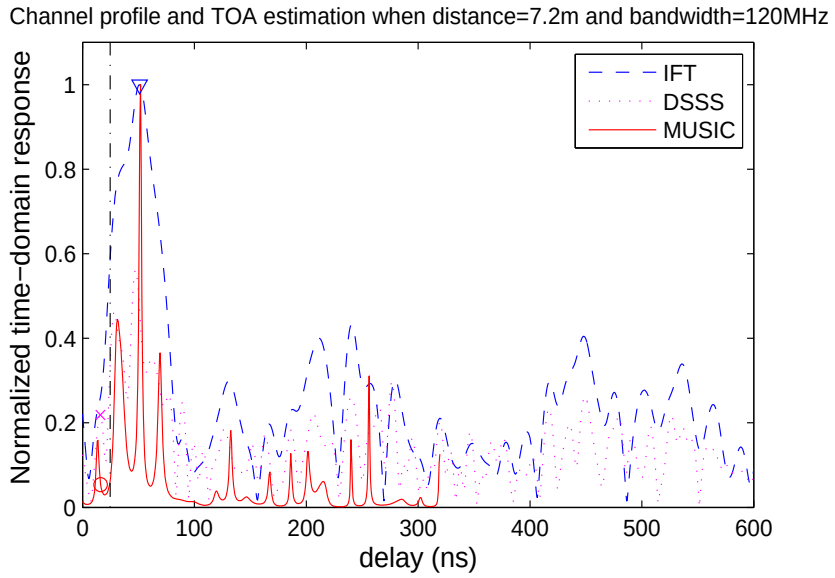

Figure 4.12: Channel profile and TOA estimation results for OLOS scenario(7.2m distance)

path, causing positive ranging error. Super-resolution algorithms are good at mitigating this kind of errors and show superiority to other algorithms, which can be observed from Fig 4.11. When the Tx is moved further away from the Rx, the determinant of DME shifts to the dynamic range of the receiver, which is similar to the situation for the LOS sce-

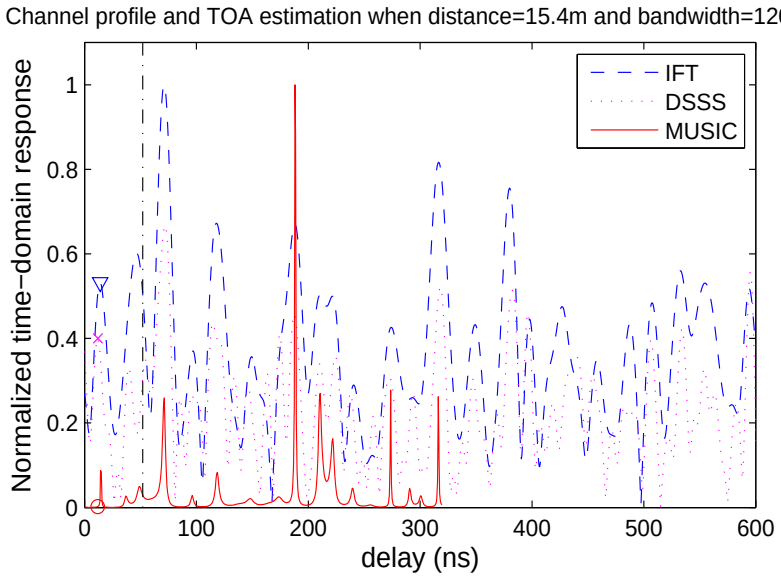

Figure 4.13: Channel profile and TOA estimation results for OLOS scenario(15.4m distance)

nario at greater distances. However, this serious degradation of ranging accuracy happens at distances greater than 8m for OLOS scenario instead of 25m for the LOS scenario.

The effect of distance on DME for the UDP scenario when bandwidth is 120MHz is shown in Fig 4.14and Fig 4.15.

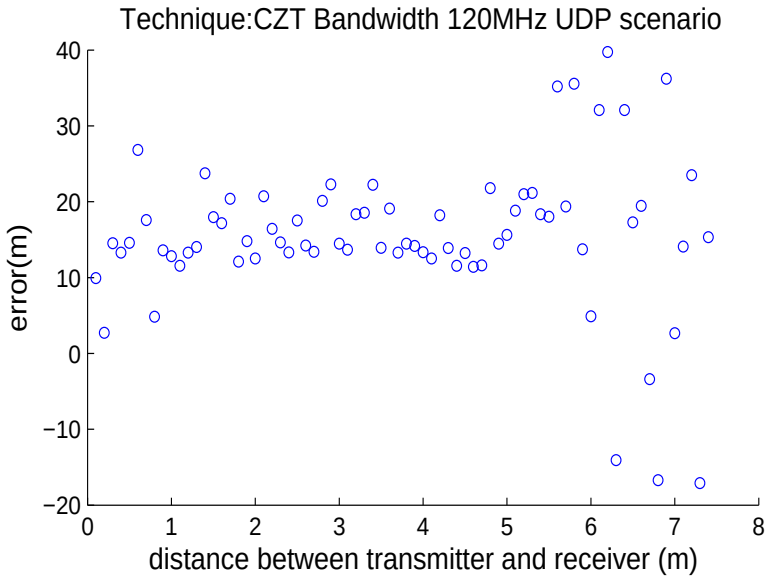

Figure 4.14:

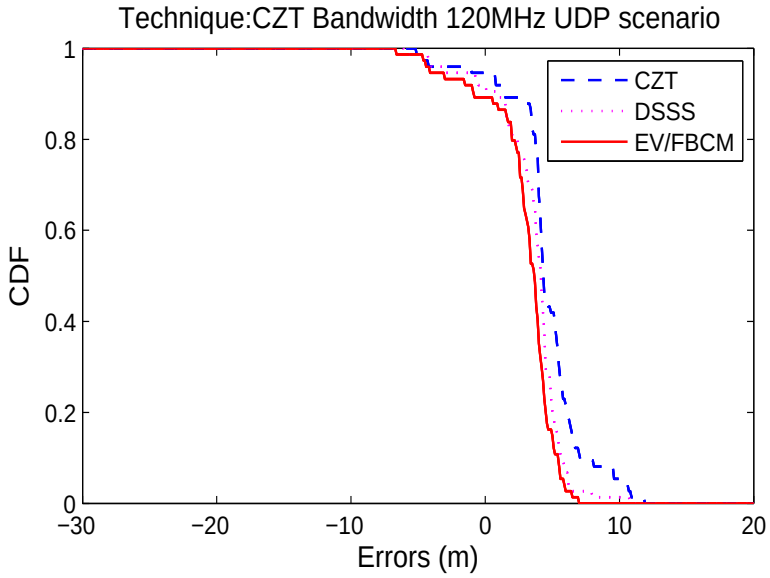

Figure 4.15: OLOS scenario performance comparison of 3 algorithms

First, we note that the maximum measurement distance between the Tx and Rx is only 7.4 m and the DME shows significant positive value on most of the measurement points even when the Rx is close to the Tx, which is caused by the unavailability of the DLOS path in the UDP scenario. With the least available information about the DLOS path among all scenarios, it is intuitive that the DME in the UDP scenario is greatest among all the multipath conditions. The typical channel profile in UDP scenario with large positive DME is shown in Fig 4.16.

Notice that the DME with the CZT method is around $50ns \times 10^{-9}s/ns \times 3 \times 10^{8}m/s = 15m$, which is almost three times the distance between Tx and Rx. in figure, as seen in 4.16. The dynamic range problem also plays an important role for TOA estimation in a UDP scenario at greater distance value, which is reflected in Fig 4.14 as some measurement points with significant negative DME value. One such typical channel profile in UDP scenario is shown in Fig 4.17.

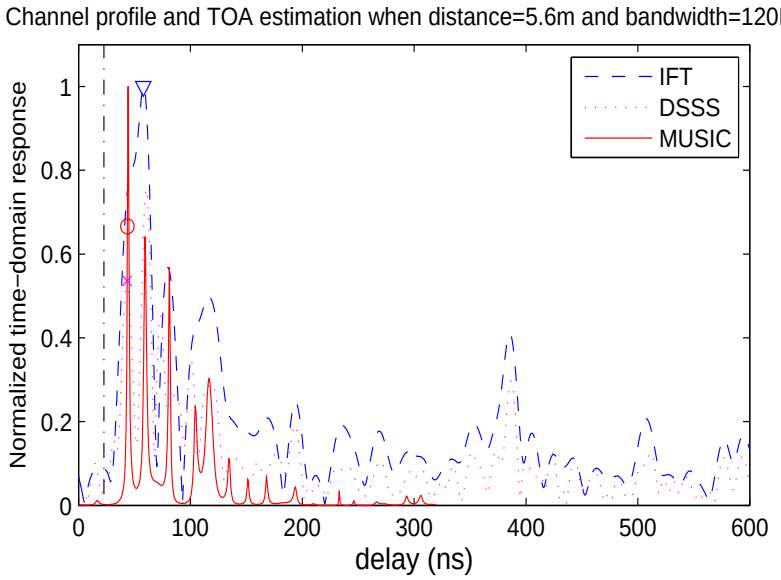

Figure 4.16: Channel profile and TOA estimation results for UDP scenario(5.6m distance)

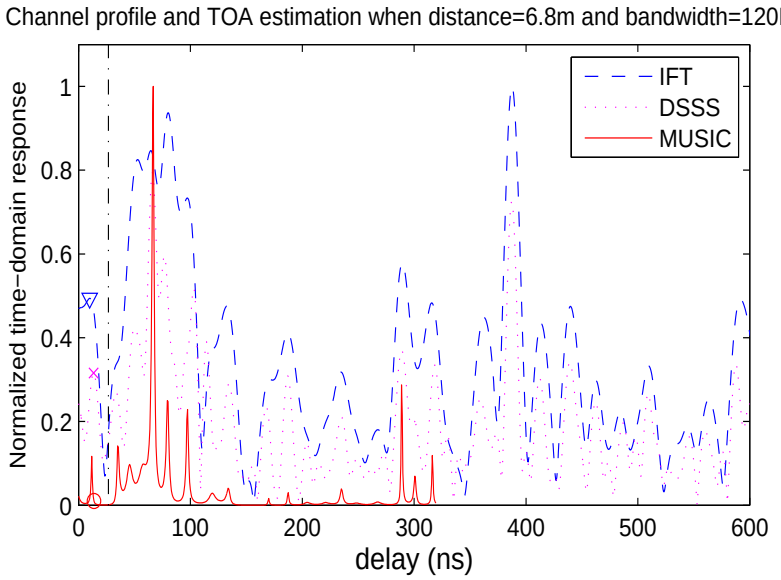

Figure 4.17: Channel profile and TOA estimation results for UDP scenario(5.6m distance)

4.2.2 Effect of Bandwidth on TOA estimation

From our analysis of the influence of distance on DME, we have gained the intuition that the TOA estimation accuracy varies significantly in different multipath environment due to the differences among scenarios in DLOS path availability and the power-distance

gradient. With the loss of DLOS path, the UDP scenario presents a major obstacle to achieving accurate TOA estimation. Therefore, the mean and STD of the DME are expected to be higher when compared with other scenarios such as LOS or OLOS.

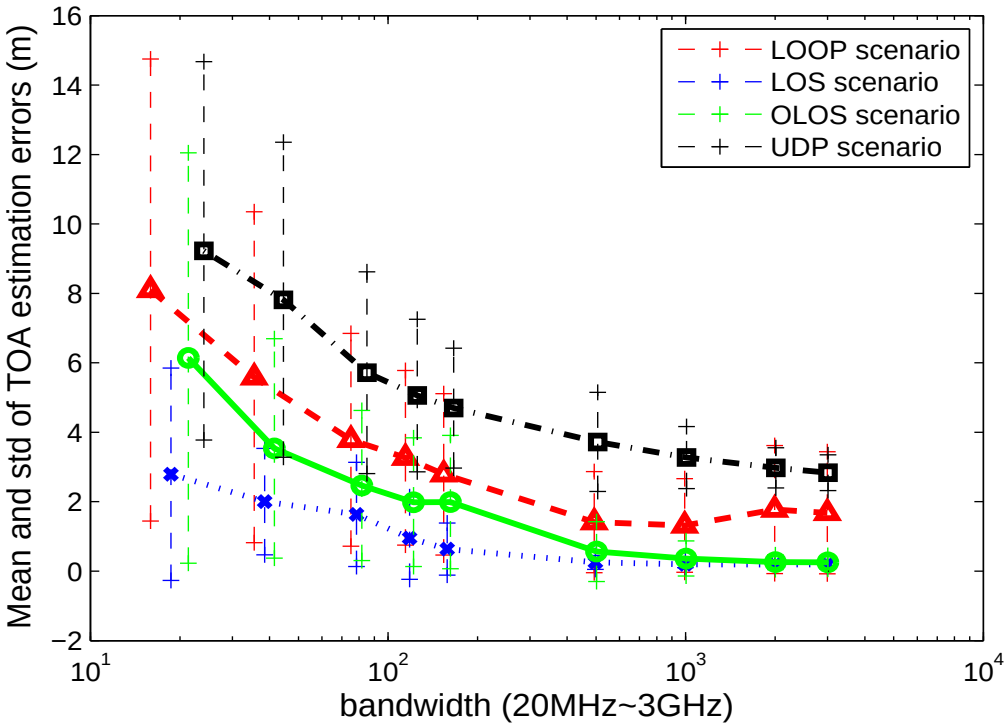

Figure 4.18: Mean and STD of DME for LOOP, LOS, OLOS and UDP scenarios. The vertical lines denote the STD around each mean value

Fig 4.18 confirms that the performance of the basic IFT TOA estimation technique degrades as the environment gets harsher. Among the four measurement scenarios, UDP introduces the highest value of DME and can't be remedied by use of wider bandwidth. Even with 3GHz bandwidth, there is more than 3m DME in the UDP scenario when the distance range between the Tx and Rx is only 7m. Notice that the DME in OLOS is most sensitive to bandwidth availability. When bandwidth is scarce, The DME in OLOS is much higher than that in the LOS scenario. However, when the system operates in an environment with ample bandwidth, say, more than 1GHz bandwidth, the TOA estimation

technique can perform in the OLOS scenario as well as in the LOS scenario.

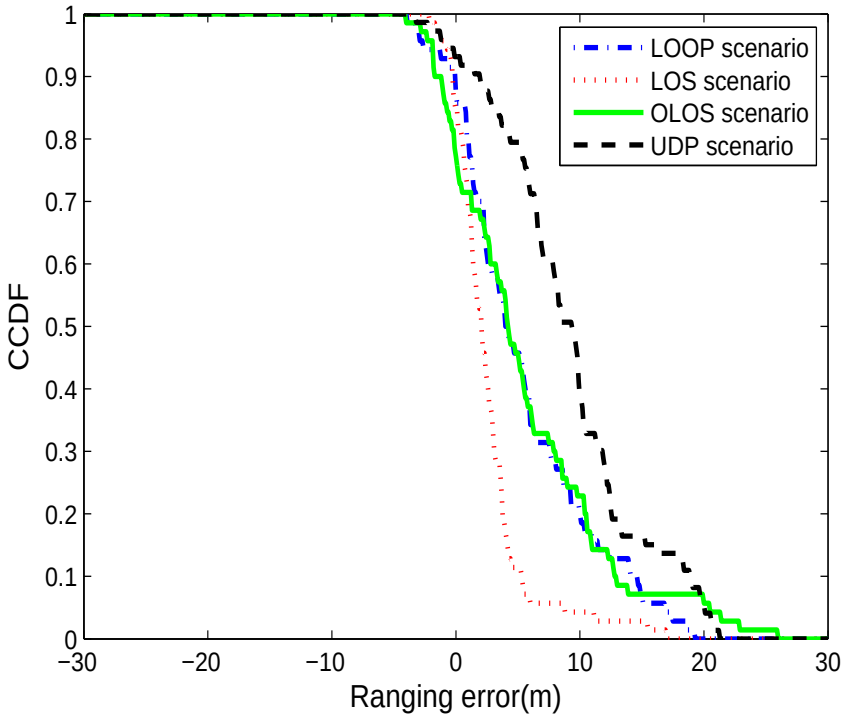

Figure 4.19: CCDF of ranging errors for LOS, OLOS, LOOP and UDP multipath conditions at 20MHz bandwidth

Figure 4.19 shows the CCDF of ranging errors in different multipath environments at low bandwidth (20MHz). The differences in ranging error among the four scenarios could be explained in terms of the multipath and the strength of the DLOS path. For the LOS and OLOS scenarios, the FDP is always the SP and the power of FDP (SP) is relatively strong. Therefore, the only source of DME is the combination of multipath components due to the limitation of bandwidth. The paths arrive in clusters and the higher bandwidth splits those clusters into distinguishable paths. For the loop and UDP scenarios, the major difficulty for accurate ranging is correctly selecting the FDP. The power of both the FDP and most of the multipath components is reduced significantly, making the FDP either below the sensitivity threshold of the Rx or weaker than some side-lobe peaks of the SP.

Nevertheless, the performance of TOA estimation techniques in all scenarios improves with increasing system bandwidth. Meanwhile, the DME improvement for the loop and UDP environments is limited. Figure 4.20 shows the CCDF of ranging errors at higher bandwidth.

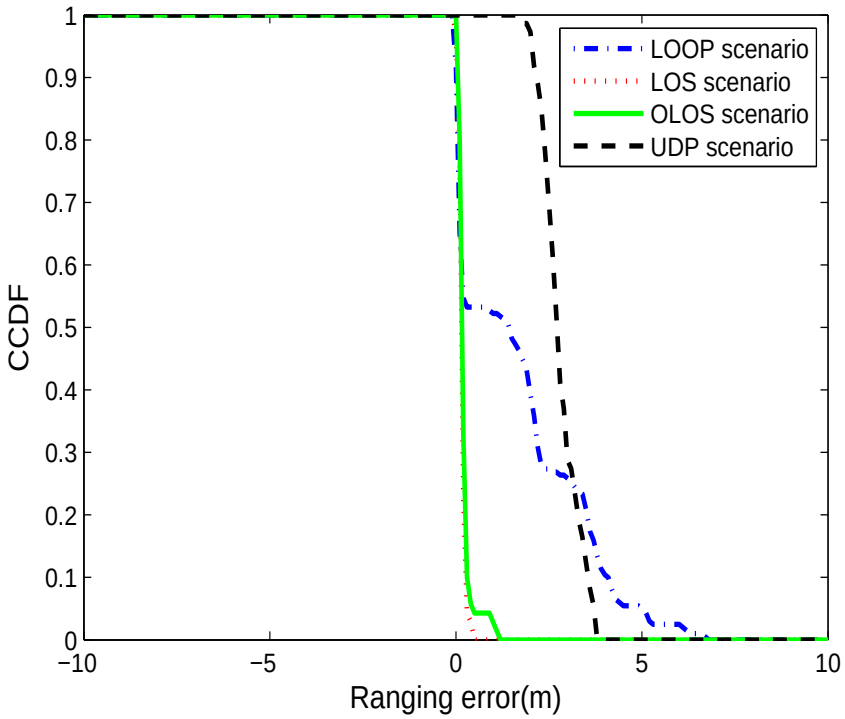

Figure 4.20: CCDF of ranging errors for LOS, OLOS, LOOP and UDP multipath conditions at 3GHz bandwidth

Comparing the two CCDFs at different bandwidths illustrates the improvement of TOA estimation accuracy in all scenarios. However, the performance of the TOA estimation technique in the Loop and UDP scenario is restricted by other factors other than just bandwidth. As will be discussed later, different TOA estimation techniques, though having the ability to reduce average distance error by some means, all failed to perform satisfactorily in UDP scenarios.

4.2.3 Effects of TOA Estimation Algorithms

Up to this point, we have studied the effect of distance, and operating environment on ranging accuracy. Another important issue is comparing the performance of different TOA estimation algorithms with the same constraints, such as same environment and same bandwidth availability. This topic is crucial for the practical implementation of a positioning system since normally the system bandwidth and the multipath condition are fixed for a single localization system. Meanwhile, although intuitively, advanced TOA estimation algorithms such as the DSSS technique and superresolution algorithm outperform simple IFT method. This advantage in performance is gained at the cost of much heavier computation load. Therefore, we need the following comparison results to decide if it is worthwhile to implement an advanced TOA estimation algorithm for a given positioning system.

In the following paragraphs, we will compare the performance of the TOA estimation algorithms, namely IFT, DSSS, and EV/FBCM, which were described in Section 5.1 . Their performance in different bandwidths and multipath conditions will be analyzed. The goal of this analysis is to provide a reference for the positioning system designer when deciding which algorithm is optimal for a certain bandwidth and operating environment. Following the process of previous section, the comparison is made between LOS, OLOS, LOOP, and UDP scenarios, with bandwidth availability ranging from 20MHz$\sim$3GHz.

Fig 4.21 illustrates the performance of IFT, DSSS and EV/FBCM algorithm for LOS scenario in terms of mean and standard deviation of DME at different bandwidths.

At lower bandwidth, EV/FBCM performs slightly better than the DSSS algorithm and IFT method. However, due to the availability of DLOS path in the LOS scenario and fewer reflectors in the environment, all the algorithms perform satisfactorily when the available bandwidth is wider than 200MHz. Even with scarce bandwidth as low as 20MHz, the mean of DME is less than 3m.

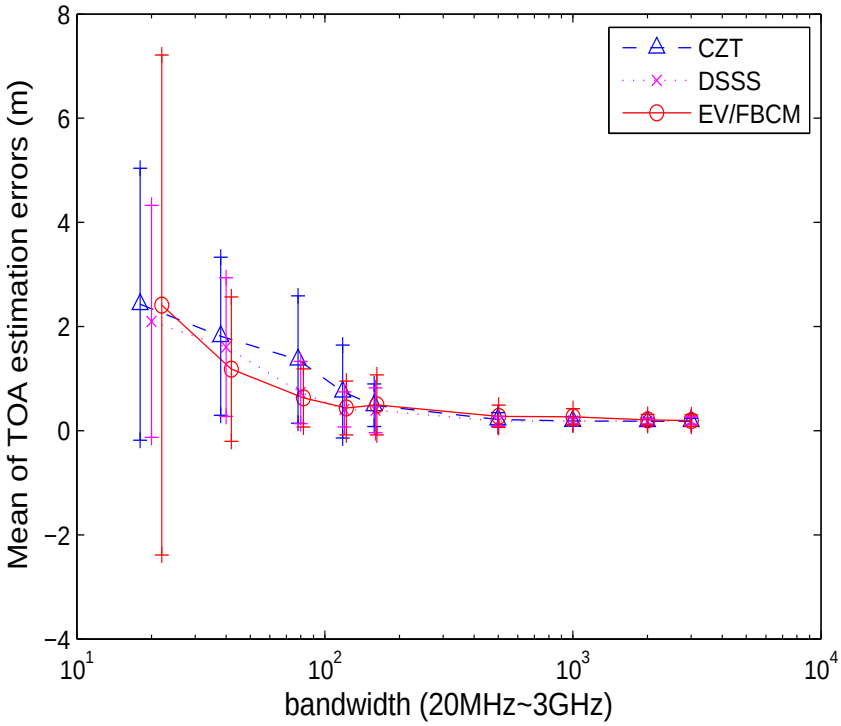

Figure 4.21: Mean and STD of ranging errors in LOS using different TOA estimation algorithms

At 20MHz bandwidth, Fig 4.22 compares the CCDF of the three TOA estimation algorithms showing the slight edge for EV/FBCM. This is not surprising since the main barrier for accurate ranging in LOS scenario is bandwidth limitation, and EV/FBCM has the ability to resolve the FDP more accurately. Figure 4.23 shows the CCDF at 1GHz.

With the increase in bandwidth, the DME for all algorithms approaches zero and the standard deviation of DME is also reduced. Therefore, we have no doubt that using advanced algorithms such EV/FBCM in LOS scenario is not worthwhile since they require much more computation resources and increase the positioning system's reaction time.

For the OLOS scenario, as shown in Fig 4.24, the EV/FBCM algorithm and the DSSS algorithm apparently perform better than the simple IFT method, especially at bandwidths lower than 500MHz. The explanation for this is that the power of the FDP is reduced seri-

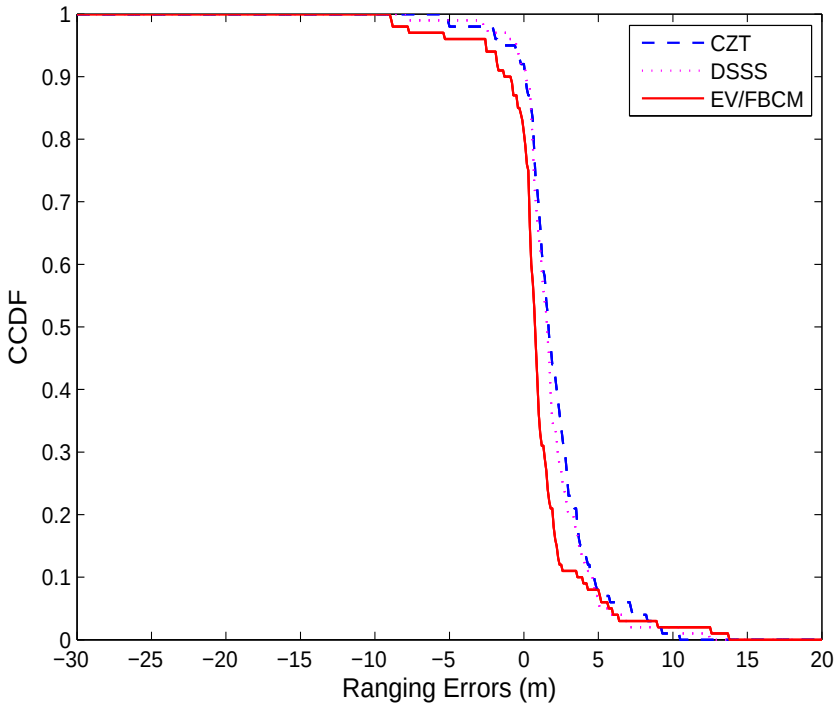

Figure 4.22: CCDF of ranging errors for LOS using different TOA estimation algorithms at 20MHz bandwidth

ously by some kind of blockage (not metallic). Most of the time in an OLOS scenario, the FDP is not the SP anymore. Hence, sometimes the peak detection algorithm will mistakenly interpret the SP or some sidelobe peaks of the SP as the DLOS path. Furthermore, the multipath condition in the OLOS scenario is more severe compared with that of LOS scenario, creating a further barrier to accurate ranging. At 20 MHz, the mean of ranging error for IFT is 6.3m while it is 5m and 5.1m for DSSS and EV/FBCM respectively. When the bandwidth exceeds 500MHz, the advantage of DSSS and EV/FBCM algorithm almost vanishes.

The EV/FBCM algorithm and DSSS algorithm significantly improves the TOA estimation performance at bandwidths less than 500MHz. However, the more complex EV/FBCM algorithm doesn't show any advantage over the DSSS algorithm. As a result,

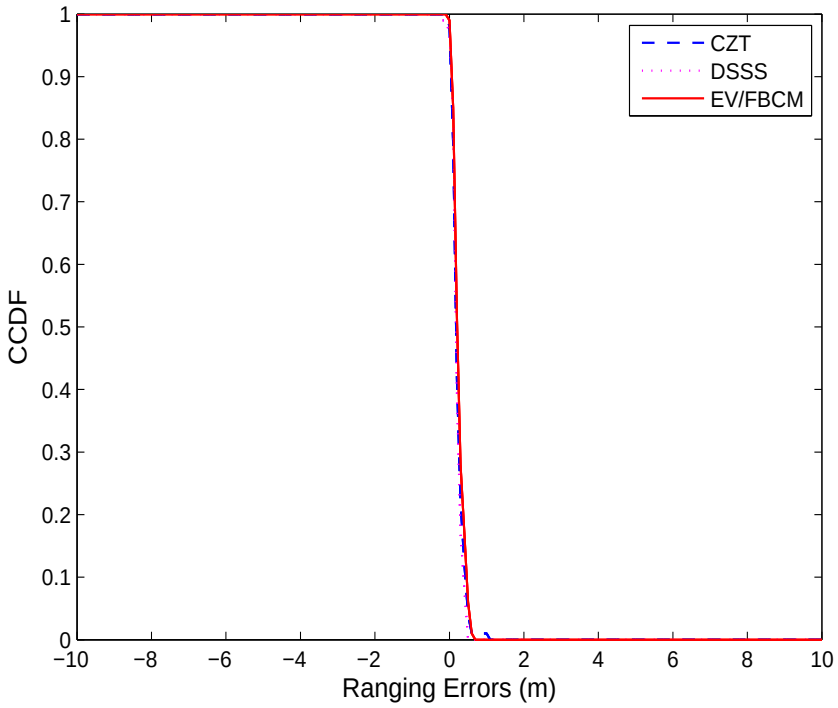

Figure 4.23: CCDF of ranging errors for LOS using different TOA estimation algorithms at 1GHz bandwidth

it is reasonable to implement the DSSS algorithm for TOA estimation in an OLOS scenario at lower bandwidth, since it has the best performance while consuming less computational resource than the EV/FBCM algorithm. However, when bandwidth is wider than 500MHz, IFT algorithm is more attractive since it can provide similar accuracy with lowest cost.

In UDP scenarios, EV/FBCM provides a significant advantage over the other two algorithms. Although the amount of the advantage decreases with the increasing bandwidth. Figure 4.27 shows the mean and STD of ranging error for UDP conditions. Notice that the EV/FBCM outperforms the other algorithms even at higher bandwidths.

Although the DLOS path is not available in UDP scenario due to metallic shadowing or the joint effect of power loss and shadowing, the EV/FBCM is able to select a path

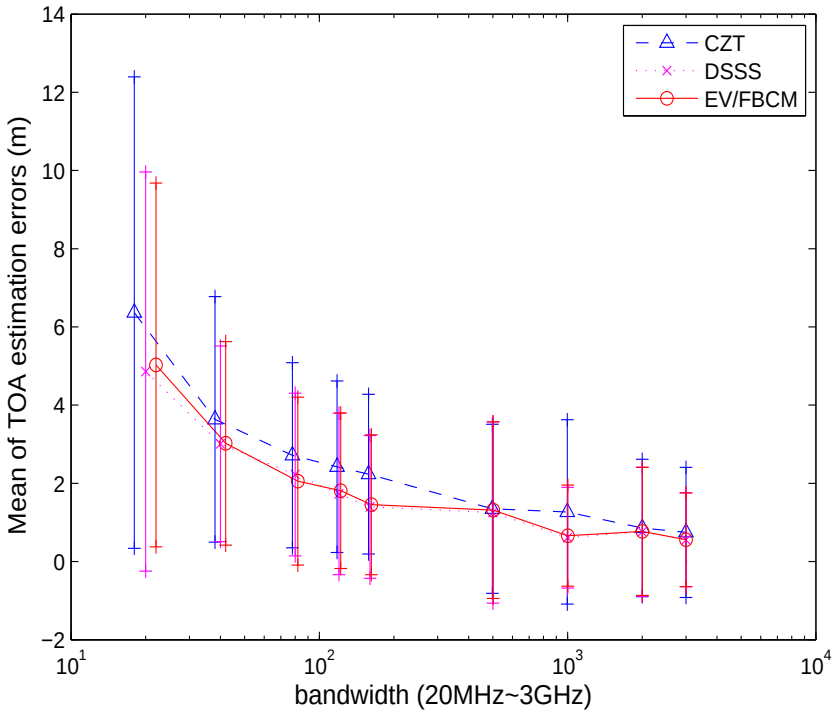

Figure 4.24: Mean and STD of ranging errors in OLOS using different TOA estimation algorithms

closer to the DLOS path compared with the other 2 algorithms. One such channel profile and estimation result are illustrated in Fig 4.28. Another issue we should emphasize is the unavoidable larger DME in the UDP scenario compared with that in other scenarios. This is confirmed by the CCDF curves in Fig 4.29 and 4.30. Even at the bandwidth of 1GHz, none of the three algorithms can provide satisfactory performance. Therefore, more recent research focuses on how to construct a cooperative localization network to avoid as many UDP situations as possible.

Finally, we will look into the performance of different algorithms in the Loop scenario, which comprises of LOS, OLOS and UDP conditions and resembles a realistic office environment. Figure 4.31 presents the mean and standard deviation of DMEs at different bandwidths. Notice that the DSSS and EV/FBCM algorithms outperform the IFT

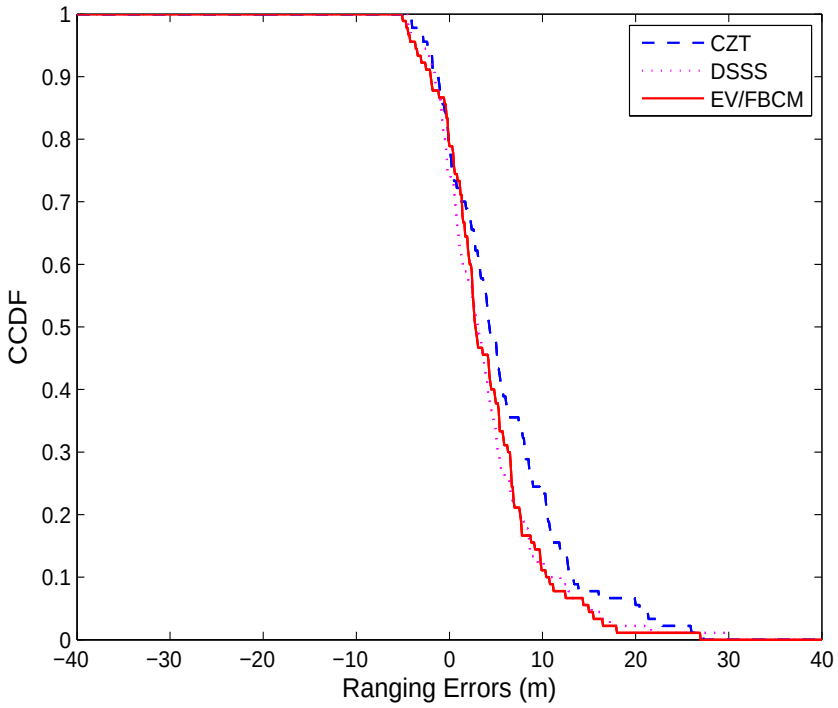

Figure 4.25: CCDF of ranging errors for OLOS using different TOA estimation algorithms at 20MHz bandwidth

algorithm at bandwidths lower than 500MHz, and the three algorithms provide similar accuracy at higher bandwidths. At bandwidth around 20∼40MHz, the DSSS and EV/FBCM algorithms are able to provide 1m lower DME than the IFT algorithm. In addition, the CCDF of the estimation algorithms for the Loop environment shows how the DSSS and EV/FBCM algorithms perform better than the IFT algorithm in lower bandwidth and how this advantage diminishes at wider bandwidth.

Although DSSS and EV/FBCM outperform the IFT algorithm at lower bandwidths, the EV/FBCM algorithm doesn't show any advantage over the simpler DSSS algorithm, which is similar to the situation in the OLOS scenario. Therefore, the optimal choice of TOA estimation techniques in Loop scenarios is the DSSS algorithm when the bandwidth is narrow (less than 500MHz) and the IFT algorithm when the bandwidth is wide.

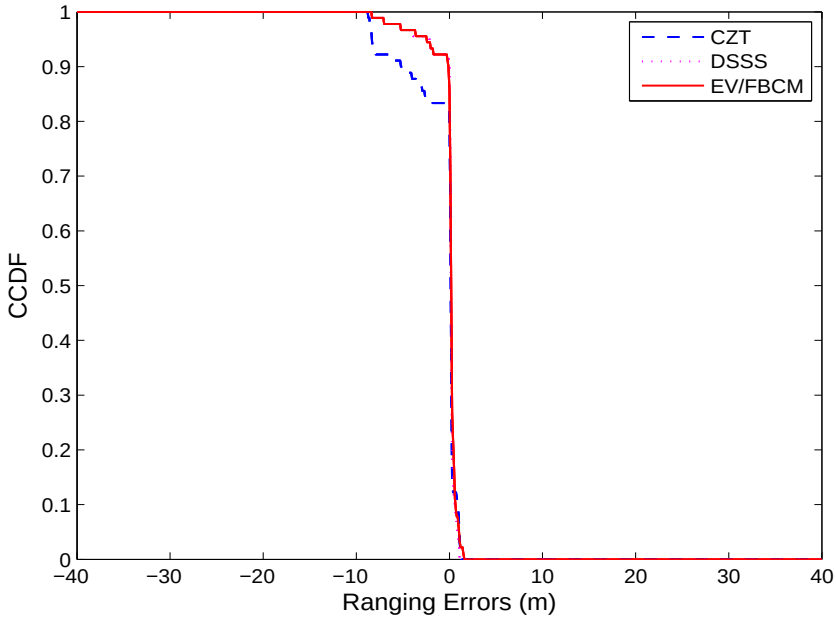

Figure 4.26: CCDF of ranging errors for OLOS using different TOA estimation algorithms at 1GHz bandwidth

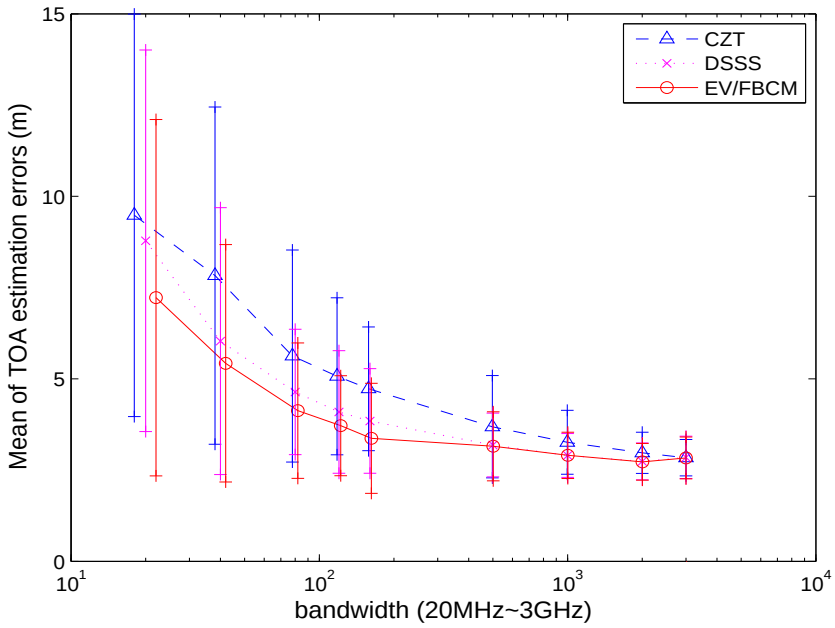

Figure 4.27: Mean and STD of ranging errors in UDP using different TOA estimation algorithms

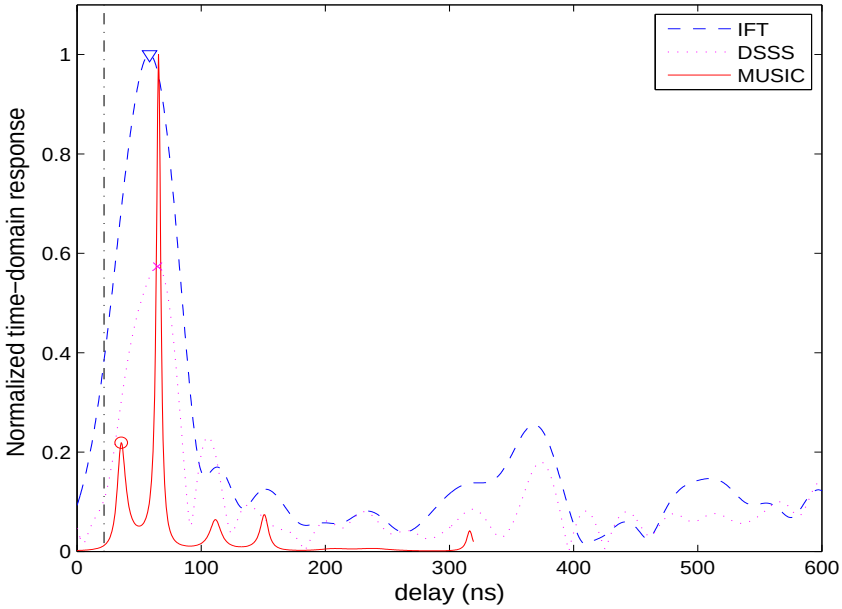

Figure 4.28: Mean and STD of ranging errors in UDP using different TOA estimation algorithms

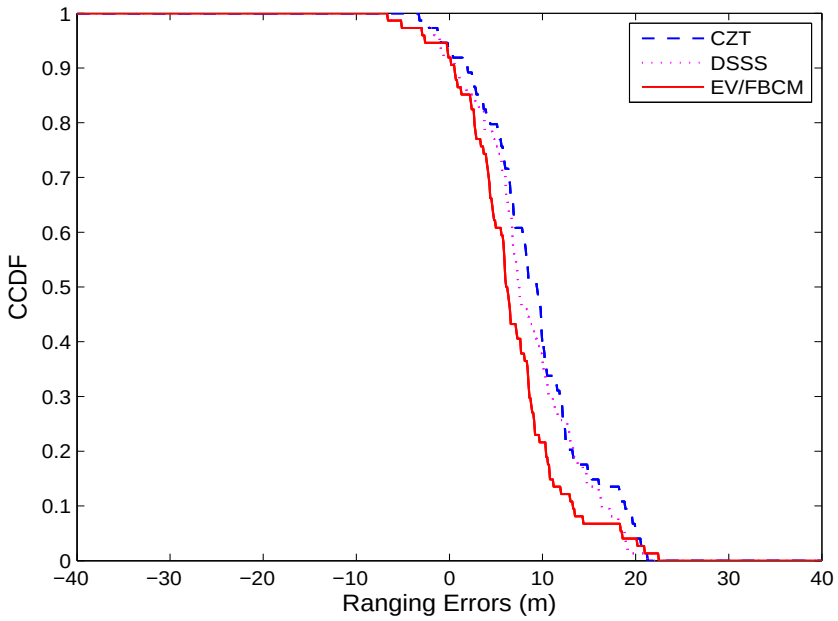

Figure 4.29: CCDF of ranging errors for UDP using different TOA estimation algorithms at 20MHz bandwidth

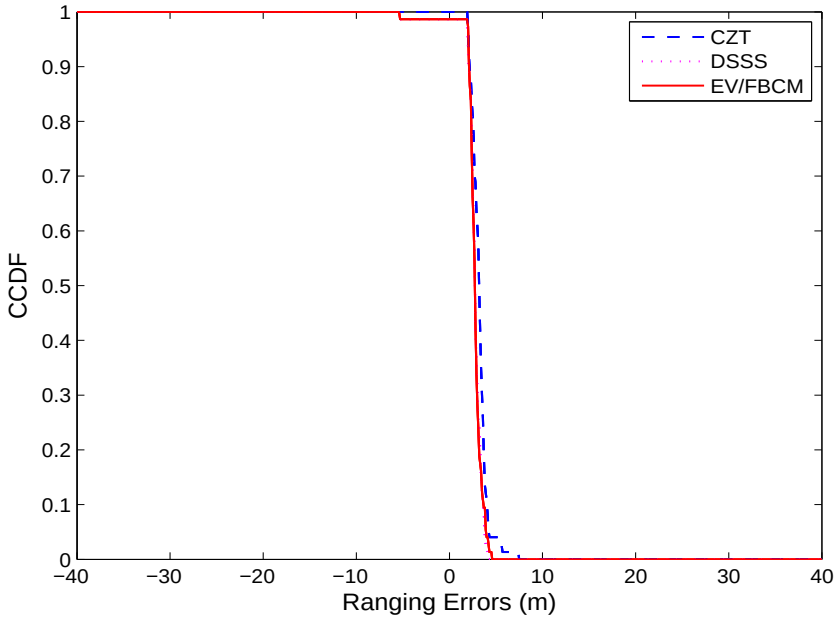

Figure 4.30: CCDF of ranging errors for UDP using different TOA estimation algorithms at 1GHz bandwidth

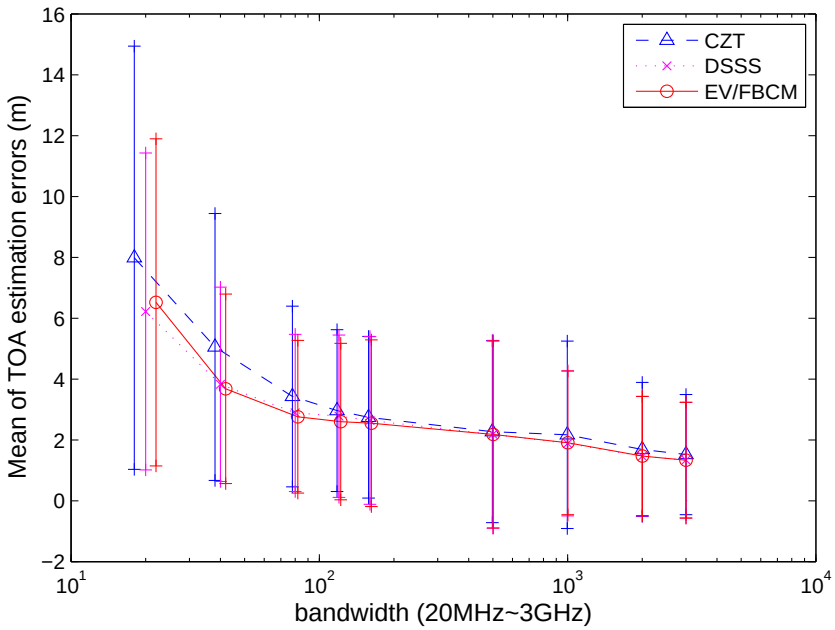

Figure 4.31: Mean and STD of ranging errors in Loop scenario using different TOA estimation algorithms

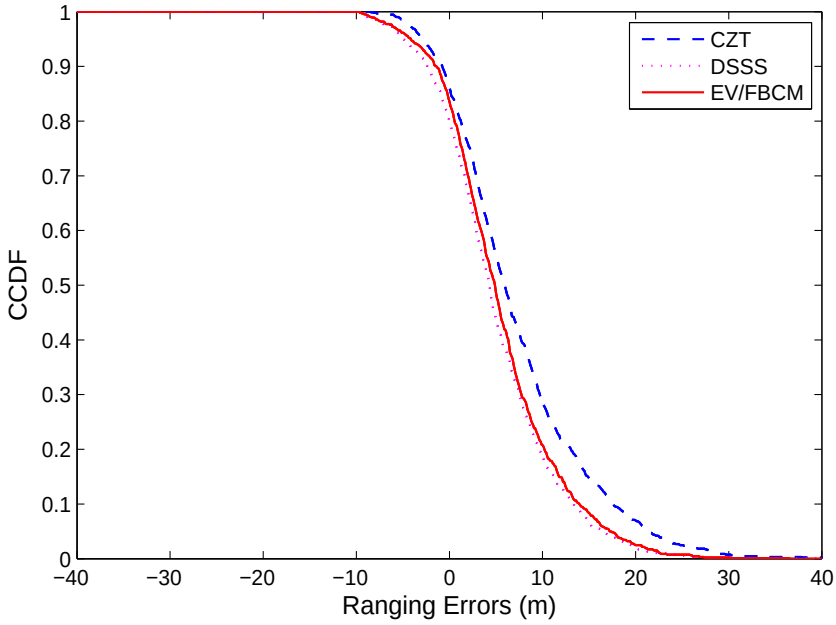

Figure 4.32: CCDF of ranging errors for Loop using different TOA estimation algorithms at 20MHz bandwidth

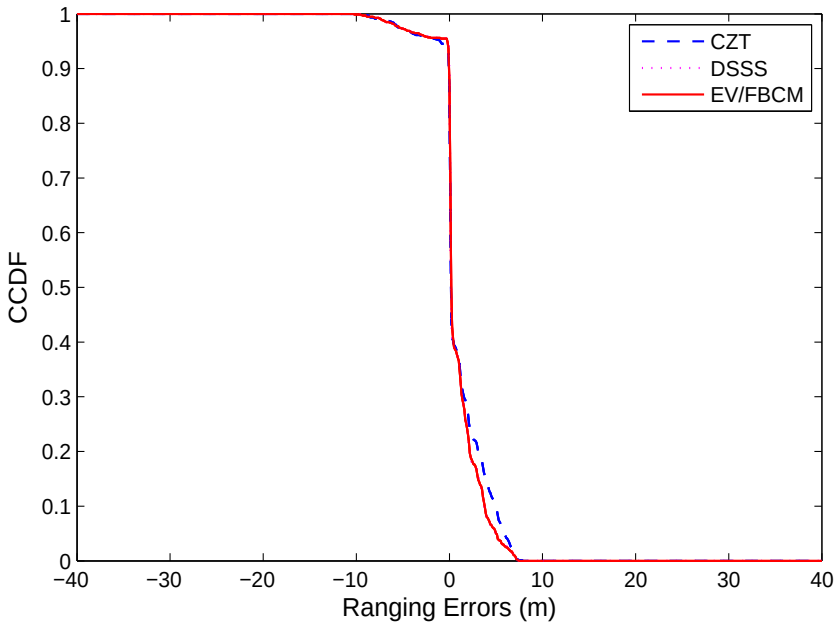

Figure 4.33: CCDF of ranging errors for Loop using different TOA estimation algorithms at 1GHz bandwidth

Chapter 5

Sensitivity Analysis for Multipath Diversity

As we mentioned before, In TOA based indoor geolocation systems, the large positioning errors are often caused by the UDP conditions where the DP can't be detected due to obstructions. However, other multipath conditions such as obstructed line of sight (OLOS) can not guarantee satisfactory accuracy either when the available bandwidth is low or the received DLOS path power is weak (possibly caused by long distance between the transmitter and receiver, or the threshold for picking paths is not chosen properly, causing the sidelobes of the windowing function to interpreted as fake peaks). The bandwidth of the system plays an important role in determining the accuracy of TOA estimation. In general, as the bandwidth increases the distance measurement error decreases. However, for harsh environments such as UDP scenarios, using the TOA of DP alone is not sufficient to provide promising positioning.

In recent years,many extensive researches have been carried out in order to mitigate the ranging errors from UDP links. Utilizing multipath diversity when the DP is not reliable comes naturally since there are always other paths available in UDP conditions.

However,this technique requires a deeper knowledge of propagation characteristics. Previous research on channel modeling didn't consider the dynamic behavior of the multipath channel, such as the appearance and disappearance of paths due to movement of the MT. This is mainly due to the lack of dynamic measurement campaigns to support realistic modeling of a dynamic channel. The motion of the MT introduces both small and large scale variations in the received signal. For the sake of this research, we focused mainly on the large scale variations induced by the motion of the MT, such as fluctuations of the number of active multipath components (MPCs), transitions where paths appear and disappear, variations in the propagation delays and powers, and the changes in the direction of arrivals as the MT moves along its trajectory.

For indoor geolocation, the time difference of arrival (TDOA) of a certain path as the MT moves along its pathway is important. Assuming we have DLOS path ranging on points uniformly spaced along the pathway, we can keep track of the difference between the TOAs of this particular path and the DLOS path at these predefined points. If the DLOS path is blocked at some locations during the MT's motion but that particular path is still available, we can use the difference information and the path length of the particular path to calculate the length of DLOS path, which is the desired distance between the transmitter and MT. This concept was first proposed in [7]. The concept of using multipath components other than the DLOS path is illustrated in Fig 5.1

As the receiver moves, certain MPCs might exhibit 'smooth' behavior in the UDP region. The differential changes of these MPCs' TOA and AOA are related to the concept of path persistency. Therefore, the persistency of MPCs is an important issue in mitigating the UDP error. To explain path persistency, we will consider the following channel model [1]

$$h(t,\theta) = \sum_{k=0}^{N-1} \alpha_k p(t-\tau_k, \theta-\theta_k) e^{j\varphi_k} \tag{5.1}$$

where N is the number of MPCs, $p(t)$ is the pulse (with a certain bandwidth ω) transmit-

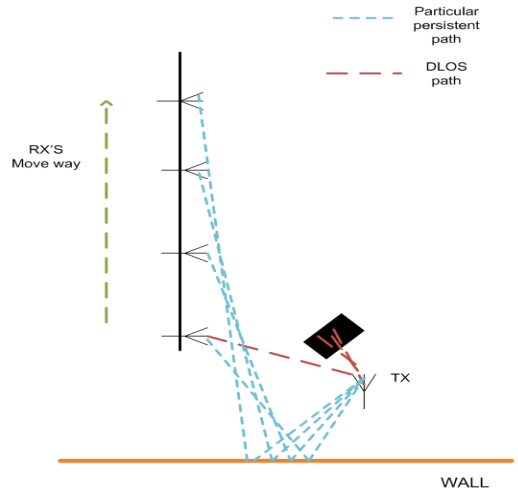

Figure 5.1: Illustration of using indirect paths

ted, and $\alpha_k, \tau_k, \theta_k, \varphi_k$ are the amplitude, propagation delay (TOA), angle of arrival(AOA) and phase of the kth MPC, respectively, which can be considered as traceable features of the paths. Persistency is basically the lifetime of a particular path during which its traceable features exhibit differential changes in accordance with the receiver's differential motion. If we can track the paths that exhibit persistent behavior even when the DP is not present, then we can use this additional information to properly adjust the ranging measurements for true distance [7]. Due to the challenge of AOA measurement, from now on, we only consider the TOA as traceable features to looking at the path persistency. The basic concept of path persistency is shown in Fig 5.2.

Because we want to use other multipath components to mitigate the distance measurement error in UDP conditions, we are interested in the number of available MPCs. The number of resolvable multipath components is important for evaluating the performance of various types of diversity, modulation and equalization techniques (e.g., RAKE receiver) [29]. A multipath component measured in a particular profile is defined to arrive at the receiver at a particular excess delay bin τ_k if the integrated power within a discrete

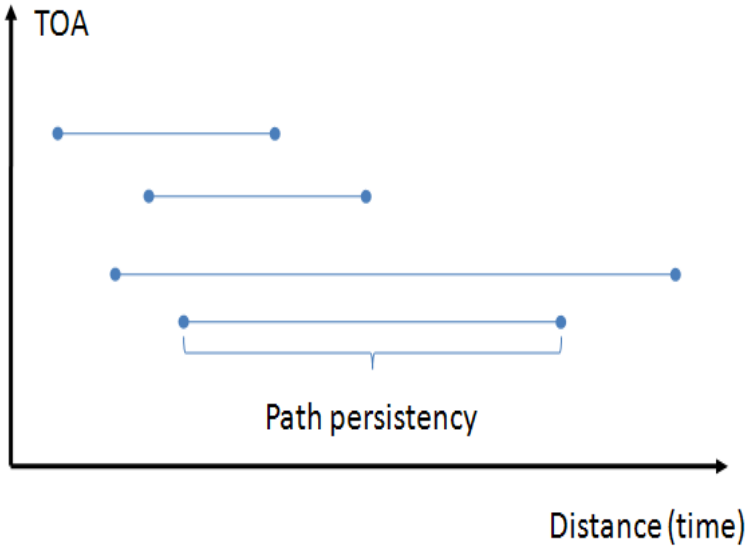

Figure 5.2: Path persistency

excess delay interval β_k^2 (fig 5.3) is greater than the minimum detectable signal threshold of the receiver. No multipath component exists if β_k^2 does not exceed the minimum detectable signal threshold at the excess delay bin τ_k.

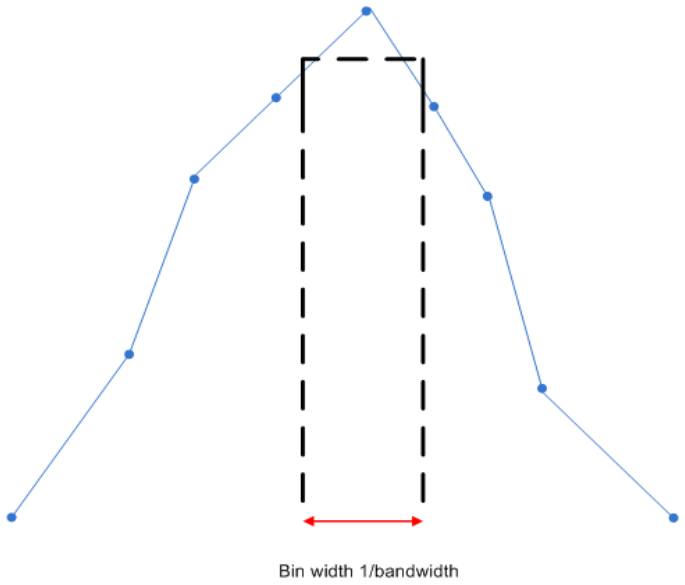

Figure 5.3: Illustration of counting multipath components

Several researchers have analyzed the number of available multipath components in

the sense of static channel modeling [30, 29]. They looked into the behavior of the number of MPCs at certain locations with different transmitter receiver separated distances. Then they studied the distribution of the number of MPCs for telecommunication applications. However, due to measurement system limitation and target difference, they haven't look at the the dynamic behavior of number of MPCs and the effect of bandwidth, threshold for picking paths, and UDP occurrence on the number of MPCs, which is also important for indoor geolocation. The analysis of the dynamic behavior of the number of MPCs in different multipath conditions would provide an insight into the resources that can be used to aid the localization in harsh environments.

Another issue crucial to using the other multipath components when the DP is not detectable is the appearance and disappearance of paths due to movement of the receiver or MT, which is also referred as path persistency in indoor geolocation applications [7]. Figure 5.4 illustrate the relationship between the TOA of the direct path and the path reflected from a wall for a simplified scenario. As the mobile receiver moves along the horizontal direction, during part of its route, the direct path is blocked, but the reflected path is still available. The change in distance in the receiver direction of motion is related to the length of the of the DP by: $dxcos\alpha = dl_{dp}$. As the geometry of Fig 5.4 shows, for the reflected path length, we have $dxcos\beta = dl_{rp}$. Therefore, we can calculate the change in the length of the direct path from the change in the reflected path using

$$dl_{dp} = dl_{rp}\frac{cos\alpha}{cos\beta} \tag{5.2}$$

In other words, knowing the angle β, between the arriving path and the direction of movement, and the angle α, between the direction of movement and the DP, we can estimate the changes of the length of the DP from the changes of the length of the reflected path. This basic principle can be extended to paths reflected from many objects and to the three-dimensional case as well [27].

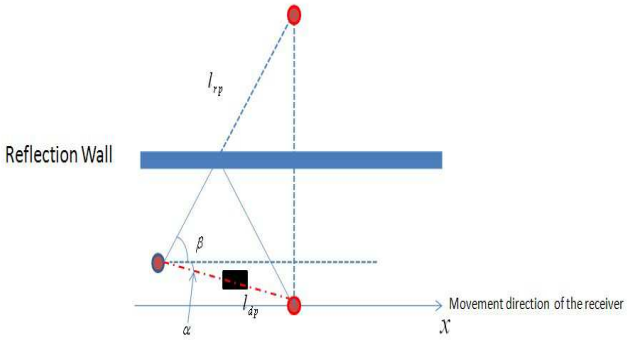

Figure 5.4: Basic two path environement

In this chapter, the comprehensive measurement database is used for dynamic analysis. The main focus here is the dependency between the distance-related number of MPCs and the effect of bandwidth, threshold for picking paths, and UDP occurrence on the number of MPCs and path persistency. In section 5.1, the distance dependency or number of MPCs is modeled for different scenarios, and the effect of bandwidth, threshold for picking paths and UDP occurrence on number of MPCs is also studied. Section 5.2 first introduces the concept of average path lifetime (APL) and average path displacement (APD), then discribes the effect of bandwidth, threshold for picking paths and UDP occurrence on path persistency .

5.1 Behavior of the Number of MPCs

The number of MPCs has been studied in [30, 31] for telecommunication applications. The author mainly looked into the distribution of the number of MPCs at some selected locations. However, more research is needed for modeling the effect of distance, bandwidth

and OLOS UDP occurrence on the number of MPCs for indoor geolocation applications. Since the number of MPCs is sensitive to the threshold value used in post-processing, we also specify the threshold used for picking MPCs from this point.

5.1.1 Distance Dependency of Number of Paths

As mentioned earlier, Fig 3.10 substantiates the following observations: When the Tx is close to the Rx, the number of MPCs is small due to the strong LOS component and the threshold for picking paths (which means we only consider those paths within α dB of the strongest paths as eligible paths). Most MPCs are below the threshold at the beginning. As the Rx moves away from the Tx, more paths will be resolved due to the reduction of the strength of the strongest path. After a certain break point, the number or MPCs will start to decrease due to distance reducing the strengths of more paths and bringing them below the noise floor threshold. Our inference is validated by the measurement result which is shown in Fig 5.5.

However, for OLOS condition (Fig 5.6), due to at least one wall of separation, even when the Tx and Rx are at the closest distance, the strongest path between them is much weaker compared with that in the LOS condition. Hence, all the resolvable paths above the noise floor will be counted as eligible paths. The cutoff effect of threshold for picking paths is weaker. As the receiver moves away, the number of MPCs will keep decreasing due to more paths becoming weaker than the noise floor. In the end, resolvable paths disappear when the receiver moves beyond the coverage of the Tx. In our case, this limitation for OLOS is around 16m.

For UDP condition depicted in Fig(5.7), the number of MPCs decreases with distance between the Tx and Rx similarly as the behavior in the OLOS scenario. However, since the anechoic chamber made of metallic material always exists between the Tx and Rx, the The power of all the MPCs is further reduced compared with that in OLOS condition.

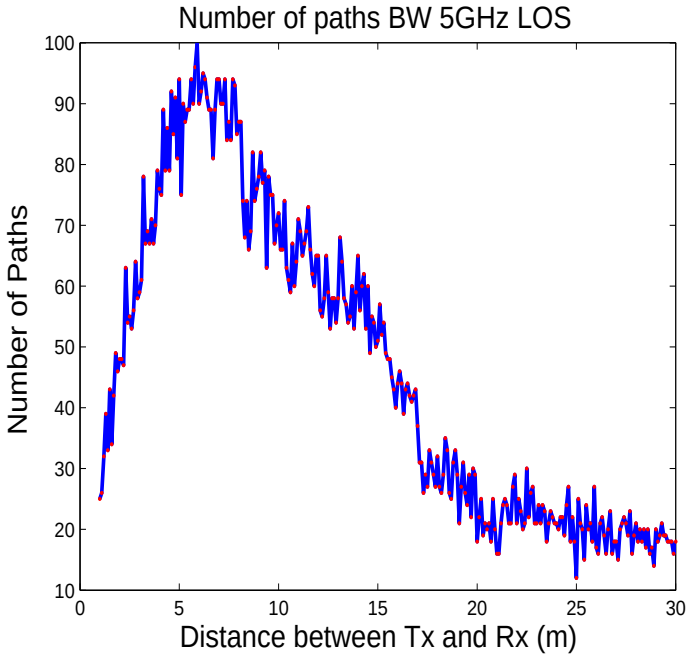

Figure 5.5: LOS scenario number of paths dynamic behavior

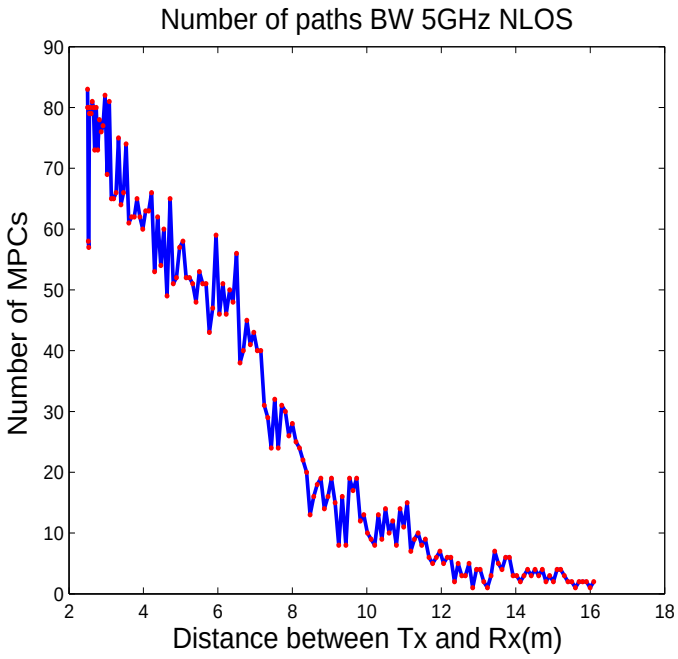

Figure 5.6: OLOS scenario number of paths dynamic behavior

Therefore, for the same distance between the Tx and Rx, there are fewer MPCs above the noise floor. Meanwhile, the coverage of resolvable paths in UDP condition is only around 8m.

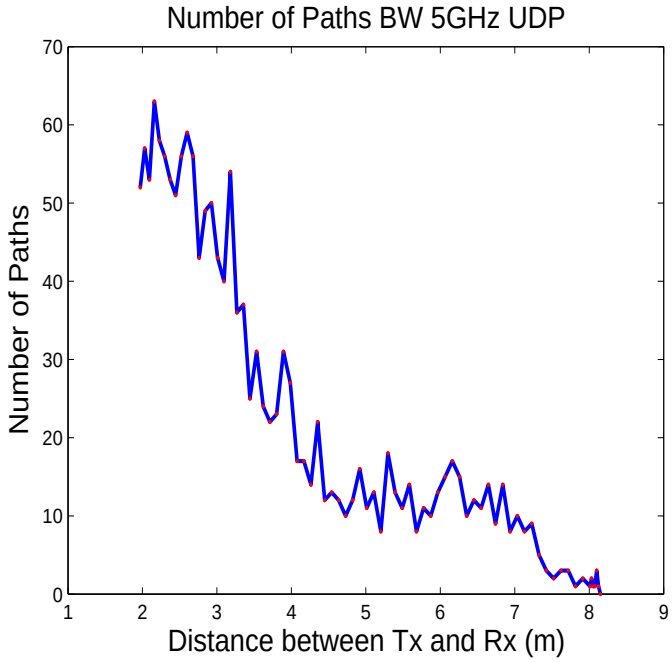

Figure 5.7: OLOS scenario number of paths dynamic behavior

5.1.2 Other Parameters Affecting the Number of Paths

By analyzing measurement data from a LOS scenario, we observed a Rayleigh-like dependency between the number of MPCs and distance. Hence, we first try to model the relationship between number of MPCs and distance as a Rayleigh-like function as :

$$N = A\frac{de^{(\frac{-d^2}{2\sigma^2})}}{\sigma^2} + \chi_{LOS}, \tag{5.3}$$

where d is the distance between the Tx and Rx in m. and A, σ and χ_{LOS} are the parameters need to be estimated. χ_{LOS} is a random variable that can be conveniently modeled

with a normal distribution $\chi_{LOS} \sim N(0, \sigma_{\chi_{LOS}})$. Naturally, one expects an increase in the number of MPCs with an increase in bandwidth, an increase in threshold for picking paths, and a decrease in noise floor. For our specific environment and measurement system, we fixed the threshold for picking paths at 30dB and noise floor at -90dB. However, the results showed that the Rayleigh-like function can't fit the measured data well when the distance between the Tx and Rx is larger than 20m, as in figure 5.8 .

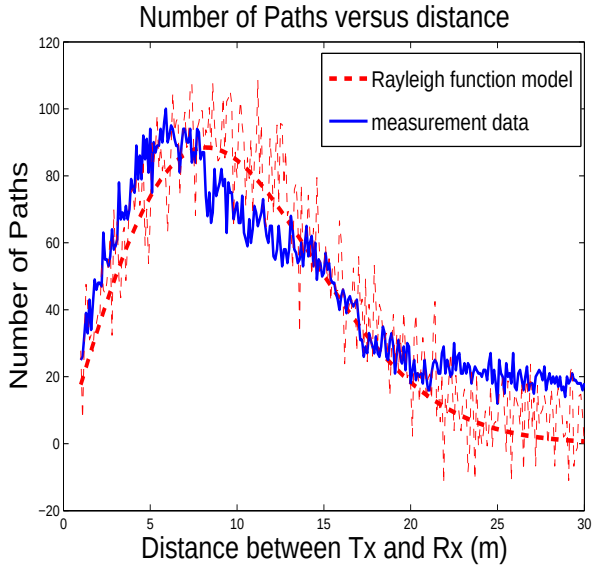

Figure 5.8: Rayleigh model

Hence, we propose to model the dependence of number of MPCs and distance in LOS condition as a two-piece exponential function. A distance break point exists and for our LOS scenario, the break point is around 6.5m. The model based on non-linear least square regression is as:

$$\begin{cases} N = (2 - e^{0.1032(d-d_{bp})}) \cdot N_{max_{LOS}} + \chi_{LOS}, \ \text{d} \leq d_{bp} \\ \\ N = e^{-0.0956(d-d_{bp})} \cdot N_{max_{LOS}} + \chi_{LOS}, \ \text{d} > d_{bp} \end{cases} \tag{5.4}$$

where $N_{max_{LOS}}$ is the number of MPCs at the break point distance, which is related

to the bandwidth (in MHz) f as:$N_{max_{LOS}} = f^{0.547}$, χ is a random variable with normal distribution $\chi_{LOS} \sim N(0, \sigma_{\chi_{LOS}})$, and $\sigma_{\chi_{LOS}}$ is related to bandwidth f as: $\sigma_{\chi_{LOS}} = f^{0.212}$. Figures 5.11 and 5.12 show the relation between $N_{max_{LOS}}$ and bandwidth and the CDF of measured and simulated number of MPCs using our two-piece model for LOS scenario respectively. Figure 5.13 compares the performance of each model in RMSE value at different bandwidth, which demonstrates the superiority of the two-piece model over Rayleigh-like function model at higher bandwidth.

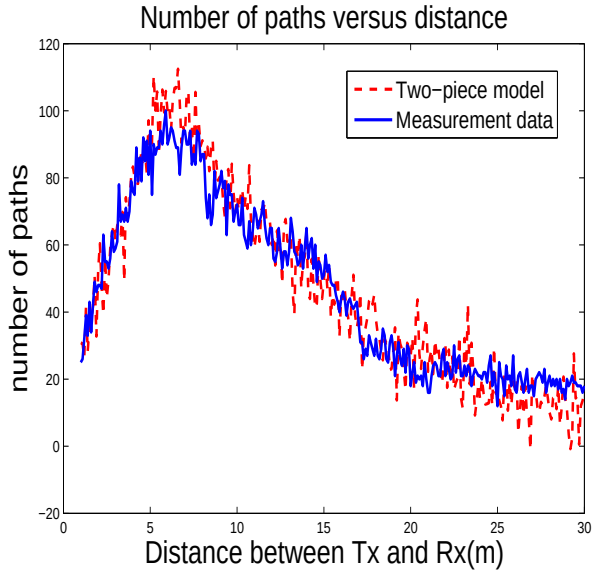

Figure 5.9: Two piece model

For the NLOS scenario, the relationship between the number of MPCs, distance and bandwidth can be modeled as

$$N = e^{-0.1309d} \cdot N_{max_{NLOS}} + \chi_{NLOS}, \tag{5.5}$$

where $N_{max_{NLOS}}$ is the number of MPCs when the Rx is at the closest distance to the Tx, which is related to the bandwidth f as $N_{max_{NLOS}} = f^{0.5273}$, and χ_{NLOS} is a random variable with normal distribution $\chi_{NLOS} \sim N(0, \sigma_{\chi_{NLOS}})$, where $\sigma_{\chi_{NLOS}}$ is related to the

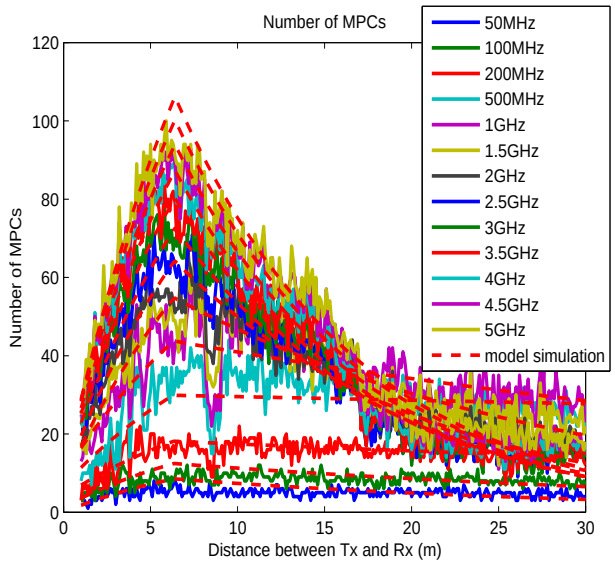

Figure 5.10: Two piece model performance for different bandwidths without χ variable

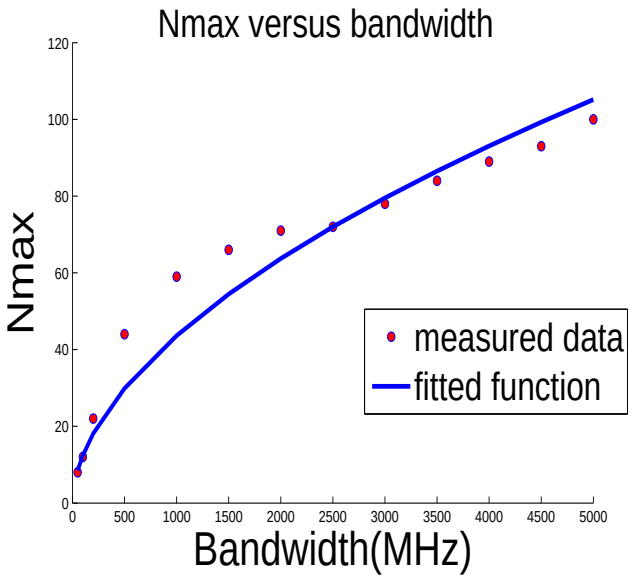

Figure 5.11: Nmax versus bandwidth

bandwidth f as: $\sigma_{\chi_{NLOS}} = f^{0.2645}$. Figure 5.15 and 5.16 show the relationship between $N_{max_{NLOS}}$ and bandwidth, and the CDF of measured and simulated number of MPCs using our model for NLOS scenario. Comparing Figs 5.12 and 5.16, model fits the number of MPCs for LOS conditions slightly better than that for NLOS condition. This is reason-

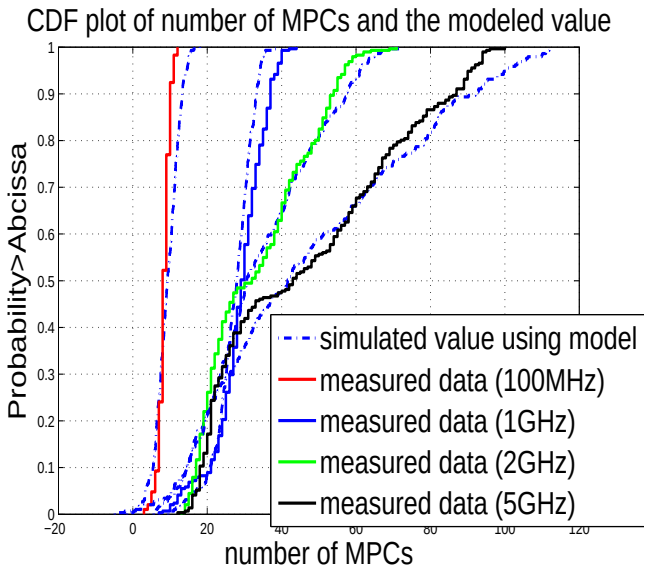

Figure 5.12: CDF of measured and simulated number of MPCs

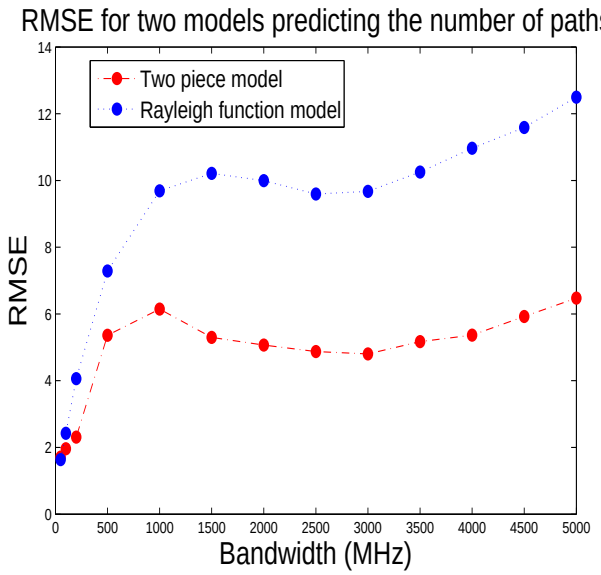

Figure 5.13: RMSE of calculated number of paths using two models at different bandwidth

able because NLOS condition is much more complex than LOS condition caused by the blockage of walls and micro-metalic objects.

For a UDP scenario the relationship between the number of MPCs, distance and band-

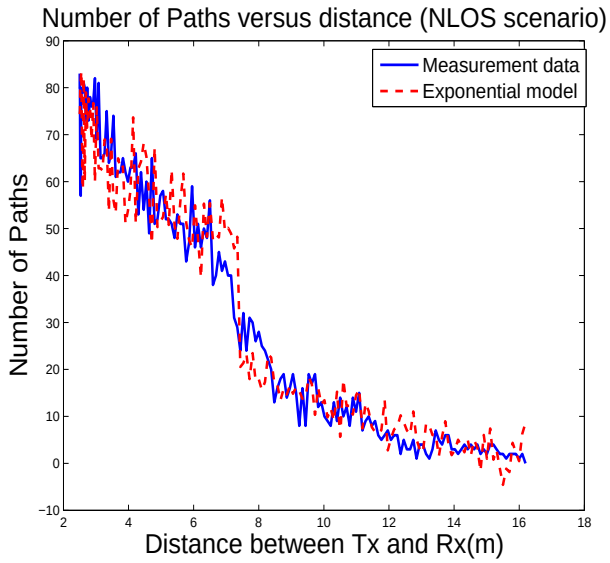

Figure 5.14: exponential function model for number of paths at OLOS scenario

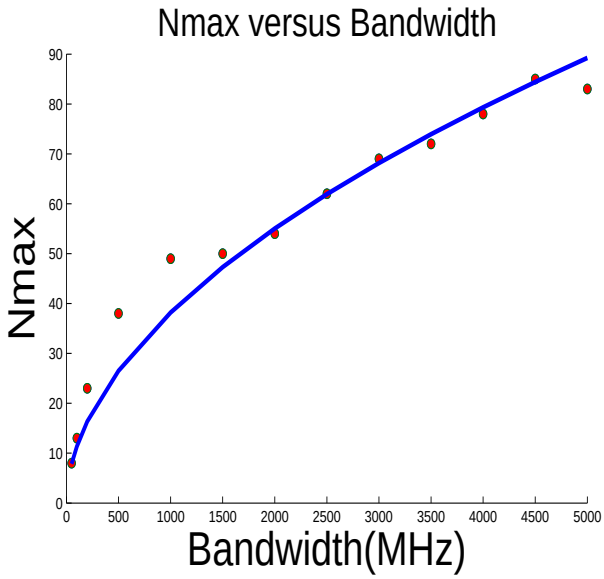

Figure 5.15: Nmax versus bandwidth for OLOS environment

width can be modeled as

$$N = e^{-0.4714d} \cdot N_{max_{UDP}} + \chi_{UDP}, \tag{5.6}$$

where $N_{max_{UDP}}$ is still a parameter related to the bandwidth f, which can be modeled

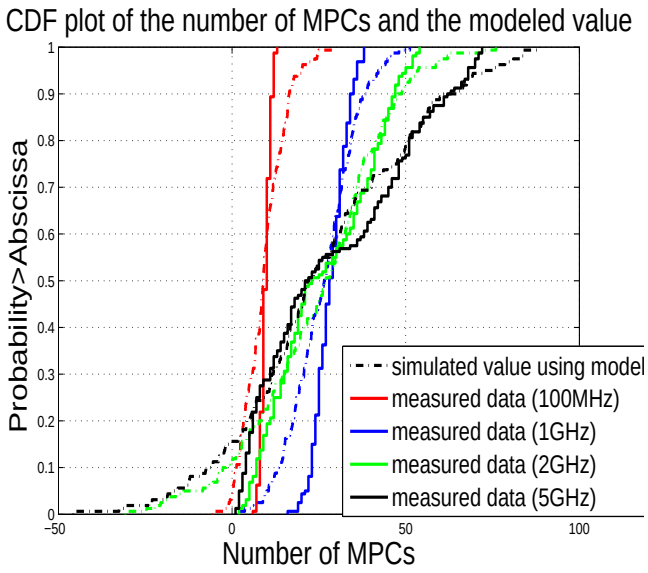

Figure 5.16: CDF of measured and simulated number of MPCs in OLOS scenarios

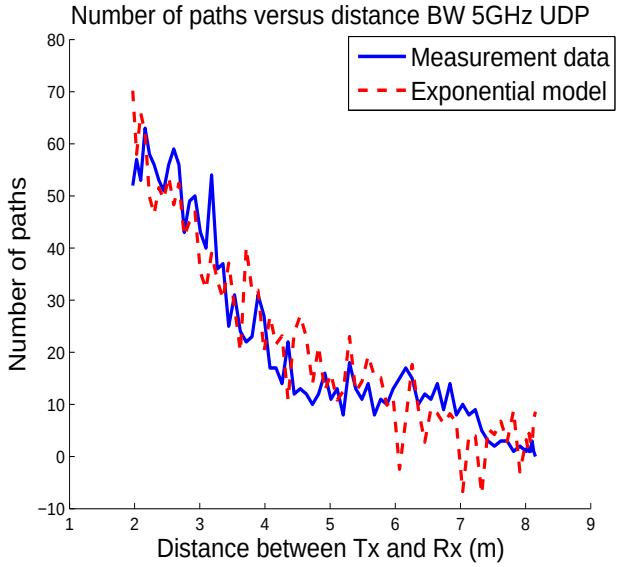

Figure 5.17: exponential function model for number of paths at UDP scenario

as $N_{max_{UDP}} = f^{0.5844}$, and χ_{UDP} is a random variable with normal distribution $\chi_{UDP} \sim N(0, \sigma_{\chi_{UDP}})$,where $\sigma_{\chi UDP}$ is related to the bandwidth f as:$\sigma_{\chi_{UDP}} = f^{0.1835}$. Figure 5.18 and 5.19and 5.20 show the relationship between $N_{max_{UDP}}$ and bandwidth, the results of model fitting for different bandwidth, and the CDF of measured and simulated number of

MPCs using our model for the UDP scenario. The CDF results show our model for the number of MPCs matches well with the measured data in UDP scenario.

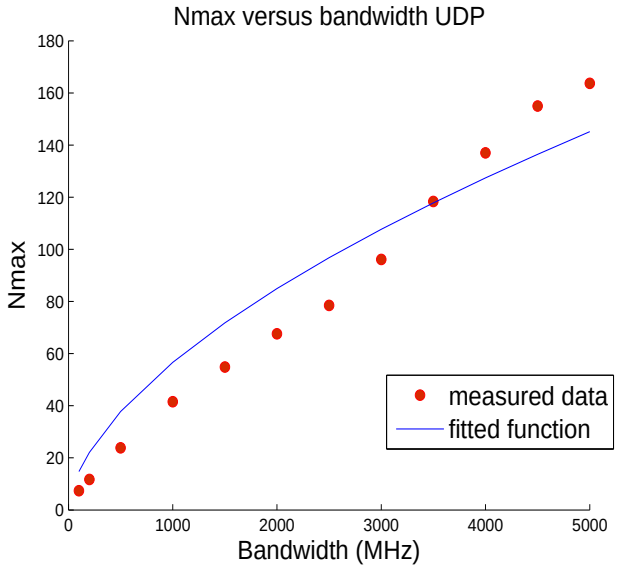

Figure 5.18: Nmax versus bandwidth for UDP environment

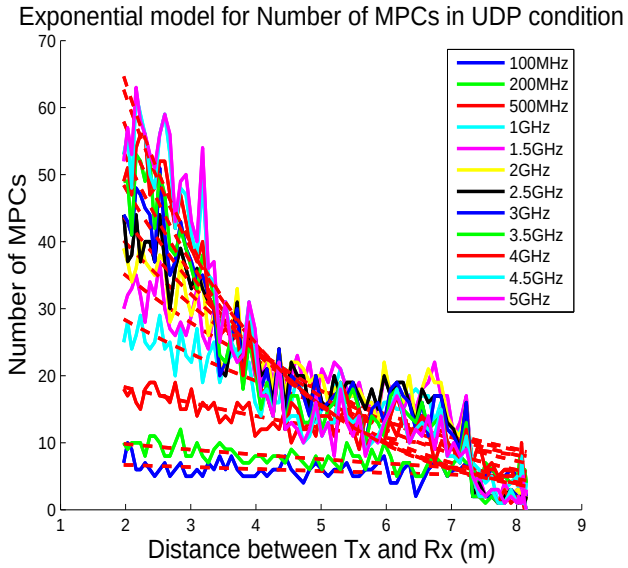

Figure 5.19: exponential model performance for different bandwidths without χ variable in UDP scenario

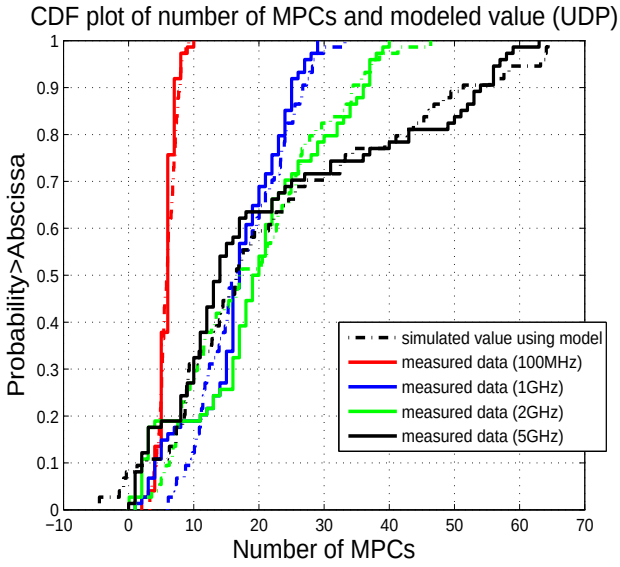

Figure 5.20: CDF of measured and simulated number of MPCs in UDP scenarios

5.2 Behavior of Path Persistency

The concept of path lifetime or path persistency has been proposed in [7, 31]. It denotes the lifetime of a particular path in which its traceable features exhibit differential changes in accordance with the receiver's differential motion. Due to the limitation of our measurement system, we only look into the TOA of persistent paths.

5.2.1 What is Path Persistency?

To illustrate how we defined path persistency in terms of TOA, it is necessary to introduce two different resolution terms used in time domain - the response resolution and the range resolution. Time domain response resolution is defined as the ability to resolve two closely-spaced responses, or a measure of how close two responses can be to each other and still be distinguished from each other. It is inversely proportional to the measurement frequency span, and is also affected by the window function used in the transform.

For example, using a normal window in the bandpass mode, we can calculate the

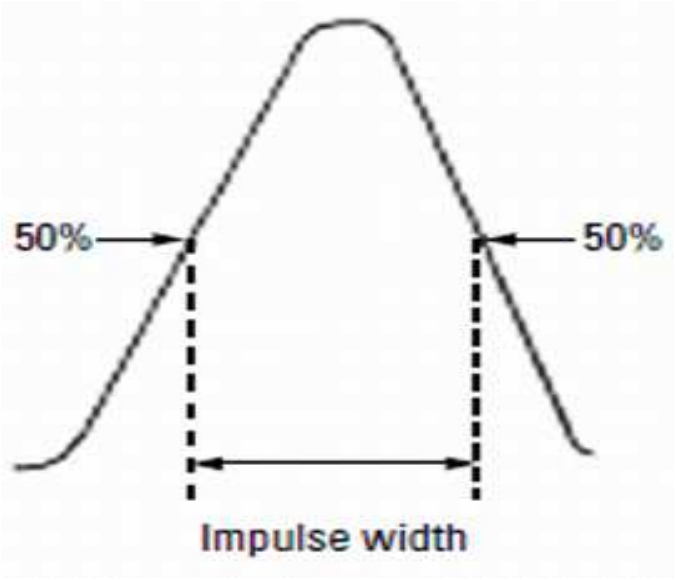

Figure 5.21: Response resolution is equal to the 50% points of the impulse width

response resolution for responses of equal amplitude as: Response resolution$= 50\%$ impulse width$\times$speed of light as indicated in Fig 5.21.

Time domain range resolution is defined as the ability to locate a single response in time. If only one response is present, range resolution is a measure of how closely we can pinpoint the peak of that response. The range resolution is equal to the digital resolution of the display, which is the time domain span divided by the number of points on the display. Range Resolution$=T_{span}/$(Points-1)

Figure 5.22shows the TOA of the earliest 10 paths' length during the movement of the Rx around the loop environment. We get the intuition that the paths' TOA exhibit differential changes in accordance with the motion of the receiver in the direct detected path (DDP) conditions, which occur at the beginning and ending parts of the route. The solid line is the actual distance and the dotted lines are the earliest 10 paths' length calculated by TOA multiplied by the speed of light.

Our measurement step size is 0.1m, which means a maximum difference in TOA of $\delta_\tau = 0.1/C = 0.33ns$, ($C = 3 \times 10^8 m/s$) for a persistent path from one measurement

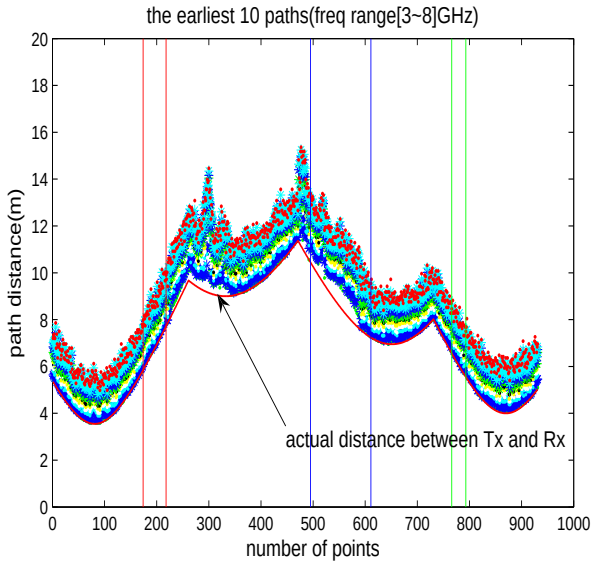

Figure 5.22: Path length of the earliest 10 paths during the measurement loop

location to the next. If the TOA difference of a particular path between several consecutive measurement points is within δ_τ, then the distance range of these measurement points is defined as the path lifetime of this path, which is illustrated in figure 5.23. Here we should point out that δ_τ refers to spatial resolution. It does not refer to the response resolution, which is determined by signal bandwidth.

In this thesis, we investigated the effect of bandwidth, path detection threshold (α)and NLOS, UDP occurrence on path persistency of the strongest path (SP) and first detected path (FDP), which are important for geolocation application based on measurement results. The parameter we focused on is the average path life time (APL), and average path displacement (APD).

APL and APD were first proposed in [7]. Buildings with simple internal structures and with less clutter will provide better tracking under UDP conditions than buildings with a large number of walls and metallic objects. Hence the number of persistent regions (NPR) on an RX's pathway is a metric useful in the characterization of buildings. APL is the mean length of all different persistent regions on the RX's motion path and is an

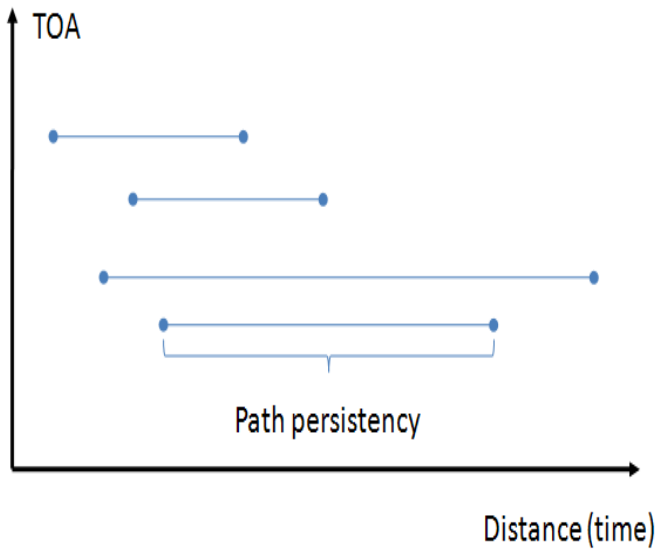

Figure 5.23: Concept of path persistency

indicator of the average lifetime of a certain path. It shows for how long a path will be persistent in units of distance. It can be written as

$$APL = \frac{\sum_{i=1}^{NPR} l_i}{NPR}, \tag{5.7}$$

where l_i is the lifetime of each persistent path in meters. Notice that low number of persistent regions indicates higher APL meaning paths are more persistent.

The other metric is the APD which shows how much TOA difference there is between different persistent regions on the average. It can be represented as

$$APD = \frac{\sum_{k=1}^{NTD} dp_i}{NTD}, \tag{5.8}$$

where dp_i is the amount of displacement in meters when a switch occurs from one persistent path to another and NTD is the number of total displacements.

5.2.2 Parameters Affecting Path Persistency

For the loop scenario, which contains mixed channel profiles (LOS OLOS and UDP), the path persistency results are summarized in Table 5.1 and Fig 5.24.

Table 5.1: APL (m)and APD (m)for FDP and SP For Different Bandwidths and α=10,20,30dB for the Loop scenario

		Bandwidth				
		128MHz	320MHz	800MHz	2GHz	5GHz
FDP	α	APL APD	APL APD	APL APD	APL APD	APL APD
	10dB	0.02 1.74	0.07 0.72	0.15 0.36	0.15 0.53	0.20 0.33
	20dB	0.02 1.45	0.09 0.47	0.24 0.16	0.52 0.09	1.28 0.03
	30dB	0.02 1.50	0.09 0.46	0.27 0.14	1.61 0.02	7.71 0.003
SP	10∼30dB	0.08 8.09	0.14 7.54	0.18 6.41	0.31 2.70	0.38 2.70

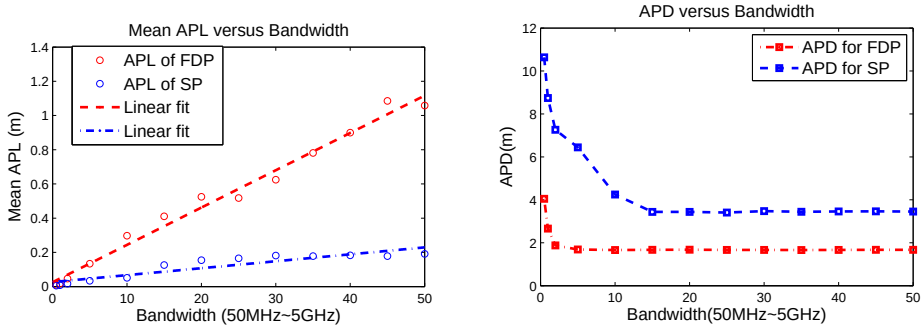

(a) APL versus BW (b) APD versus BW

Figure 5.24: APL and APD versus Bandwidth and the linear fit ($\alpha = 20dB$)

Based on these results, we observed that

1.For the same α, the APL of both FDP and SP increases with bandwidth. The relationship between the mean APL of FDP and bandwidth when $\alpha = 20dB$ can be modeled as:

$$APL = 0.0218BW + 0.0256 \tag{5.9}$$

where BW is the bandwidth in units of 100MHz. The RMSE for this model is 0.046m. Choosing 20dB has been found to be suitable for detecting paths While the relationship between the mean APL of SP and bandwidth can be modeled as :

$$APL = 0.0041BW + 0.0264 \tag{5.10}$$

The RMSE for this model is 0.028m.

2.The APL of FDP is always larger than that of the SP since the power of paths suffers easily in UDP conditions causing the SP to switch to another path more often.

3.The APL and APD of the strongest path are not sensitive to α since no matter which α we choose, the power of SP is always within the α dB range of itself.

4.The APD of both the FDP and SP decreases as the bandwidth increases, but the APD of FDP and SP stays at around 1.8m for FDP and 3.5m for SP for bandwidth greater than 0.5GHz for FDP and 1.5GHz for SP respectively.

For the LOS scenario, the path persistency results are summarized in Table 5.2 and Fig 5.25.

Table 5.2: APL (m)and APD (m)for FDP and SP For Different Bandwidths and α=10,20,30dB for the LOS scenario

		Bandwidth				
		100MHz	500MHz	1GHz	2GHz	5GHz
	α	APL APD	APL APD	APL APD	APL APD	APL APD
FDP	10dB	0.22 1.56	0.74 1.14	1.61 1.15	2.39 1.25	13.90 1.25
	20dB	0.22 1.49	0.73 0.79	1.87 0.80	3.00 0.78	9.23 0.79
	30dB	0.23 1.48	0.70 0.75	1.86 0.76	3.00 0.75	1.65 0.74
SP	10$\sim$30dB	0.26 2.89	0.58 3.89	1.15 4.20	1.37 4.11	1.15 4.17

Based on these results, we observed that:

1. Most of the time, the APL of both FDP and SP increases with bandwidth. For the same bandwidth, the mean APL of FDP increases as the threshold value α decreases.

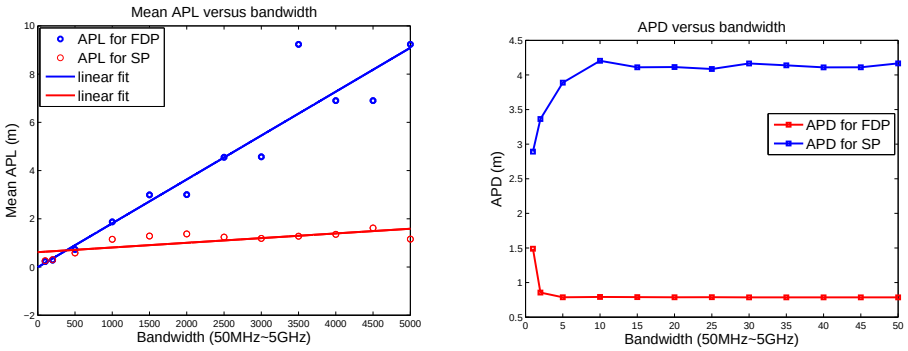

(a) APL versus BW (b) APD versus BW

Figure 5.25: APL and APD versus Bandwidth and the linear fit ($\alpha = 20dB$) for LOS scenario

The relationship between the mean APL of FDP and bandwidth when $\alpha = 20dB$ can be modeled as:

$$APL = 0.182BW - 0.01 \tag{5.11}$$

where BW is the bandwidth in units of 100MHz. The RMSE for this model is 0.972m. Choosing 20dB is reasonable since a 10dB threshold for picking paths would eliminate most of the multipath components, making the number of available MPCs insignificant, while if a 30dB threshold is used, the first path would be non-persistent, which is not the fact for the LOS scenario. The relationship between the mean APL of SP and bandwidth can be modeled as

$$APL = 0.0194BW + 0.6141 \tag{5.12}$$

The RMSE for this model is 0.274m.

2.The APL of FDP is always larger than that of the SP which is in accordance with the results for the loop scenario.

3.The APL and APD of the strongest path are not sensitive to the threshold α for picking paths .

4. The APD of FDP in the LOS scenario decreases as the bandwidth increases. How-

ever, the APD for SP increases with bandwidth. The APD of FDP and SP stay at about 0.75m and 4m for the bandwidth greater than 1GHz.

For NLOS or OLOS scenario, the path persistency results are summarized in table 5.3 and figure 5.26.

Table 5.3: APL (m)and APD (m)for FDP and SP For Different Bandwidths and α=10,20,30dB for the NLOS scenario

		Bandwidth				
		100MHz	500MHz	1GHz	2GHz	5GHz
	α	APL APD	APL APD	APL APD	APL APD	APL APD
FDP	10dB	0.11 3.01	0.25 1.65	0.37 1.62	0.48 1.63	0.69 1.83
	20dB	0.11 3.06	0.25 1.69	0.40 1.68	0.57 1.73	0.69 1.90
	30dB	0.11 3.07	0.25 1.69	0.40 1.68	0.57 1.73	0.69 1.90
SP	10∼30dB	0.12 11.35	0.20 7.58	0.25 8.32	0.47 8.02	0.55 7.93

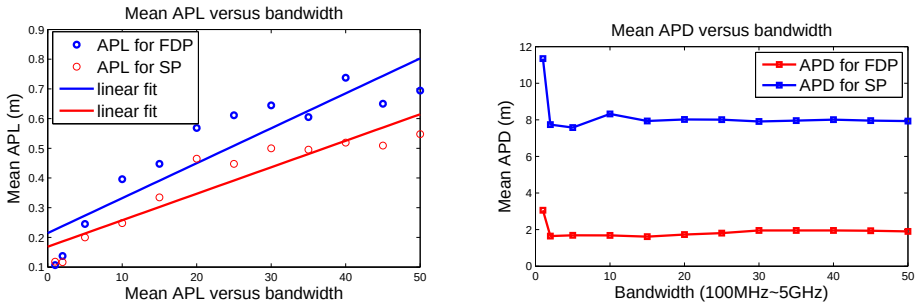

(a) APL versus BW (b) APD versus BW

Figure 5.26: APL and APD versus Bandwidth and the linear fit ($\alpha = 20dB$) for NLOS scenario

Based on these results, we observe that: 1. the APL of both FDP and SP increases with bandwidth. However, comparing with the results for the LOS scenario, the APL of FDP decreases due to walls and metallic objects blockage between the Tx and Rx. For the same bandwidth, the mean APL of the FDP is not very sensitive to the threshold α. The relationship between the mean APL of FDP and bandwidth when $\alpha = 20dB$ can be modeled as

$$APL = 0.012BW - 0.215 \tag{5.13}$$

where BW is the bandwidth in units of 100MHz. The RMSE for this model is 0.0851m. The relationship between the mean APL of SP and bandwidth can be modeled as :

$$APL = 0.009BW + 0.169 \tag{5.14}$$

The RMSE for this model is 0.057m.

2.The APL of the FDP is always larger than that of the SP, which is in accordance with the results for Loop and LOS scenario.

3.The APL and APD of the strongest path are not sensitive to the threshold α for picking paths.

4. The APD of both FDP and SP decreases as the bandwidth increases. The APD of FDP and SP stay at about 2m and 8m after the bandwidth reaches 1GHz.

For the UDP scenario, the path persistency results are summarized in Table 5.4 and Fig 5.27.

Table 5.4: APL (m)and APD (m)for FDP and SP For Different Bandwidths and α=10,20,30dB for the UDP scenario

		Bandwidth				
		100MHz	500MHz	1GHz	2GHz	5GHz
FDP	α	APL APD	APL APD	APL APD	APL APD	APL APD
	10dB	0.12 3.10	0.14 1.57	0.32 1.76	0.21 1.52	0.27 1.56
	20dB	0.12 2.97	0.16 1.59	0.12 1.25	0.19 0.93	0.31 0.89
	30dB	0.12 3.12	0.20 1.65	0.15 1.38	0.18 1.07	0.33 1.02
SP	10$\sim$30dB	0.10 5.29	0.16 5.27	0.18 6.00	0.15 4.73	0.20 4.73

Based on these results, we observe that:

1. the APL of both FDP and SP increases with bandwidth. However, in contrast with the results for of LOS and OLOS scenario, the APL of the FDP decreased significantly due to the wall and micro-metal blockage between the Tx and Rx, causing the FDP to jump among several different MPCs. For the same bandwidth, the mean APL of FDP is

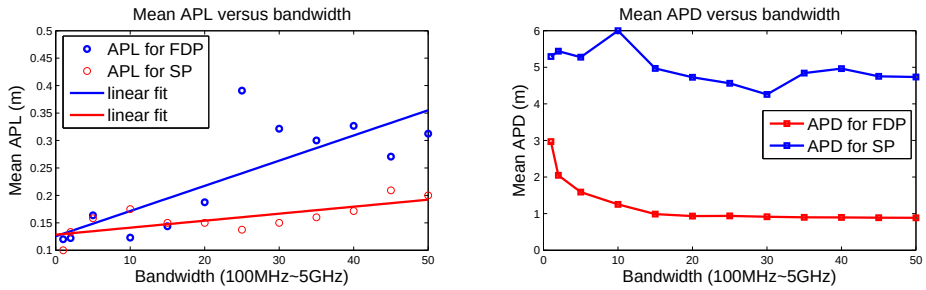

(a) APL versus BW (b) APD versus BW

Figure 5.27: APL and APD versus Bandwidth and the linear fit ($\alpha = 20dB$) for UDP scenario

not very sensitive to the threshold value α. The relationship between the mean APL of FDP and bandwidth when $\alpha = 20dB$ can be modeled as

$$APL = 0.005BW + 0.126 \tag{5.15}$$

where BW is the bandwidth in units of 100MHz. The RMSE for this model is 0.057m. The relationship between the mean APL of SP and bandwidth can be modeled as :

$$APL = 0.001BW + 0.128 \tag{5.16}$$

The RMSE for this model is 0.019m.

2.The APL of FDP is always larger than that of the SP but the difference between them is not as significant as that for LOS and NLOS scenarios.

3.The APL and APD of the strongest path is not sensitive to the threshold α for picking paths .

4. The APD of both FDP and SP decreases as the bandwidth increases. The APD of FDP and SP stay at about 1m and 4m for the bandwidth above 1GHz.

Chapter 6

Conclusions and Future Work

6.1 Conclusions

In this thesis, we have analyzed the effect of distance, bandwidth, environment and threshold for picking paths on Multipath parameters such as distance measurement error, number of MPCs, and path persistency. The measurement database was constructed with the collaboration of Ferit Akgul during the summer of 2008. The measurement campaign was conducted in four different scenarios. The measurement campaign was different from previous measurement campaigns in that we used a robot assisted measurement system to achieve spatially continuous measurements.

We begin our research with a review of existing indoor localization techniques was presented. Due to the harshness of indoor propagation environments, there is the need to study the dynamic channel behavior in depth in order to avoid or remedy the ranging errors induced by UDP occurrence and multipath combination. Among different solutions devised by researchers in the literature, one innovative way to combat TOA estimation inaccuracy caused by UDP occurrence is to use the TOA information of indirect paths together with geometric methods to calculate the lengths of the DLOS path . Recognizing

the value of this technique, we were motivated to analyze the behavior of number of available paths and path persistency, which are important in the use of this technique.

First, we studied the effect of distance, bandwidth and multipath environment on TOA estimation techniques. When the environment's influence on TOA estimation is considered, the LOS scenario provides the lowest ranging error because the presence of strong DLOS path. The performance of TOA estimation algorithms is more sensitive to bandwidth in OLOS scenario. All the TOA estimation algorithms perform poorly in the UDP scenario although the use of higher bandwidth helps to reduce the ranging error to some extent. Based on our processed results, the optimal choice for the localization system designer is to implement the simple IFT algorithm in the LOS scenario, DSSS algorithm in the OLOS scenario with limited bandwidth, and the IFT algorithm with large bandwidth, and superresolution algorithm in the UDP scenario with limited bandwidth while using the IFT algorithm with large bandwidth. .

Then, the models for number of MPCs were built based on data from three different indoor environments, and a statistical method was used to find the best-fit model. According to the models we developed, the number of MPCs is very sensitive to the threshold for picking paths, and to the noise floor threshold, which should be carefully selected by the localization system designer. The number of MPCs generally decreases as the distance increases while larger bandwidths always provide better path resolvability and more MPCs. Harsher environments such as the UDP scenario will cause the number of MPCs to drop more quickly as the distance increases, so that the coverage of the UDP scenario is the smallest compared with other scenarios.

For path persistency, we first illustrated the definition of path persistency and its importance for tracking when the DLOS path is not available. Then we gave the definition of two parameters, APL and APD which were used for comparing the path persistency under different constraints. From our processed results, it is clear that the multipath components

generally behave more persistently in LOS and OLOS scenario than they do in the UDP scenario, and larger bandwidth and higher threshold for picking paths also contributes to finding a more persistent path.

6.2 Future Work

Accurate indoor geolocation remains a challenging problem that still needs further research. The work of this thesis will provide other researchers with increased knowledge of the behavior of multipath parameters pertinent to indoor geolocation. Better algorithms are needed for utilizing indirect paths to calculate the length of the direct path in practical implementation. Another potentially useful approach for mitigating the influence of UDP occurrence and multipath environment is to implement a cooperative localization system to avoid as many UDP links as possible or to use other sources of localization information such as inertial measurement to aid the RF localization system. For the selection of differernt TOA estimation algorithms, one possible further research direction is to design new algorithms that can switch among different techniques dynamically based on the known parameters such as system bandwidth and operating environment. Gathering moeore measurement data in different environments is also desirable. A more extensive database will be valuable in refining our models to achieve closer correspondence to real-world propagation environments.

Appendix

Appendix A

More CCDF Graphs

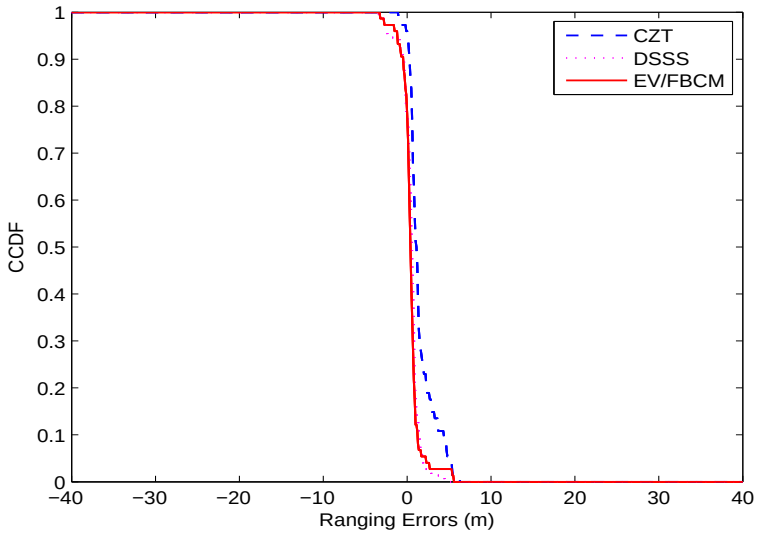

Figure A.1: CCDF of ranging errors for LOS using different TOA estimation algorithms at 80MHz bandwidth

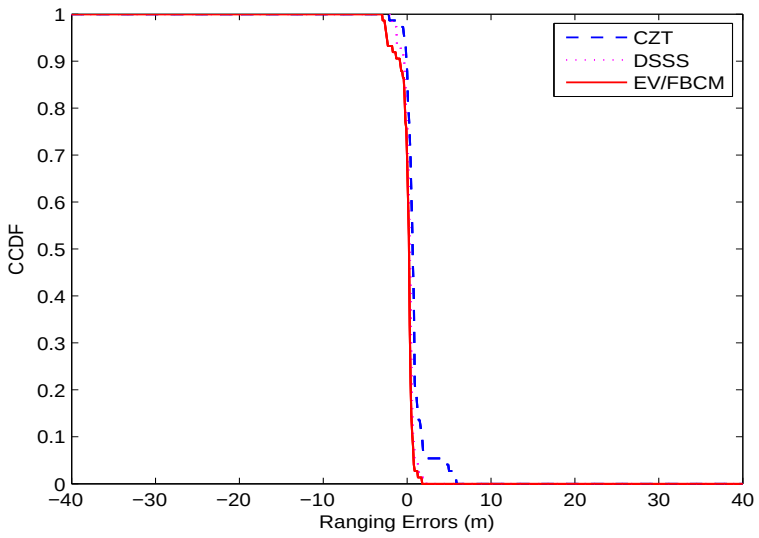

Figure A.2: CCDF of ranging errors for LOS using different TOA estimation algorithms at 120MHz bandwidth

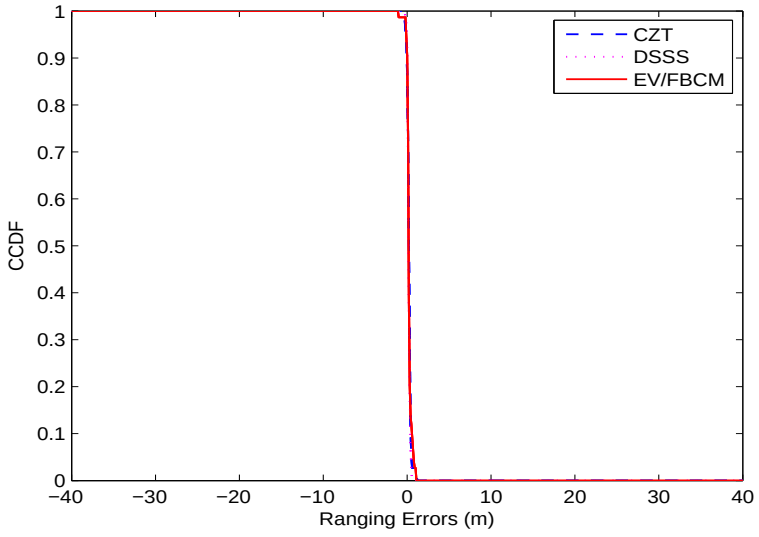

Figure A.3: CCDF of ranging errors for LOS using different TOA estimation algorithms at 500MHz bandwidth

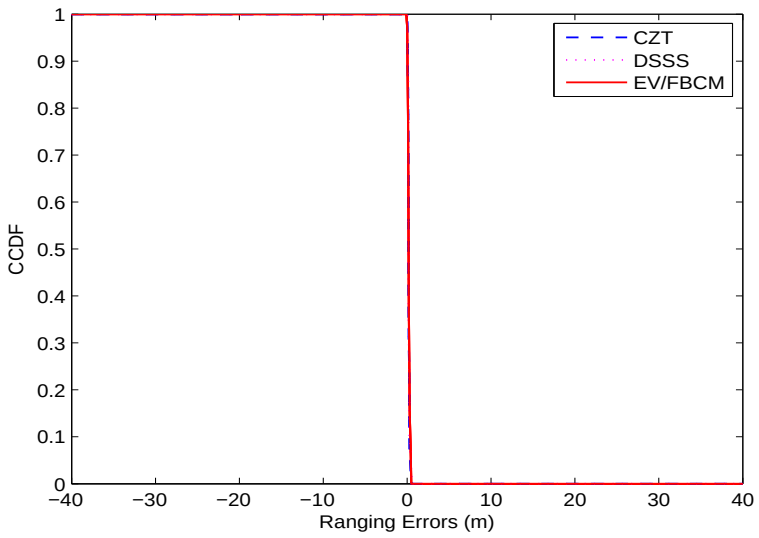

Figure A.4: CCDF of ranging errors for LOS using different TOA estimation algorithms at 2GHz bandwidth

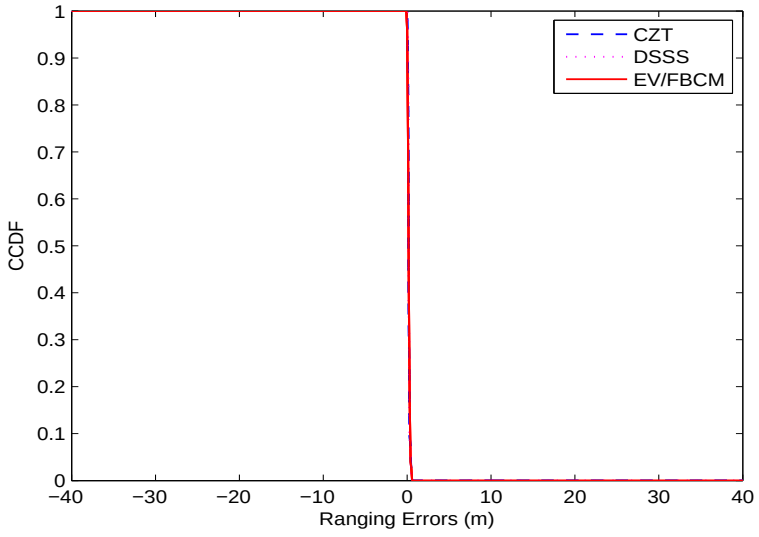

Figure A.5: CCDF of ranging errors for LOS using different TOA estimation algorithms at 3GHz bandwidth

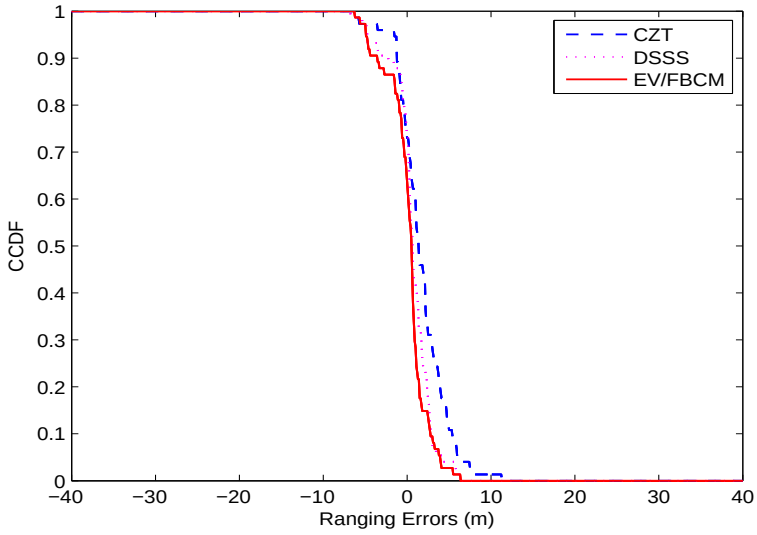

Figure A.6: CCDF of ranging errors for OLOS using different TOA estimation algorithms at 80MHz bandwidth

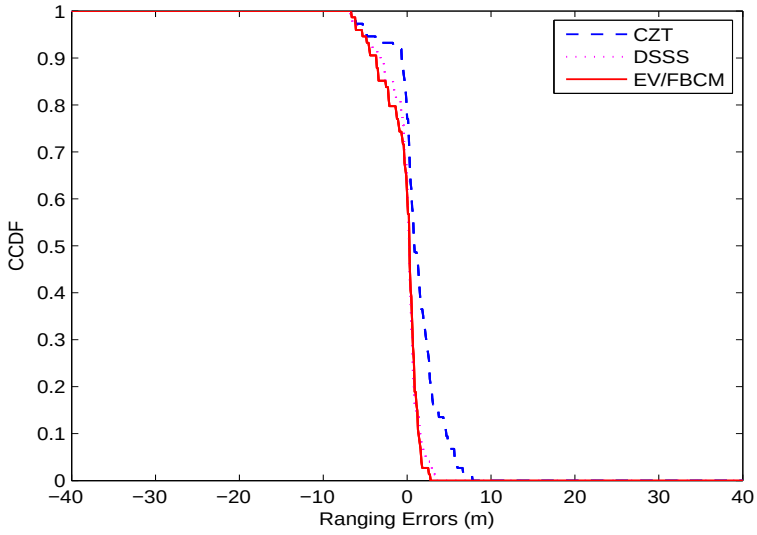

Figure A.7: CCDF of ranging errors for OLOS using different TOA estimation algorithms at 120MHz bandwidth

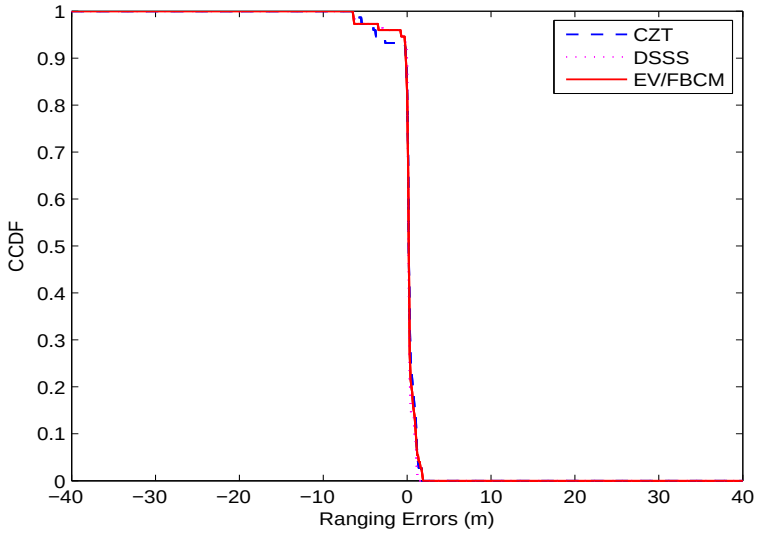

Figure A.8: CCDF of ranging errors for OLOS using different TOA estimation algorithms at 500MHz bandwidth

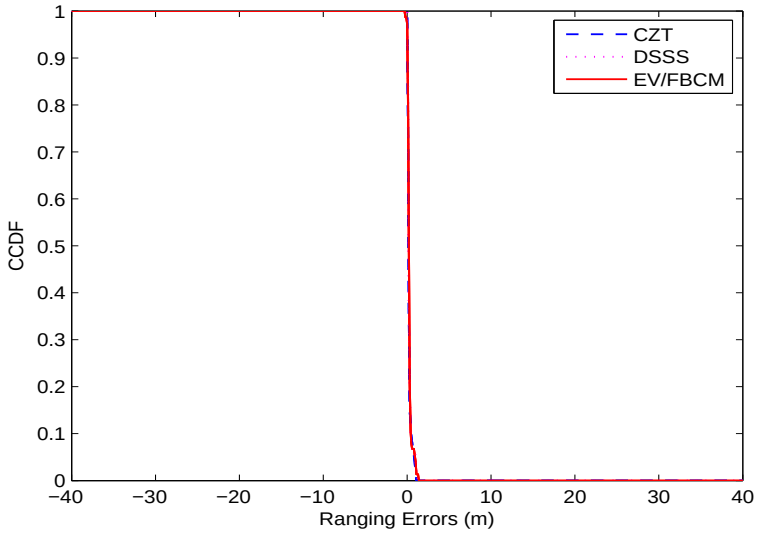

Figure A.9: CCDF of ranging errors for OLOS using different TOA estimation algorithms at 2GHz bandwidth

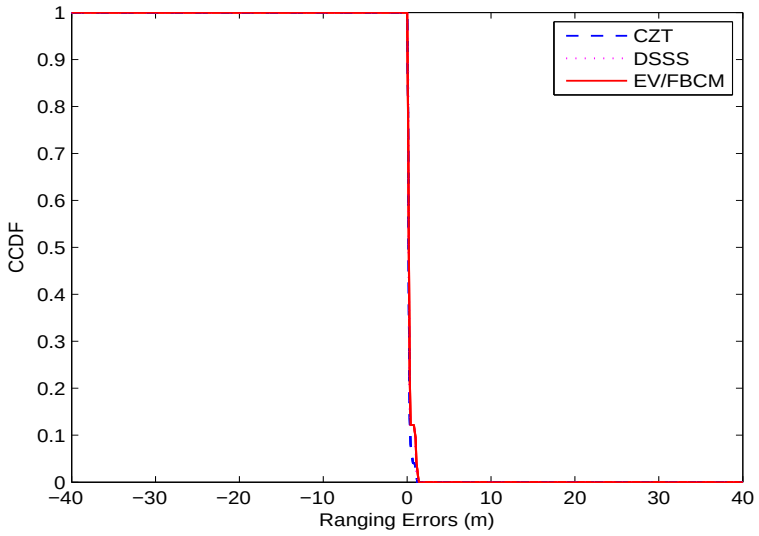

Figure A.10: CCDF of ranging errors for OLOS using different TOA estimation algorithms at 3GHz bandwidth

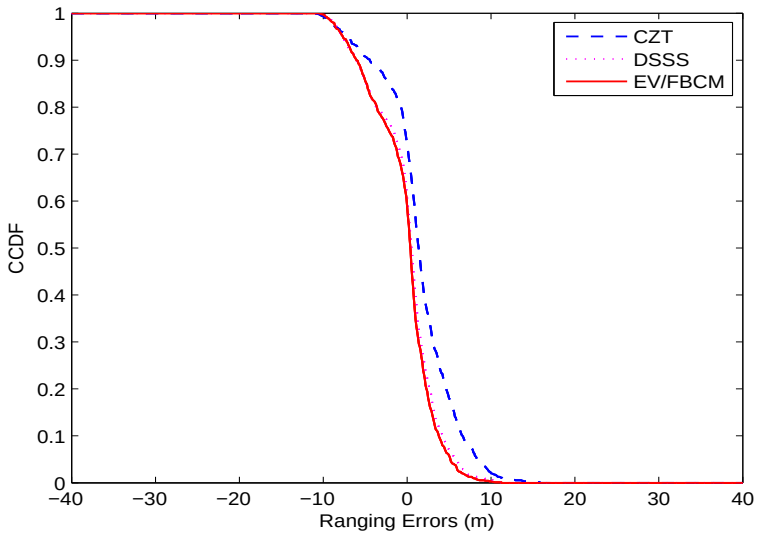

Figure A.11: CCDF of ranging errors for Loop scenario using different TOA estimation algorithms at 80MHz bandwidth

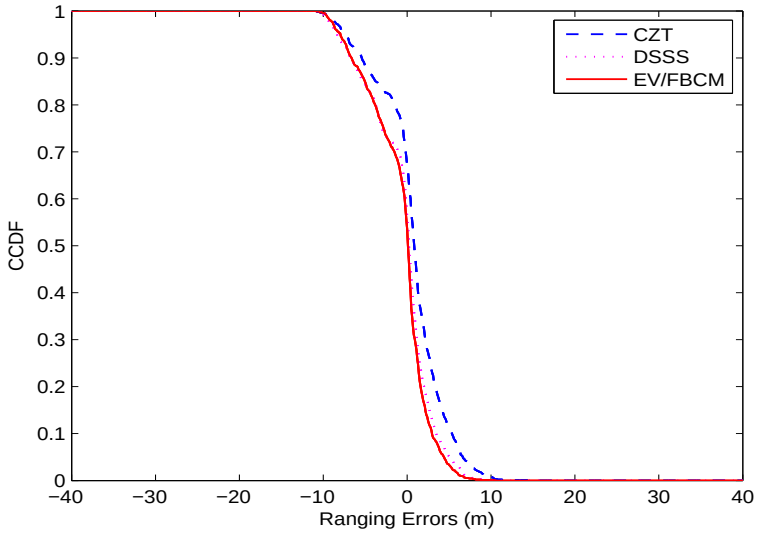

Figure A.12: CCDF of ranging errors for Loop scenario using different TOA estimation algorithms at 120MHz bandwidth

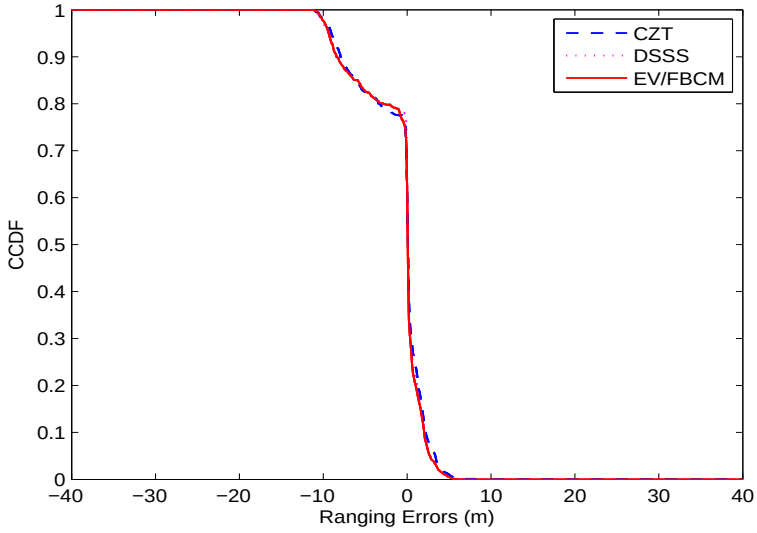

Figure A.13: CCDF of ranging errors for Loop scenario using different TOA estimation algorithms at 500MHz bandwidth

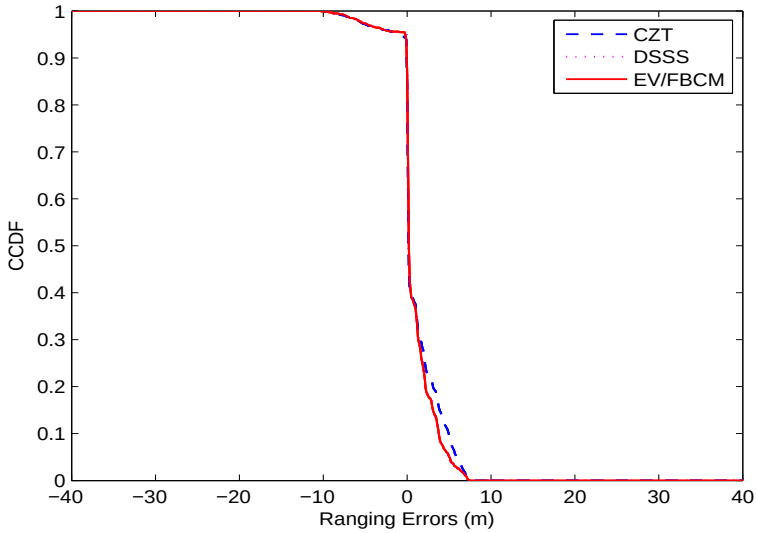

Figure A.14: CCDF of ranging errors for Loop scenario using different TOA estimation algorithms at 2GHz bandwidth

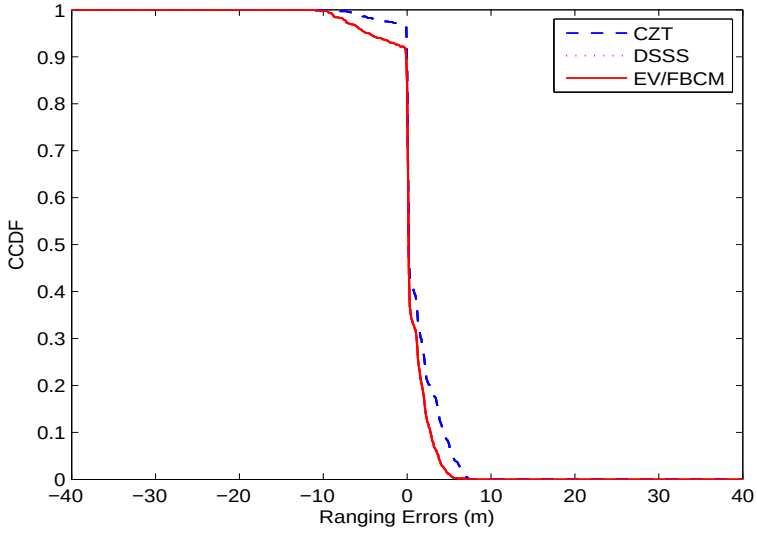

Figure A.15: CCDF of ranging errors for Loop scenario using different TOA estimation algorithms at 3GHz bandwidth

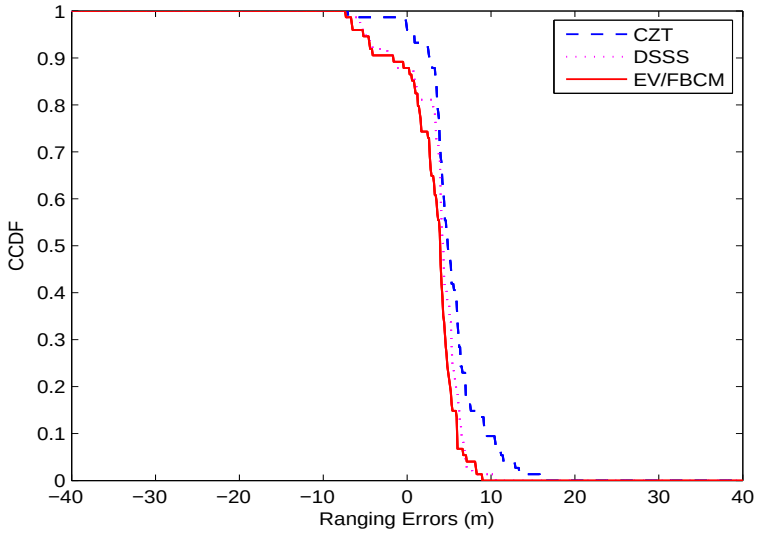

Figure A.16: CCDF of ranging errors for UDP scenario using different TOA estimation algorithms at 80MHz bandwidth

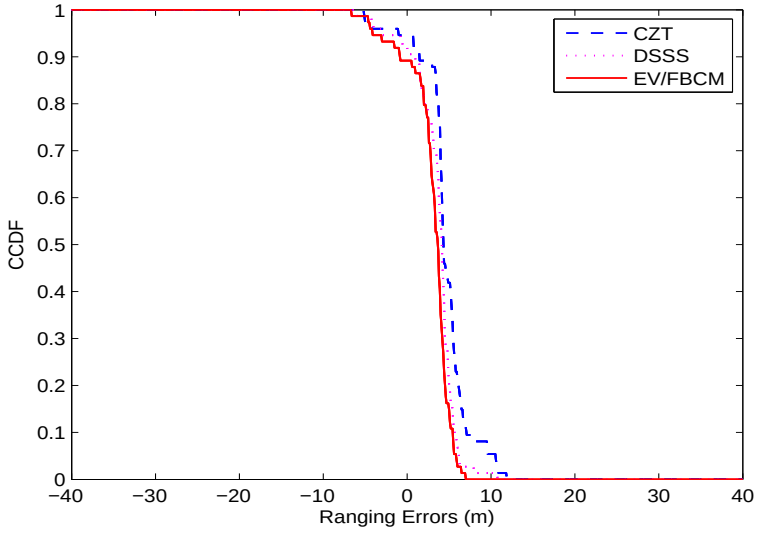

Figure A.17: CCDF of ranging errors for UDP scenario using different TOA estimation algorithms at 120MHz bandwidth

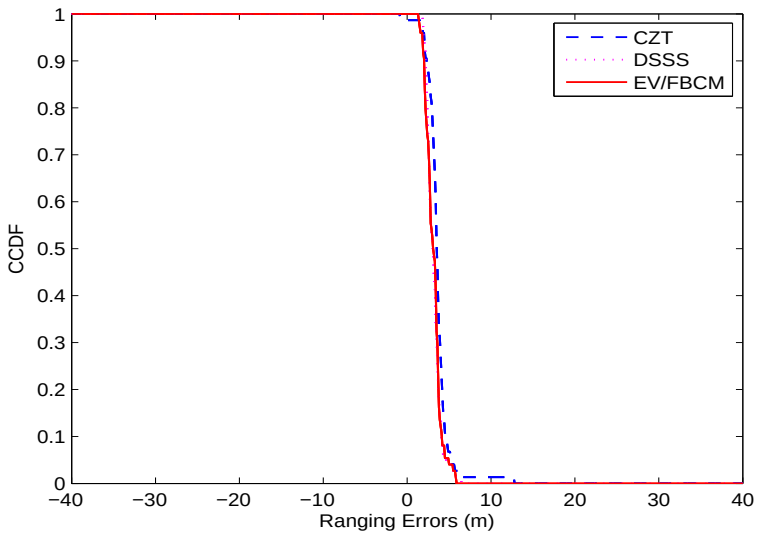

Figure A.18: CCDF of ranging errors for UDP scenario using different TOA estimation algorithms at 500MHz bandwidth

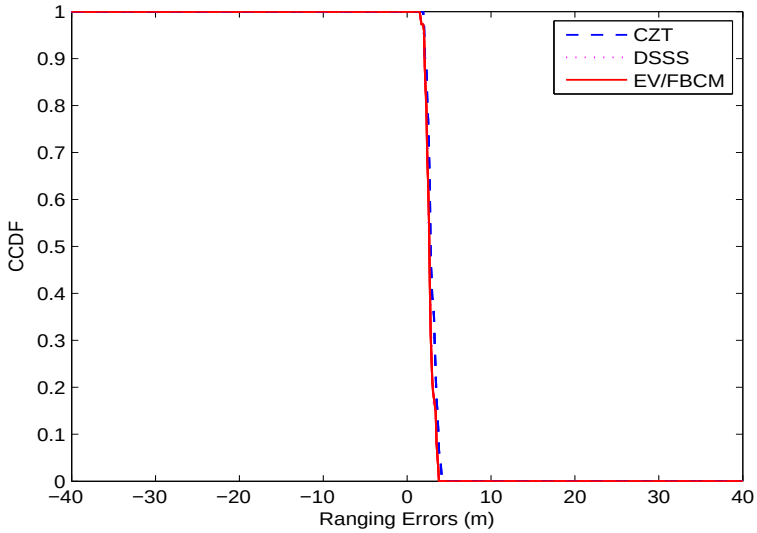

Figure A.19: UDP scenario using different TOA estimation algorithms at 2GHz bandwidth

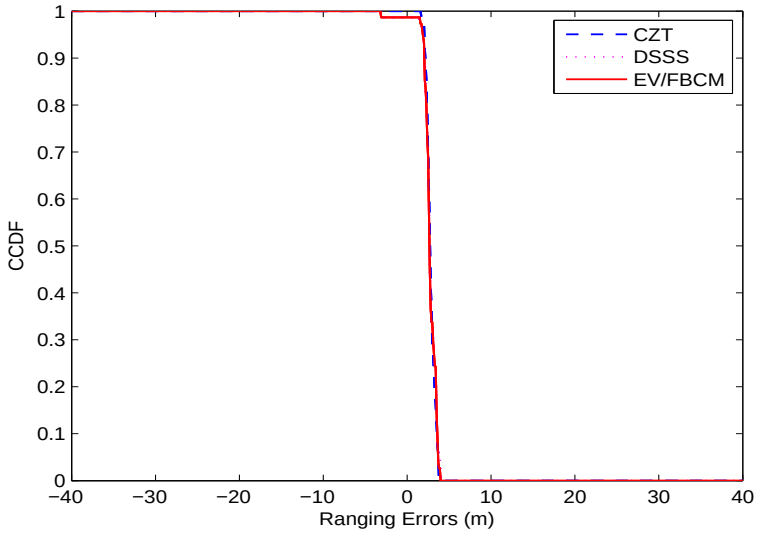

Figure A.20: UDP scenario using different TOA estimation algorithms at 3GHz bandwidth

Appendix B

MATLAB Codes for Parsing Data

```
%% convert network analyzer data to time domain
close all
clear all
clc
%%%%%%%%%%%%%%%%%%%%%%%%%%%%%%%%%%%%
%%  For calculating Tx-RX distance
%%%%%%%%%%%%%%%%%%%%%%%%%%%%%%%%%%%%
% Nfile=291;      %Number of measurement points
% txloc = [9 6.95];     %fixed transmitter point
% rxloc1 = [(13:-0.05:0)' 10.5*ones(segm(1),1)  ];
% rxloc2 = [zeros(segm(2),1) (10.45:-0.05:0)' ];
% rxloc3 = [(0.05:0.05:13)' zeros(segm(3),1)  ];
% rxloc4 = [13*ones(segm(4),1) (0.05:0.05:10)' ];
% rxloc = [rxloc1; rxloc2; rxloc3; rxloc4];  %Receiver points
%calculate distance between Tx and Rx
% for k=1:size(rxloc,1)
%     dist(k) = norm(rxloc(k,:) - txloc);
% end
```

```
%%%%%%%%%%%%%%%%%%%%%%%%%%%%%%%%%%%%
%%%%%%%%%%%%%%%%%%%%%%%%%%%%%%%%%%%%
%% SETTINGS
%%%%%%%%%%%%%%%%%%%%%%%%%%%%%%%%%%%%
%%%%%%%%%%%%%%%%%%%%%%%%%%%%%%%%%%%%
△ = 1;                  %  Delta x 5 cm processing
vec = [1:△:(Nfile-1)]; % Count vector
numpa=zeros(length(vec),1);% Number of path
makemovie = 0;              % Switch for making movie
dbase =1;
c = 3e8;                    %Speed of signal
% Noise suppression in dB%
noise_suppr_db =20;
noise_suppr =10^(noise_suppr_db/20);
% Time domain span%
tstart = 0;
tstop=320e-9;
% Frequency domain span (GHz)
BWstart = 3;
BWend = 8;
BW = BWend - BWstart;
% Average number of MPCs
avgnumpa=zeros(13,1);
drange=0;  %select whether to put the dynamic range
numpamat=zeros(length(vec),13);%matrix of number of paths
% Matrix of number of paths for CDF plot
numpamat1=zeros(Nfile,13);
% Receiver sensitivity threshold
noi = 10^(-90/20);
% side lobe threshold
side =10^(-20/20);
```

```
peak_width = 1;
% Used for calculation of APL of FDP
segcnt=1;
lenvec=zeros(1,length(vec));
lenvecmat=zeros(13,length(vec));
% Used for calculation of APL of SP
segcnt1=1;
lenvec1=zeros(1,length(vec));
lenvec1mat=zeros(13,length(vec));
flag_fig = 0;
%%%%%%%%%%%%%%%%%%%%%%%%%%%%%
tracking=0;% Switch for tracking the paths
%%%%%%%%%%%%%%%%%%%%%%%%%%%%%

%% plotting figure switches
plot_figure = 0;
% TOA of the FDP and SP versus moved distance
plot1=0;
% RMS delay versus moved
plot2=0;
% Received signal power versus moved distance
plot3=0;
% Distance between Tx and Rx
plot4=0;
% Number of MPCs versus bandwidth
plot5=0;
% Plot power of FDP and SP versus
% moved distance
plot6=0;
% Plot delay gain matrix
plot7=0;
```

```
% Plot the difference between SP and FP power as
% a function of location
plot14=0;
%%%%%%%%%%%%%%%%%%%%%%%%%%%%%%%%%%%%
%%%%%%%%%%%%%%%%%%%%%%%%%%%%%%%%%%%%

%% Switch and save for making movie
if makemovie
    mov = avifile([num2str(vec(1)) '-' num2str(vec(end)) ...
    '_' num2str(BWstart) 'G-' num2str(BWend) 'G_test_thr' ...
    num2str(abs(noi)) '_' num2str(dbase) '.avi']);
end

%%
k = vec+1;
j = 1;
%Swiching between different bandwidths
frange=1:12;   %%%for 5G
for q=frange;
    %Originate parameters for each bandwidth
    k=vec+1;
    j=1;
    segcnt=1;
    segcnt1=1;
    lenvec1=zeros(1,length(vec));
    lenvec=zeros(1,length(vec));
    numpa=zeros(length(vec),1);
    power=zeros(length(vec),1);
    pfir=zeros(length(vec),1);
    rms=zeros(length(vec),1);
    disp(num2str(q));
```

```
for i=vec
     %Display points which are times of 50
    if mod(j,50)==0
        disp(['Numpos: ' num2str(j)] )
    end
    %Load measurement data
    if avg    %Switch for averaging 2 data set
          fname1 = ['scen3_pt' num2str(i) '_1.s1p'];
          fname2 = ['scen3_pt' num2str(i) '_2.s1p'];
        [Hf1, f1] = load_chmeas_s1p_dB( fname1, flag_fig );
        [Hf2, f2] = load_chmeas_s1p_dB( fname2, flag_fig );
        %%%% Time avg
        %[zt_han1, t1] = CZT_Hanning( f1, Hf1, tstart, tstop, flag);
        %[zt_han2, t2] = CZT_Hanning( f2, Hf2, tstart, tstop, flag);

        %zt_han = (zt_han1 + zt_han2) / 2;
        %t = t1;
        %%%% Freq avg
        Hf = (Hf1 + Hf2) / 2;
        [zt_han, t] = CZT_Hanning( f1, Hf, tstart, tstop, flag);
    else
        fname = ['scen3_pt' num2str(i) '_1.s1p'];
        flag = 1; % Hanning -- > 1: apply  0: donot apply
        [Hf, f] = load_chmeas_s1p_dB( fname, flag_fig );
        factor = BW / 5;
        lim = fix(length(f)*factor);
    end
    % Vector for Switching among different BW
    bwvector=[100 200 500 1000 1500 ...
    2000 2500 3000 3500 4000 4500 5000];
    % Load frequency domain data with different
```

```
143     % Bandwidth
144     Hf=Hf((5000-bwvector(q))/(2*5000)*3200+1:...
145     (5000-bwvector(q))/(2*5000)*3200+1+bwvector(q)/5000*3200);
146     f=f((5000-bwvector(q))/(2*5000)*3200...
147     +1:(5000-bwvector(q))/(2*5000)*3200+1+bwvector(q)/5000*3200);
148     % Use chirp-Z transform to get time domain data
149      [zt_han, t] = CZT_Hanning( f, Hf, tstart, tstop, flag);
150     % Suppress noise before multipath
151     noi_ind = find(t < dist(j)/c);
152     zt_han(noi_ind) = zt_han(noi_ind)/noise_suppr;
153     % Find peaks
154     index = pkd_cir(abs(zt_han), noi, side, peak_width);
155     if index == 0
156         continue
157     end
158     numpa(j)=length(index);
159     pathindex=index;%%%%%%%
160     %%%%%%calculate the path's time of arrival %%%%%%%
161     % First path
162     firstpath(i+1) = min(t(pathindex)) * 3*10^8;
163     [val1 ind1]=sort(t(pathindex),'ascend');
164     % Strongest path
165     [val ind]=sort(20*log10(abs(zt_han(pathindex))),'descend');
166     strpath(i+1)=t(pathindex(ind(1)))*3*10^8;
167     % Calculate the magnitude difference between the FP and SP
168     pfir(j)=20*log10(abs(zt_han(pathindex(ind1(1)))));
169     pstr(j)=20*log10(abs(zt_han(pathindex(ind(1)))));
170     differp(j)=pstr(j)-pfir(j);
171     differl(j)=strpath(j)-firstpath1(j);
172
173     % Calculation for APL and APD
```

```
174     % This is for FDP
175     if i>0
176         if abs(firstpath(i+1)-firstpath(i))<0.25
177             lenvec(segcnt)=lenvec(segcnt)+1;
178        else
179             jump(segcnt)=abs(firstpath(i+1)-firstpath(i));
180             segcnt = segcnt + 1;
181         end
182     end
183     % This is for SP
184     if i>0
185         if abs(strpath(i+1)-strpath(i))<0.25
186             lenvec1(segcnt1)=lenvec1(segcnt1)+1;
187
188        else
189             jump1(segcnt1)=abs(strpath(i+1)-strpath(i));
190             segcnt1 = segcnt1 + 1;
191
192         end
193     end
194     %Calculate the RMS delay spread%%%
195     tao=sum(abs(zt_han(pathindex))...
196     .*t(pathindex)')/sum(abs(zt_han(pathindex)));
197     taosqure=sum(abs(zt_han(pathindex)).*...
198     (t(pathindex).^2)')/sum(abs(zt_han(pathindex)));
199     rms(j)=sqrt(taosqure-tao^2);
200     % Path gain
201     gain{j,:} = abs(zt_han(pathindex));
202     % Path delay
203     delay{j,:} = t(pathindex);
204     % Total received power at each point
```

```
205     power(j)=sum(gain{j,:}.*gain{j,:});
206     for ii=1:length(delay)
207         len(ii) = length(delay{ii,:});
208     end
209
210     if plot_figure
211         figure(2)
212         plot(t*1e9,20*log10(abs(zt_han)),'g','LineWidth',2)
213         title(['Point: ' num2str(i) ])
214         xlabel('Time (ns)')
215         ylabel('Path power (dB)')
216         ylim([-130 -30])
217         grid
218         hold on
219         plot(t(index)*1e9,20*log10(abs(zt_han(index))),'k*')
220         hold on
221         plot([dist(i)/c*1e9 dist(i)/c*1e9], [-130 30],'r--');
222     end
223     if makemovie
224         F = getframe(gca);
225         mov = addframe(mov,F);
226     end
227     hold off
228 j=j+1;
229 end
230
231
232 % Delay matrix
233 delaymat = zeros(length(delay),max(len));
234 % Gain delay matrix
235 gainmat = zeros(length(delay),max(len));
```

```
% Number of MPCs matrix
numpamat(:,q)=numpa;
% Persistent region matrix
% For FDP
lenvecmat(q,:)=lenvec;
% For SP
lenvecmat1(q,:)=lenvec1;
% FDP's APL for different bandwidth
meanlenvec(q)= mean(lenvec(find(lenvec)))*0.1;
% FDP's APD for different bandwidth
meanjump(q)=mean(jump);
% SP's APL for different bandwidth
meanlenvec1(q)=mean(lenvec1(find(lenvec1)))*0.1;
% SP's APD for different bandwidth
meanjump1(q)=mean(jump1);
% Average number of MPCs at different bandwidth
avgnumpa(q)=mean(numpa);
end




%if plot10
   %figure(13)
   %ii=1:931
   %plot(ii*0.05,firstpath(ii));
   %xlabel('the unfolded path length to the starting point');
   %ylabel('distance of the first path(m)');
   %title('bandwidth=100MHz');
   %ylim([0 30]);
```

```
    %figure(14)
    %ii=1:931
    %plot(ii*0.05,strpath(ii));
    %xlabel('the unfolded path length to the starting point');
    %ylabel('the length of strongest path(m)');
    %title('bandwidth=100MHz');
    %ylim([0 30]);
% end


if plot8
    figure(8)
    q=0:12
    plot((1-2/25*q)*50,avgnumpa(q+1));
    xlabel('bandwidth(100MHz)');
    ylabel('average number of paths during the round trip');
    title('number of paths versus bandwidth');
end

if plot1
    figure(1)
    i=1:931
    plot(i,firstpath(i),'g.');
    hold on
    plot(i,dist(i),'r');
    ylim([0 20])
    %hold on
    %legend('first path','second path',
    %'third path','forth path','fifth path','actual distance')
    plot([174 174],[0 20],'r',[218 218],...
    [0 20],'r',[560 560],[0 20],'b',...
```

```
    [611 611],[0 20],'b',[766 766],[0 20],'g',[793 793],[0 20],'g');
    xlabel('number of points');
    ylabel('path distance(m)');
    title('the first path(freq range[3¬8]GHz)');
    figure(2)
    i=1:931
    plot(i,strpath(i),'g.');
    hold on
    plot(i,dist(i),'r');
    hold on
    %legend('strongest path','second strongest',
    plot([174 174],[0 30],'r',[218 218],[0 30]...
    ,'r',[560 560],[0 30],'b',[611 611],[0 30]...
    ,'b',[766 766],[0 30],'g',[793 793],[0 30],'g');
    ylim([0 30]);
    xlabel('number of points');
    ylabel('path distance(m)');
    title('the strongest path (freq range[3¬8]GHz)');
end

if plot2
    figure(3)
    ii=1:length(rms)
    plot(ii,rms*10^9,'r');
    xlabel('the unfolded path length to the starting point');
    ylabel('rmsdelay(ns)');
    hold on
    plot([174 174],[0 100],'r',...
    [218 218],[0 100],'r',[560 560],[0 100]...
    ,'g',[611 611],[0 100],'g',[766 766]...
    ,[0 100],'b',[793 793],[0 100],'b');
```

```
    title('rms delay(5GHz)')
end


if plot3
    figure(4)
    jj=1:length(power)
    plot(jj,10*log10(power(jj)),'r');
    hold on
    plot([174 174],[-75 -40],...
    'r',[218 218],[-75 -40],...
    'r',[560 560],[-75 -40],'b',[611 611],[-75 -40],'b');
    xlabel('the unfolded path length to the starting point');
    ylabel('power(dBm)');
end


if plot4
    figure(5)
    ii=1:931
    plot(ii*0.05,dist(ii),'b');
    xlabel('unfolded path length from starting point');
    ylabel('distance between Tx and Rx(m)');
    title('distance variation during the measurement');
end


if plot5
    figure(6)
    jj=1:length(numpa)
    [ax,h(1),h(2)]=plotyy(jj,numpa(jj),jj,dist(jj));
```

```
360      legend(h,'number of paths','distance between the Tx and Rx')
361      hold on;
362      % plot([174 174],[0 300],'r',[218 218],[0 300],
363      %'r',[495 495],[0 300],'g',[611 611],[0 300],'g',
364      %[766 766],[0 300],'b',[793 793],[0 300],'b');
365      xlabel('number of the measurement points');
366      ylabel('number of paths for the threshod used for DP detection');
367      title('number of paths when bandwith is 5GHz(noi threshold -85dB)');
368      plot(dist,numpa');
369      axis([1 15 0 90]);
370  end
371
372
373
374  if plot6
375      figure(7)
376      jj=1:931
377      plot(jj,differp(jj),'o');
378      hold on
379      plot([174 174],[0 40],'r',[218 218]...
380      ,[0 40],'r',[560 560],[0 40],'g',...
381      [611 611],[0 40],'g',...
382      [766 766],[0 40],'b',[793 793],[0 40],'b');
383      xlabel('number of points');
384      ylabel('difference of magnitude between the FP and SP(dB)');
385      title(' difference of gain between SP and FP versus location');
386
387      figure(8)
388      jj=1:931
389      plot(jj,pfir(jj));
390      hold on
```

```
391     plot([174 174],[-90 -40],'r',[218 218]...
392     ,[-90 -40],'r',[560 560],[-90 -40],'g',...
393     [611 611],[-90 -40],'g',[766 766],[-90 -40],'b',[793 793],[-90 -40],'b');
394     xlabel('number of points');
395     ylabel('magitude of the FP(dB)');
396     title(' magnitude of FP versus location');
397
398     figure(9)
399     jj=1:931
400     plot(jj,pstr(jj));
401     hold on
402     plot([174 174],[-85 -45],'r',...
403     [218 218],[-85 -45],'r',[560 560],[-85 -45],...
404     'g',[611 611],[-85 -45],'g',[766 766],...
405     [-85 -45],'b',[793 793],[-85 -45],'b');
406     xlabel('number of points');
407     ylabel('magitude of the SP(dB)');
408     title(' magnitude of SP versus location');
409
410     figure(10)
411     jj=1:931
412     plot(jj,differl(jj),'o');
413     ylim([0 18]);
414     hold on
415     plot([174 174],[0 18],'r',...
416     [218 218],[0 18],'r',[560 560],[0 18],'g',...
417     [611 611],[0 18],'g',[766 766],[0 18],'b',[793 793],[0 18],'b');
418     xlabel('number of points');
419     ylabel('difference of path length between the FP and SP(m)');
420     title(' difference of path length between SP and FP versus location');
421 end
```

```
422
423 if plot7
424     figure(11)
425     pp=zeros(max(len),931);
426     for ii=1:931
427         pp(:,ii)=ii*ones(max(len),1);
428     end
429     mesh(pp,delaymat',(10*log10(gainmat))');
430
431 end
432
433
434 if makemovie
435     mov = close(mov);
436 end
437 %grid
```

Bibliography

[1] K. Pahlavan, X.Li, and J.-P.Makela, "Indoor geolocation science and technology," *IEEE Commun.Mag*, vol. Vol. 40, no. No. 2, pp. 112–118, 2002.

[2] K. Pahlavan and A. H. Levesque, *Wireless Information Networks. Second Edition.* Boston: Artech Houses, 1996.

[3] E. D. Kaplan, *Understanding GPS principles and applications.* New York: John Wiley and Sons Inc, 2005.

[4] M. J. M. et al, "Wireless enhanced 9-1-1 service-making it a reality," *Bell Labs Tech. J.*, pp. 188–202, Autumn 1996.

[5] H. Koshima and J.Hoshen, "Personal locator services emerge," in *IEEE Spectrum*, pp. 41–48, Feb. 2000.

[6] P.Jensfelt, *Approaches to mobile robot localization in indoor environments*. PhD thesis, Royal Institute of technology,Sweden, 2001.

[7] F. O. Akgul and K. Pahlavan, "Path persistency for high precision ranging in different building architectures," in *IEEE Personal Indoor Mobile Radio Communications Conference (PIMRC)*, February 2007.

[8] S. Gezici et al, "Localization via ultra-wideband radios," *IEEE Signal Processing Magazine*, July 2005.

[9] B. Denis, J. Keignart, and N. Daniele, “Impact of nlos propagation upon ranging precision in uwb systems,” in *IEEE conference on Ultra Wideband Systems and Technologies*, 2003.

[10] D. E. Gustafson, J. M. Elwell, and J. A. Soltz, “Innovative indoor geolocation using rf multipath diversity,” in *IEEE Position, Location, And Navigation Symposium(ION)*, April 2006.

[11] “Ekahau indoor positioning software website.”

[12] V. Bahl, P. Padmanabhan, “Radar: an in-building rf-based user location and tracking system,” in *INFOCOM 2000. Nineteenth Annual Joint Conference of the IEEE Computer and Communications Societies. Proceedings. IEEE*, vol. 2, pp. 775–784, 2000.

[13] M.GHAVAMI, L.B.MICHAEL, and R.KOHNO, *ultra wideband signals and systems in communication engineering.* NJ: John Wiley and Sons, Ltd, 2004.

[14] X.Li, *Super-Resolution TOA estimation with Diversity Techniques for Indoor Geolocation Appllications*. PhD thesis, Worcester Polytechnic Institute, 2003.

[15] M. Heidari, F. O. Akgul, and K. Pahlavan, “Identification of the absence of direct path in indoor localization systems,” in *IEEE Personal Indoor Mobile Radio Communications Conference (PIMRC)*, 2007.

[16] Y. Ye, F. O. Akgul, and K. Pahlavan, “Effect of bandwidth, path detection threshold and udp occurrence on multipath parameters pertinent to indoor geolocation,” in *IEEE Wireless and Microwave technology (WAMICON)*, April 2009.

[17] J. Beneat, K. Pahlavan, and P.Krishnamurthy, “Radio channel characterization for indoor and urban geolocation at different frequencies,” in *Proc. IEEE PIMRC*, September 1999.

[18] B. Alavi, K. Pahlavan, X. Li, and N.Alsindi, “Indoor geolocation distance error modeling with uwb technology,” in *Proceedings of IASTED 2nd International Conference on Communication and computer networks CCN 2004*, November 2004.

[19] E. D. Zand, K. Pahlavan, and J. Beneat, “Frequency domain measurement for indoor geolocation,” in *IEEE Personal Indoor Mobile Radio Communications Conference (PIMRC)*, 2003.

[20] “Evolution robotics.”

[21] S.S.Ghassemzadeh, R.Jana, C. Rice, W.Turin, and V.Tarokh, “A statistical path loss model for in-home uwb channels,” in *IEEE Ultra Wideband Systems and Technologies,Digest of Papers*, 2002.

[22] J. Schroeder, S. Galler, K. Kyamakya, and K. Jobmann, “Nlos detection algorithms for ultra-wideband localization,” in *Positioning, Navigation and Communication (WPNC) 4th workshop on*, 2007.

[23] J.Werb and C.Lanzl, “Designing a positioning system for finding things and peopleindoors,” in *IEEE spectrum*, vol. 35, September 1998.

[24] D.Manolakis, V.Ingle, and S.Kogon, *Statistical and Adaptive Signal Processing.* McGraw-Hill Co.,Inc, 2000.

[25] R.Schmidt, *A signal subspace approach to multiple emitter location and spectral estimation.* PhD thesis, Stanford Univ, Stanford, CA, 1981.

[26] K. Pahlavan, P. Krishnamurthy, and J.Beneat, “Wideband radio propagation modeling for indoor geolocation applications,” *IEEE Commun.Mag*, April 1998.

[27] K. Pahlavan, F. O. Akgul, M. Heidari, A. Hatami, J. M. Elwell, and R. D. Tingley, “Indoor geolocation in the absence of direct path,” *IEEE wireless communications*, Jan 2007.

[28] B.Alavi, *Distance Measurement Error Modeling for Time-of-arrival Based Indoor Geolocation*. PhD thesis, Worcester Polytechnic Institute, 2006.

[29] T. Rappaport, S. Seidel, and K. Takamizawa, “Statistical channel impulse response models for factory and openplan building radio communicate system design,” *IEEE transaction on communications*, May 1991.

[30] H.Hashemi, “Impulse response modeling of indoor radio propagation channels,” *IEEE Journal on Selected Areas in Communications*, vol. 11, September 1993.

[31] C.-C. Chong, C.-M. Tan, D. I.Laurenson, S. Mclaughlin, M. A.Beach, and A. R.Nix, “a novel wideband dynamic directional indoor channel model based on a markov process,” *EURASIP Journal on Wireless Communications*, vol. 4, no. 4, 2005.